FRMD4A REGULATES THE ENTRY OF WEST NILE VIRUS INTO GLIOBLASTOMA CELLS

PANG JUNXIONG, VINCENT

NATIONAL UNIVERSITY OF SINGAPORE

2009

FRMD4A REGULATES THE ENTRY OF WEST NILE VIRUS INTO GLIOBLASTOMA CELLS

PANG JUNXIONG, VINCENT
[B.Sc. (Hons.), NUS]

A THESIS SUBMITTED

FOR THE DEGREE OF MASTER OF SCIENCE IN

INFECTIOUS DISEASES, VACCINOLOGY AND

DRUG DISCOVERY

DEPARTMENT OF MICROBIOLOGY

NATIONAL UNIVERSITY OF SINGAPORE

2009

MATERIALS FROM THIS STUDY HAVE BEEN PRESENTED AT THE FOLLOWING CONFERENCE

JX Pang and ML Ng. (2008). *FRMD4A*, a FERM domain-containing gene, regulates the permissivity of A172 glioblastoma cells towards West Nile virus infection. *9th Asia Pacific Microscopy Conference (APMC9)*. Jeju, Korea. (Oral presentation) (APMC9 travel scholarship)

ACKNOWLEDGEMENTS

I would like to express my sincere thanks and gratitude to the following people for their contributions during this one year of fruitful research:

Professor Mary Ng– For her supportive supervision and steadfast guidance, and for spending her weekends reviewing this thesis.

Madam Loy Boon Pheng– For her efficient running of the laboratory, and her professionalism in maintaining the logistical and safety issues in the laboratory.

Terence Tan, Bhuvana, Yeo Kim Long, Chong Munkeat, Edwin, Adrian, Melvin, Anthony, Su Min and Li Shan– For their generous advice and support, and also for their Flavivirology spirit and fun in the laboratory.

Mr. Clement Khaw (Nikon Imaging Centre, Biopolis)– For his prompt expert advice on confocal microscopy imaging services.

My wife, Xiaoman, all family members and friends– For their emotional support and encouragements.

TABLE OF CONTENTS

LIST OF TABLES

LIST OF FIGURES

SUMMARY

West Nile virus (WNV) is a mosquito-borne flavivirus. It can cause fatal meningoencephalitis in infected victims especially in elderly and immunocompromised. This re-emerging virus has recently caused large epidemics in the Western Hemisphere. Despite advances in WNV research, the mechanism of its molecular pathogenesis is still not well understood. It has also been shown that different cell types have different permissivity to WNV infection. Differential permissivity could be one of the factors that contribute to different degree of pathogenesis. Hence, by exploring the transcriptome profile of two different cells with differential permissivity, a better understanding of the molecular pathogenesis of WNV could be attained.

The initial studies on different human host cells have found that A172 cells (glioblastoma) were not as permissive as HeLa cells (cervical adenocarcinoma) to WNV (Sarafend) infection. Based on the results of a previous study by Koh and Ng (2005) on the global transcriptome profiles of these two different host cells, differentially expressed *FRMD4A* and *INDO* were selected as the genes of interest. The gene expression profile of *FRMD4A* and *INDO* were further validated by reverse-transcription and real-time polymerase chain reaction (PCR). Silencing of *FRMD4A* and *INDO* in A172 cells showed ten-fold increase and no increase in virus titre, respectively. Hence, *INDO* was dropped out as it showed no anti-viral role and *FRMD4A* was chosen for further research. It was also observed that *FRMD4A* only expressed in A172 cells and not HeLa cells. This showed that *FRMD4A* is an anti-viral host factor that can resist WNV infection, found only in A172 cells.

Based on indirect immunofluorescence confocal microscopy, FRMD4A was observed to interact with the activated $\alpha_v\beta_3$ integrin via the FERM domain at the N-terminal of FRMD4A protein. Activated $\alpha_v\beta_3$ integrin have been shown previously to mediate WNV entry via the activated focal adhesion kinase (FAK) pathway. Through bioinformatics analyses, it was observed that FERM domain of FRMD4A may compete with FAK binding event to the activated $\alpha_v\beta_3$ integrin. As a result, the level of phosphorylation of FAK was affected that might have hindered the entry of WNV. Hence, this study provided insights into how *FRMD4A* regulates the entry of WNV via the activated $\alpha_v\beta_3$ integrin pathway in A172 cells, making them less permissive to WNV infection. The entry event is often a major determinant of virus tropism and pathogenesis (Schneider-Schaulies, 2000). Understanding this early event of virus infection in more details will provide opportunities to develop strategies to reduce the burden of WNV infection.

INTRODUCTION

The completion of the Human Genome Project has revolutionised biomedical sciences gradually towards functional genomics. Functional genomics involve the analyses and understanding of many genes (and proteins) functions and their interactions simultaneously. As a result, an overall biological mechanism of how certain phenotypes arise can be proposed and this can enhance the progress of drug discovery and vaccine developments against the emerging infectious diseases.

Techniques of functional genomics include high-throughput methods for gene expression profiling at the transcript and protein levels, and the application of bioinformatics. DNA microarray and two-dimensional gel electrophoresis are the common methods for gene expression profiling at the transcript and protein level, respectively. Both DNA microarrays and proteomics hold great promise for the study of complex biological systems with applications in molecular medicine (Celis *et al.*, 2000). A vast amount of gene and protein expression data is usually generated and these data may provide information in understanding the regulatory events involved in normal and diseased processes.

Flaviviruses are emerging pathogens of increasingly important public health concern in the world. For some flaviviruses such as West Nile virus (WNV), although much has been learned about their molecular biology, neither effective vaccine nor antiviral therapy is available yet. In order to generate an effective vaccine, the vaccine must be immunogenic enough to generate an effective humoral immune response, producing neutralising antibodies but not too reactogenic that it is harmful to the host. In addition, an effective vaccine has to provide protection against all different

serotypes and strains of the virus. As such, even though the development of safe and effective vaccines remains to be critical for controlling the disease in the long run, alternatively, antiviral therapy is an approach to be developed in parallel as well

Since WNV alternates between insect vectors and vertebrates in nature, any cellular proteins that this virus uses during replication would be expected to be evolutionarily conserved. Of particular interest will be the identification of cell protein(s) used for virus attachment and entry, and elucidation of molecular mechanisms involved in virus replication. Viruses use cell proteins during many stages of their replication cycles, including attachment, entry, translation, transcription/replication, and assembly. Viruses also interact with cell proteins to alter the intracellular environment or cell architecture so that it is more favourable for virus replication. The replication can also inactivate intracellular defence mechanisms, such as apoptosis and interferon pathways. Mutations in cell proteins involved can cause disruptions of these critical virus-host interactions. These virus-host interactions may thus represent novel targets for the development of new anti-viral agents.

A DNA microarray genomic study was carried out previously by Koh and Ng (2005) to elucidate host factors involved in the different permissiveness of HeLa and A172 cell lines to WNV (Sarafend) infection. Based on the findings, an attempt was therefore made to further investigate whether any of these differentially expressed host factors play a role in anti-viral mechanism in A172 cells as it may be one the factors that caused brain inflammation. This host factor may also represent novel target for the development of new anti-viral agents.

CHAPTER 1

LITERATURE REVIEW

1.1. History of West Nile Virus

West Nile virus (WNV) was first isolated in 1937 from the blood of a febrile adult woman participating in a malaria study in the West Nile region of Uganda (Smithburn *et al.*, 1940). Before the fall of 1999, WNV was considered to be relatively unimportant as a human and animal pathogen and it was classified under the genus *Flavivirus* under the family *Flaviviridae* by a cross-neutralisation test (Calisher *et al.*, 1989). It is a member of the Japanese encephalitis virus serogroup of flaviviruses, which includes a number of closely related viruses that also cause human disease, including *Japanese encephalitis virus* (JEV) in Asia, *St. Louis encephalitis virus* (SLEV) in the Americas, and *Murray Valley encephalitis virus* (MVEV) in Australia (Mackenzie *et al.*, 2002; Gubler *et al.*, 2007). These viruses have a similar transmission cycle, with broad vector range such as *Culex* species mosquitoes serving as the enzootic and/ or epizootic vectors and broad vertebrate host range such as birds serving as the natural vertebrate host, humans and domestic animals, such as horses, are generally thought to be incidental hosts.

1.2. Epidemiology of West Nile Virus Infection

From 1937 to 1999, epidemic of infection only occurred occasionally (Romania and Morocco in 1996; Tunisia in 1997; Italy in 1998; Figure 1-1) and infection of human, birds and horses were generally asymptomatic or mild. In

addition, neurologic disease and death were very uncommon (Murgue *et al.,* 2001; Murgue *et al.,* 2002; Hurlburt *et al.,* 1956).

Figure 1-1. Epidemics caused by West Nile virus, 1937–2006. The red stars indicate epidemics that have occurred since 1994 that have been associated with severe and fatal neurologic disease in humans, birds, and/or equines (adapted from Gubler DJ, 2007).

In 1999, an epidemic of WNV infection occurred in some parts of United States such as New York, Connecticut, and New Jersey (Hayes *et al.*, 2006) and the severity of the disease was seen to increase amongst those who developed clinical symptoms (Petersen and Roehrig, 2001). This WNV outbreak was suggested to be due to the introduction of WNV in spring or early summer of 1999 by an infected human arriving from Israel, which was also facing WNV epidemic in Tel Aviv at that time (Giladi *et al.*, 2001). In addition, it was found that the epidemic was due to the emergence of a new variant of WNV designated "Isr98/NY99" (Lanciotti *et al.*, 2002). This strain is characterized by a high avian death rate and an apparent increase in human disease severity as it moved westward of United States (Solomon and Winter, 2004). This was consistent with the hypothesis that there were some changes in the neurovirulent properties of the virus (Ceccaldi *et al.*, 2004).

From 1999, there were increasing number of cases with neuroinvasive disease and death (Gubler, 2007). This is likely due to the increasing numbers of migratory birds that fly south to Central and South America in the fall and back north to the United States and Canada along specific flyways in the spring (Gubler, 2007). These migratory birds presented an increased risk of spreading WNV, resulting in the increasing number of cases. West Nile virus infection was observed via several novel modalities of transmission to humans besides advances in transportation and globalisation. These include transplacental transmission to the foetus, transmission via breast milk, blood transfusion, or laboratory contamination through percutaneous inoculation (Peterson and Roehrig, 2001; Hayes and O'Leary, 2004).

Wild bird species develop high levels of viremia after WNV infection and are able to sustain viremic levels of WNV of at least 10^5 PFU/ml of serum (the minimum level estimated to be required to infect a feeding mosquito) for days to weeks. They are the main reservoir hosts in endemic regions for the virus, which can initiate epizootics outside the endemic areas (Bernard *et al.*, 2001; Petersen and Roehrig, 2001).

West Nile virus has been isolated from *Culex, Aedes, Anopheles, Minomyia, and Mansonia* mosquitoes in Africa, Asia, and the United States, but *Culex* species are the most susceptible to WNV infection (Burke and Monath, 2001; Ilkal *et al.*, 1997). *Culex* mosquitoes feed on infected wild bird species. This increases the possibility of vertical transmission from mosquito to eggs since infected wild birds can have high levels of viremia (Turell *et al.*, 2000). Natural vertical transmission of WNV in *Culex* mosquitoes in Africa has been reported and is expected to enhance

virus maintenance in nature (Miller *et al.*, 2000). Humans and horses are incidental hosts with low viremic levels and it is still unknown what roles they play in the transmission cycle of WNV (Gubler, 2007).

The existing WNV isolates are grouped into two genetic Lineages (1 and 2) on the basis of signature amino acid substitutions or deletions in their envelope proteins (Berthet *et al.*, 1997). Due to antigenic cross-reactivity between different flaviviruses, techniques such as *in situ* hybridization and sequence analyses of real-time polymerase chain reaction (PCR) products are required to unequivocally identify WNV as the causative agent in infections (Briese *et al.*, 2002; Lanciotti *et al.*, 2002). All members belong to the same clade share more than or equal to 98% homology with each other (Figure 1-2), thus suggesting that they all had a common ancestor. All WNV isolates that are associated with human diseases are found in Lineage 1, while Lineage 2 viruses are mainly restricted to endemic enzootic infection in Africa (Jia *et al.*, 1999; Lanciotti *et al.*, 2002).

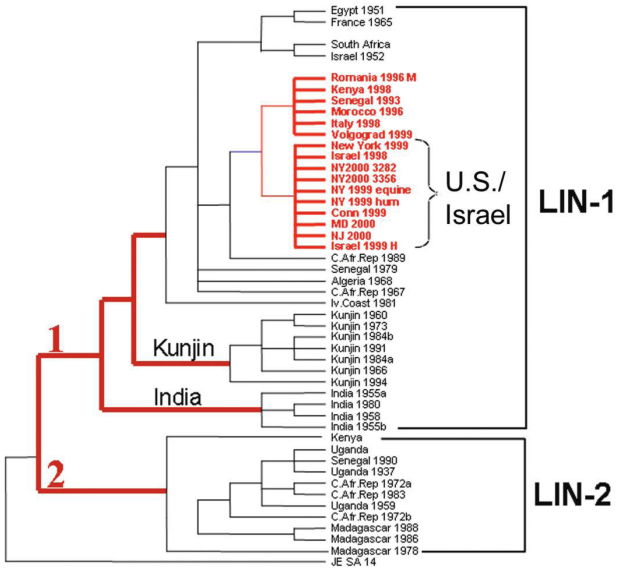

Figure 1-2 Phylogenetic tree of West Nile viruses based on sequence of the envelope gene. Viruses were isolated during the epidemics indicated by red stars in Figure 1-1, all of which belong to the same clade, suggesting a common origin. Figure appears courtesy of the Centers for Disease Control and Prevention (adapted from Gubler DJ, 2007)

1.3. Clinical Manifestations of West Nile Virus Infection

According to the Centre for Disease Control and Prevention (CDC), WNV infections may be asymptomatic or may result in illnesses of variable severity sometimes associated with central nervous system (CNS) involvement. West Nile Fever (WNF) is the most common symptom observed in humans. The course of the fever is sometimes biphasic, and a rash on the chest, back, and upper extremities often develops during or just after the fever (Burke and Monath, 2001). When the CNS is affected, clinical syndromes ranging from febrile headache to aseptic meningitis to encephalitis may occur (Omalu *et al.*, 2003, Briese *et al.*, 2000), and these are usually indistinguishable from similar syndromes caused by other arboviruses, and hence, may lead to misdiagnosis. The brainstem, particularly the medulla, is the primary central nervous system (CNS) target. Humans aged 60 and older have an increased risk of developing this fatal disease (Sampson *et al.*, 2000; Chowers *et al.*, 2001). WNV meningitis is characterized by fever, headache, stiff neck, and pleocytosis. WNV encephalitis is characterized by fever, headache, and altered mental status ranging from confusion to coma with or without additional signs of brain dysfunction (e.g., paresis or paralysis, cranial nerve palsies, sensory deficits, abnormal reflexes, generalized convulsions, and abnormal movements). Flacid paralysis and muscle weakness, similar to polio-like syndrome, have also been reported in the absence of fever or meningo-encephalitis (Li *et al.*, 2003; Arturo *et al.*, 2003).

Histopathological studies revealed that, WNV could be detected but in different viral titres in all major organs such as liver, kidney, heart and spleen, and in most part of the brain (88%), including glial cells and neurons (Steele *et al.*, 2000). Neuropathogenicity was also observed in infected animals whereby it is similar to

poliomyeloencephalitis. It was characterized by T-lymphocytes and, to a lesser extent, macrophage infiltration within the CNS, with multifocal glial nodules and some nueronophagia (Cantile *et al.*, 2001). As high levels of WNV-reactive serum IgM antibodies could still be detected in confirmed human cases (Roehrig *et al.*, 2003) and in animal studies (Xiao *et al.*, 2001) of WNV encephalitis as long as 1.5 years after onset, there is a possibility of viral persistence within the CNS.

1.4. Virus Morphology

West Nile virus belongs to the family *Flavivirdae*. The virions are small (~50nm in diameter), spherical, enveloped, and have a buoyant density of ~1.2g/cm^3. The WNV genome is a single-stranded RNA of positive polarity (mRNA sense) and is 11,029 bases in length, containing a single open reading frame (ORF) of 10,301 bases. The virus contain three structural proteins which include the majority of flavivirus antigenic and functional determinants (Heinz and Roehrig, 1990): a nucleocapsid protein (C protein, 14kDa), a lipid membrane protein (M protein, 8kDa), and a large envelope glycoprotein (E protein, 55kDa). Figure 1-3 shows the structure of the virus particle and Figure 1-4 shows the structural arrangement of the envelope proteins. The E glycoprotein is the principal stimulus for the development of neutralizing antibodies and it contains a fusion peptide responsible for inserting the virus into the host cell membrane. Generally, the E proteins of most flaviviruses are glycosylated, and the glycosylation of certain amino acid residues have been postulated to contribute to the pathogenicity of the virus (Beasley *et al.*, 2004). Hence, varying N-glycosylation sites could also be important in epitope definition (Seligman and Bucher, 2003).

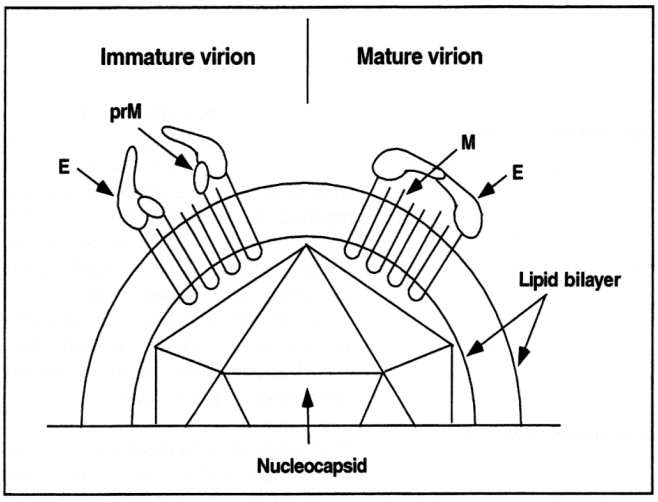

Figure 1-3. The immature and mature flavivirus virions. The heterodimers of prM and E are shown on the left (immature virion) and the homodimers of E, following cleavage of prM, on the right (mature virion). The icosahedral nucleocapsid consists of viral C protein and genomic RNA, and is surrounded by a lipid bilayer in which the viral E and prM/M proteins are embedded. Viral maturation is triggered by the cleavage of prM to pr and M proteins by the host protease furin (adapted from Shi, 2002).

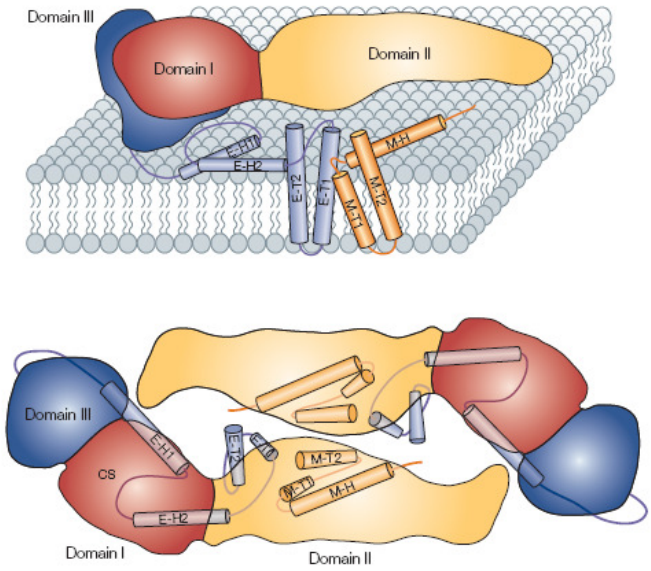

Figure 1-4. Structural arrangement of flavivirus envelope protein. Diagrams of the flavivirus ectodomain and transmembrane domain proteins side and top views. The stem and transmembrane helices of the E (E-H1, E-H2, E-T1 and E-T2) and M (M-H, M-T1 and M-T2) proteins are shown in blue and orange, respectively. The conserved amino acid sequence of the region between the two E protein stem helices is marked CS (adapted from Mukhopadhyay *et al.*, 2005).

1.5. Virus Entry, Assembly and Maturation

WNV replicates in a wide variety of cell cultures, including primary chicken, duck and mouse embryo cells and continuous cell lines from monkeys, humans, pigs, rodents, amphibians, and insects, but does not cause obvious cytopathology in many cell lines (Brinton, 1986). It was demonstrated that although embryonic stem (ES) cells were relatively resistant to WNV infection before differentiation, they became permissive to WNV infection once differentiated, and die by the process of apoptosis (Shrestha *et al.*, 2003). Since flaviviruses are transmitted between insect and

vertebrate hosts during their natural transmission cycle, it is likely that the cell receptor(s) they utilize to gain entry into the cells is a highly conserved protein (Brinton, 2002). The receptor for WNV (Sarafend) was found to be a 105-kDa protease-sensitive, N-linked glycoprotein in Vero and murine neuroblastoma 2A cells (Chu and Ng, 2003a). Subsequently, it was determined to be the $\alpha_V\beta_3$-integrin receptor (Chu and Ng, 2004b). Alternatively, WNV entry can be independent of $\alpha_V\beta_3$-integrin receptor. The virus was shown to enter via cholesterol-rich membrane microdomain (Medigeshi *et al.,* 2008)

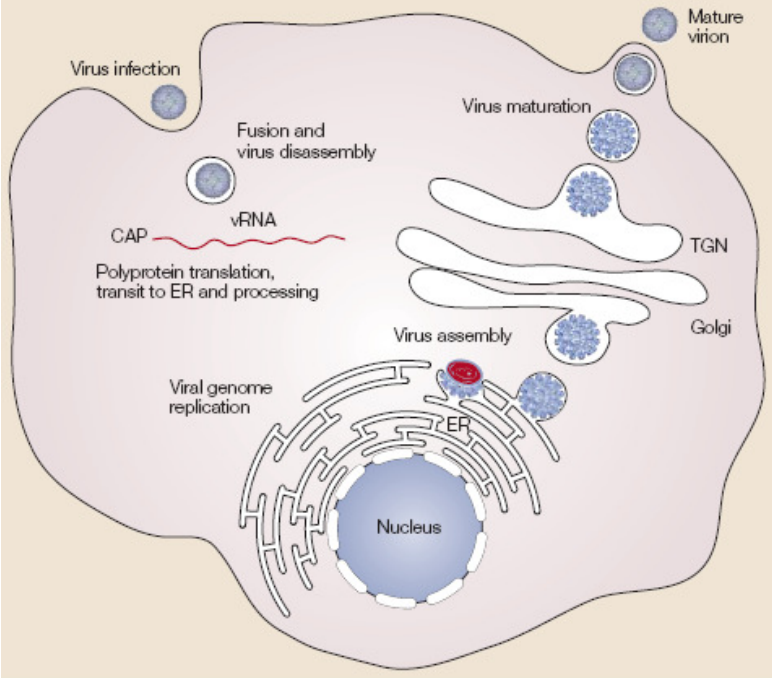

Figure 1-5. The Flavivirus replication cycle. Virions attach to the surface of a host cell and subsequently enter the cell by receptor-mediated endocytosis (see Figure). Several primary receptors and low-affinity co-receptors for flaviviruses have been identified. Acidification of the endosomal vesicle triggers conformational changes in the virion, resulting in fusion of the viral and lysosomal membranes, and particle disassembly. Once the genome is released into the cytoplasm, the positive-sense RNA is translated into a single polyprotein that is processed co- and post-translationally by viral and host proteases. Genome replication occurs on intracellular membranes. Virus assembly occurs on the surface of the endoplasmic reticulum (ER) when the structural proteins and newly synthesized RNA buds into the lumen of the ER. The resultant non-infectious, immature viral and subviral particles are transported through the trans-Golgi network (TGN). The immature virion particles are cleaved by the host protease furin, resulting in mature, infectious particles. Subviral particles are also cleaved by furin. Mature virions and subviral particles are subsequently released by exocytosis (adapted from Mukhopadhyay *et al.*, 2005).

The pathway for flavivirus entry into host cells is through clathrin-mediated endocytosis, which is triggered by an internalization signal (di-leucine or YXXΦ) in the cytoplasmic tail of the receptor (Chu and Ng, 2004a). Clathrin is assembled on the inside face of the plasma membrane to form an electron dense coat known as clathrin-coated pit. Clathrin interacts with a number of accessory protein molecules (Eps15, ampiphysin and AP2 adapter protein) as well as the dynamin GTPase which is responsible for releasing the internalized vesicle from the plasma membrane (Marsh and McMahon, 1999).

This is followed by low-pH fusion of the viral membrane with the lysosomal vesicle membrane, releasing the nucleocapsid into the cytoplasm [(Heinz and Allison, 2000) (Figure 1-5 and 1-6)]. The reduced pH causes the conformational rearrangement of the E proteins, allowing the interactions of the virus E proteins with the lysosomal membrane to form hemifusion pores for the release of viral nucleocapsids into the cytoplasm for uncoating and replication (Modis *et al.*, 2004).

The RNA genome is released and translated into a single polyprotein (Figure 1-5). The viral serine protease, NS2B-NS3, and several cell proteases then cleave the polyprotein at multiple sites to generate the mature viral proteins (Figure 1-5). The viral RNA-dependent RNA polymerase (RdRp), NS5, in conjunction with other viral nonstructural proteins and possibly cell proteins, copies complementary minus strands from the genomic RNA template, and these minus-strand RNAs in turn serve as templates for the synthesis of new genomic RNAs. Upon WNV infection, extensive reorganization and proliferation of both smooth and rough endoplasmic reticula were observed (Ko *et al.*, 1979; Murphy, 1980; Westaway and Ng, 1980; Lindenbach and

Rice, 1999). There were also induction of unique sets of membranous structures, but their functions during infection mostly remained elusive (Westaway *et al.*, 2002). One of such generic flavivirus-induced features, in both vertebrate and invertebrate cells, is the formation of vesicles packets that contains bi-layered membrane vesicles of 50-100 nm in size. These vesicles enclosed distinctively single or double-stranded 'thread-like' structures during early stages of infection (Ng, 1987).

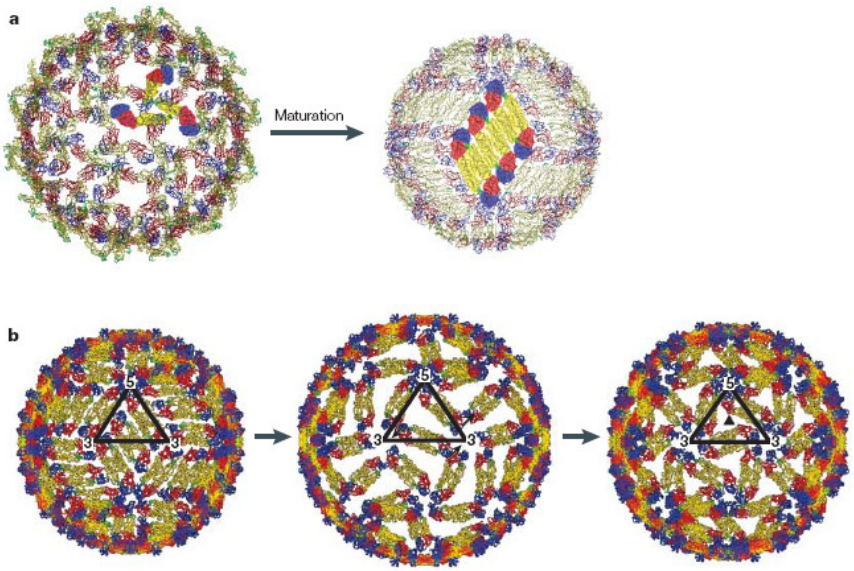

Figure 1-6 Proposed rearrangement of the E proteins during maturation and fusion. a The E proteins in the immature virus (left) rearrange to form the mature virus particle (right). **b** The E protein dimers in the mature virus (left) are shown undergoing a rearrangement to form the putative *T*=3 fusogenic intermediate structure (right) with a possible intermediate (centre). The arrows indicate the direction of the E rotation. The solid triangle indicates the position of a quasi three-fold axis. This suggested rearrangement would require a ~10% radial expansion of the particle between the intermediate (centre) and fusogenic form (right) (adapted from Mukhopadhyay *et al.*, 2005).

Flavivirus assembly occurs in association with the ER membranes (Figure 1-5). Intracellular immature virions, which contain heterodimers of E and prM proteins, accumulate in vesicles and are then transported through the host secretory pathway (Heinz *et al.*, 1994). It has been shown by electron microscopy that mature virions can be found within the lumen of endoplasmic reticulum (Matsumura *et al.*, 1977; Sriurairatna and Bhamarapravati, 1977; Hase *et al.*, 1989; Ng, 1987) at the perinuclear

area of the cytoplasm (Murphy, 1980; Westaway and Ng, 1980). The glycosylated and hydrophilic N-terminal portion of prM protein is cleaved in the *trans*-Golgi network by cellular furin or a related protease (Stadler *et al.*, 1997). The C-terminal portion (M) remains inserted in the envelope protein of the mature virion (Murray *et al.*, 1993). The prM-E proteins interaction may maintain the E protein in a stable, fusion-inactive conformation during the assembly and release of new virions (Heinz and Allison, 2000). Recently, it has been shown that the pr peptide beta-barrel structure of immature virus at neutral pH covers the fusion loop in E protein, preventing fusion with host cell membranes (Li *et al.*, 2008). Virus maturation involves 60 trimers of prM-E proteins heterodimers that project from the virus surface to dissociate and form 90 E protein homodimers, which lie flat on the virus surface. During fusion with host cell, the anti-parallel E protein homodimers dissociate into monomers, which then reassociate into parallel homotrimers (Figure 1-6) (Mukhopadhyay *et al.*, 2005).

Assembly of WN (Sarafend) virus is, however, slightly different from the process shown above, which is generally true for other flaviviruses. With the use of cryo-immunoelectron microscopy, the precursor of nucleocapsid particles from WNV was observed to be closely associated with the envelope proteins at the host cell's plasma membrane (Ng *et al.*, 2001). Instead of maturing within the endoplasmic reticulum, WNV was found to mature (cis-mode) at the plasma membrane (Ng *et al.*, 1994). This contrasts with the trans-mode of maturation observed for most flavivirus where mature virus particles are released from cells by exocytosis (Mason, 1989; Nowak *et al.*, 1989).

Egress of WNV had been observed to occur predominantly at the apical surface of polarized Vero cells, suggesting the involvement of a microtubule-dependent, polarized sorting mechanism for WNV proteins (Chu and Ng, 2002a). Previous study has shown that both E and C proteins were strongly associated and transported along the microtubules to the plasma membrane for assembly (Chu and Ng, 2002b). It was also observed in the same study that the association of E protein and microtubules was sensitive to high salt extraction but resistant to Triton X-100 and octyl glycoside extraction. This suggested that virus E protein and possibly also C protein associate effectively with the microtubules through an ionic interaction (Chu and Ng, 2002b).

1.6. Virus-Host Interactions

Infection and replication of viruses in vertebrate cells resulted in the alteration of expression of many cellular genes and these differentially expressed genes can be identified using a variety of techniques such as high-density DNA microarrays, differential display or subtraction hybridization (Manger and Relman, 2000). Such changes in host gene expression could be a cellular antivirus response, a virus-induced response that is beneficial or even essential for virus survival, or a non-specific response that neither promotes nor prevents virus infection (Saha and Rangarajan, 2003). In addition, some cell types may response differently to WNV infection (Silva *et al.,* 2007) and this make the study of WNV pathogenesis more complicated but still essential so as to develop an effective antiviral strategy.

Infection of diploid vertebrate cells with WNV has been reported to increase cell surface expression of MHC-1, which was activated by NF-κB (Kesson and King,

2001). Activation of NF-κB appeared to be mediated *via* virus-induced phosphorylation of inhibitor κB. Increased MHC-1 expression allowed intracellular virus antigens to be presented, thus increasing the cell's susceptibility to virus-specific cytotoxic T-cell (CTL) lysis (Douglas *et al.*, 1994). This increase might also enhance tissue damage and immunopathology in an infected host (King *et al.*, 1993).

West Nile virus infection was reported to induce expression of non-conserved polymorphic intracellular adhesion molecule-1 [(ICAM-1) (CD54)] and its receptor, the integrin lymphocyte related antigen-1 [(LFA-1)(CD11a/CD18)] in infected cells (Shen *et al.*, 1995). The binding of ICAM-1 to its receptor was found to increase the avidity of cellular conjugation between T cells and their target cells. This facilitated the interaction of antigen-targeted immune cells, and hence contributing to more efficient antiviral responses. WNV-specific, interferon-independent induction of ICAM-1 was observed within 2 h after infection in quiescent but not replicating fibroblasts. The increase in MHC-1 and ICAM-1 expressions were found to be cell-cycle dependent, with up-regulation in G_0 phase compared to G_1 phase (Douglas *et al.*, 1994; Shen *et al.*, 1995). E-selectin (ELAM-1, CD62E), which is a rolling receptor for leukocyte adhesion, was also found to increase maximally 2 h post-infection (p.i.), but declined to baseline levels within 24 h p.i. (Shen *et al.*, 1997). Recently, dendritic cell-specific ICAM-3-grabbing non-integrin (DC-SIGN) was shown to be able to enhance infection of cells by direct interaction with the glycosylated Lineage 1 WNV strains, which partially explained why Lineage 1 strains are more pathogenic than Lineage 2 strains (Martina *et al.*, 2008). In another perspective, this showed that cells with DC-SIGN tend to be more permissive to WNV of Lineage 1 as compared to Lineage 2 strains.

Another common outcome of virus-host interaction is the physiological process of cell death. Apoptosis, which is an active and highly conserved process of cellular self-destruction with distinctive morphological and biochemical features, was observed in WNV-infected K562 and Neuro-2a cells and was shown to be *bax* dependent (Parquet *et al.*, 2001). Apoptosis was also shown to be a major pathway of death in mouse neuronal cells infected with dengue virus (Despres *et al.*, 1996). Virus replication seemed necessary to induce apoptosis since UV-inactivated virus failed to induce apoptosis. Apoptosis of cells might also be triggered by the M ectodomain (proapoptotic sequence) of WNV and this was similarly found in Dengue virus M protein (Catteau *et al.*, 2003).

In addition, the introduction of WNV C protein into the nuclei of host cells inducing apoptosis, further contributed to the pathogenesis of flavivirus infection (Yang *et al.*, 2002). However, others found that neurons of mice infected with *Murray Valley Encephalitis* (MVE) virus did not show evidence of apoptosis, and the severity of the disease might be more linked to neutrophil infiltration and inducible nitric oxide synthetase activity in the CNS (Andrews *et al.*, 1999). Hence, the mechanism of pathogenesis could be virus-specific even though the viruses belong to the same genus. Furthermore, death-associated protein kinase-related apoptosis-inducing kinase-2 (Drak2), a member of the death-associated protein family of serine/threonine kinases, which is specifically expressed in T and B cells (Wang *et al.*, 2008b) and matrix metalloproteinase (MMP) 9 (Wang *et al.,* 2008a) was shown to facilitate WNV entry into brain, resulting in lethal encephalitis.

The role of host genetic factors often has a part to play in the outcome of WNV infection. It was found that WNV replication was less efficient in cells that produce the normal copy of Oas1b as compared to those expressing the inactive mutated form (Lucas *et al.*, 2003). Variations in the response of individuals to flavivirus infection were observed in humans as well as in other host species. In mice, the alleles of a single Mendelian dominant gene, *Flv*, can determine whether an infection is lethal (Brinton, 1986) and segregates as a Mendelian dominant trait (Sangster *et al.*, 1993). The *Flv* resistance allele functions intracellularly to reduce the amount of virus produced, and the lower production of virus resulted in a slower spread of the virus in the host, both of which served to give the host defence systems sufficient time to effectively eliminate the virus.

The host immune response is also critical in determining the outcome of human flavivirus infection. Recently, production of alpha/beta interferon (Samuel and Diamond, 2005) and cell-specific IRF-3 responses (Daffis *et al.*, 2007) were shown to protect against West Nile virus infection. The expression of these IRF-3 target genes and IFN stimulated genes, including several subtypes of alpha interferon involved both RIG-I and MDA5 proteins signaling through IPS-1 (Fredericksen et al., 2008). Both RIG-I and MDA5 are two related pathogen recognition receptors (PRRs), required for sensing various RNA viruses. In addition, early protective alpha interferon response was shown to occur through an IRF-7-dependent transcriptional signal (Daffis *et al.*, 2008).

On the contrary, there are host factors that play a part in sustaining viral replication in infected cells. Interaction between eEf1A and the 3'-terminal stem loop

of WNV (Davis *et al.*, 2007), and interactions of T cell intracellular antigen-1 related protein (TIAR) with viral components (Emmara and Brinton, 2007) was shown to facilitate West Nile virus genome RNA synthesis and inhibited the shutoff of host translation. Lastly, host cell-encoded phosphatase inhibitor, I2PP2A was shown to interact with WNV capsid protein, resulting in an increase in serine/threonine phosphatase PP2A activity, producing more infectious virus (Hunt *et al.*, 2007).

1.7. The FERM Domain Superfamily

Members of the protein 4.1 superfamily such as the closely related proteins ezrin, radixin and moesin (ERM), band 4.1, merlin, talin and protein-tryosine phosphatases (PTPs), are generally associated with the linkage of the cytoskeleton to the plasma membrane. They are involved in signal transduction pathways and played vital roles in maintaining cell integrity, motility and differentiation (Bretscher *et al.*, 2002). Some of these members are also implicated in carcinogenesis such as moesin (Kobayashi *et al.*, 2004), apoptosis and metastasis such as ezrin and merlin (Gautreau *et al.*, 1999; Hunter *et al.* 2004; Bretscher *et al.*, 2002). The 4.1 protein superfamily has a conserved region called the FERM domain which is originally named after the four proteins: Band 4.1 and ERM proteins. The FERM domain is approximately 300 amino acids in length and predominantly located at the N-terminus in the majority of FERM-containing proteins (Chishti *et al.*, 1998). There are three structural lobes within the FERM domain. The N-terminal lobe resembles ubiquitin and the central lobe resembles acyl-CoA binding proteins (Hamada *et al.,* 2000). The C-terminal lobe is structurally similar to the pleckstrin homology (PH) and phosphotyrosine binding (PTB) domains and consequently is capable of binding to both peptides and phospholipids at different sites. For example, the ERM proteins function as molecular

linkers that connect cell-surface transmembrane proteins such as CD44, CD43, ICAM-2 and ICAM-3 to the actin cytoskeleton, in a variety of cell types (Chrishti *et al.,* 1998). In addition, FERM domain of PTPL1 has a crucial role of intracellular targeting and by binding to phosphatidylinositol 4, 5-biphosphate [PtdIns (4, 5) P2], it regulates the localisation of PTPL1 (Bompard *et al.,* 2003). The FERM domain is found in tryosine kinases such as focal adhesion kinase (FAK) and Janus kinase (JAK) (Serrels *et al.,* 2007; Hilkens *et al.,* 2001). FERM domain of FAK regulates actin polymerisation by binding directly to Arp3 (Serrels *et al.,* 2007) and enhances p53 degradation that promotes cell proliferation and survival (Lim *et al.,* 2008). FERM domain of FAK also binds to integrin beta subunit directly upon activation of integrin receptor which leads to autophosphorylation of tyrosine 397 and subsequent downstream signaling processes ("outside-in" signaling) (Parsons, 2003). Recently, FERM domain of PTPN3 was shown to be essential for suppression of Hepatitis B virus gene expression (Hsu *et al.,* 2007).

1.8. Gene Silencing with microRNA

Gene silencing is a general term used to describe the reduction in gene expression level (gene knockdown) by a mechanism other than genetic modification. Gene knockdown is a preferred method than gene knockout for large scale or preliminary study. In order to observe the effect of a specific gene knockdown, antisense technology is used in the post transcriptional gene silencing to suppress the gene. This is also known as RNA interference (RNAi). There are several appropriate tools to induce RNAi, depending on the model system, the length of time you require knockdown and other experimental parameters. The tools are synthetic/ *in vitro* dicing-siRNA (McManus and Sharp, 2002) and RNAi vectors with short hairpin RNA

(shRNA) (Paddison *et al.,* 2002) or microRNA (miRNA) (Yekta *et al.,* 2004). The use of siRNA (diced siRNA or synthetic siRNA) for RNAi analysis in mammalian cells is limited by their transient nature. Hence, it is not effective to observe an accurate account of the effect of gene silencing. In addition, the use of shRNA vectors for RNAi analysis requires the screening of large number of sequences to identify active sequences and the use of Pol III promoters limits applications such as tissue-specific expression. In contrast, the use of miRNA vector for RNAi analysis is ideal as it is engineered with capabilities for tissue-specific expression with the Pol II promoters, and high, constitutive expression of the miRNA to suppress the gene of interest.

MicroRNA expressed from the transfected vector are small ssRNA sequences of ~22 nucleotides in length which naturally direct gene silencing through components shared with the RNAi pathway (Bartel, 2004). Unlike shRNAs, however, the miRNAs are found embedded, sometimes in clusters, in long primary transcripts (pri-miRNAs) of several kilobases in length containing a hairpin structure and driven by RNA Polymerase II (Lee *et al.*, 2004b), the polymerase also responsible for mRNA expression. Drosha, a nuclear RNase III, cleaves the stem-loop structure of the pri-miRNA to generate small hairpin precursor miRNAs (pre-miRNAs) which are ~70 nucleotides in length (Zeng *et al.*, 2005). The pre-miRNAs are exported from the nucleus to the cytoplasm by exportin-5, a nuclear transport receptor (Bohnsack *et al.*, 2004; Yi *et al.*, 2003). Following the nuclear export, the pre-miRNAs are processed by Dicer into a ~22 nucleotides miRNA (mature miRNA) molecule, and incorporated into an miRNA-containing RNA-induced silencing complex (miRISC) (Cullen, 2004).

1.9. Objectives of study

There is a lack of understanding of why and how A172 cells are less permissive to WNV infection. Hence, a DNA microarray genomic study was carried out previously in the laboratory to elucidate host factors involved in the differential permissiveness of HeLa and A172 cell lines to WNV (Sarafend) infection (Koh WL and Ng ML, 2005). Based on the previous findings, the objectives of this study are:

1) To investigate whether these differentially expressed host factors have any role in anti-viral mechanism in A172 cells via microRNA silencing technology. A172 cells were chosen as they resemble microglial cells, in which they are also poorly permissive to the growth of WNV and is thought to influence the neuropathogenesis of WNV infection (Cheeren *et al.,* 2005).

2) To investigate the role of the selected anti-viral host factor which may have contributed to the less permissive A172 cells, using mainly indirect immunofluorescence confocal microscopy.

CHAPTER 2

MATERIALS AND METHODS

2.1. Cell Culture

All solutions and media for cell culture were made with autoclaved reagent water of type one grade (E-pure, Barnstead, USA) and chemicals of ultra-pure grade. The following measures were taken to prevent contamination of the media and the cell cultures: Glass bottles (Schott, Germany) with screw-capped lids and non-toxic plastic blue washer were used for storage of the media. In addition, parafilm was used to seal around the cap and the neck of the bottle after tightening the cap. All cell culture and media preparations were done under aseptic conditions in a class two type A2 biohazard safety cabinet (Gelman Sciences, Australia & ESCO, USA). Cells used in this study were grown and maintained in sterile 75 cm^2 plastic tissue culture flasks with double seal cap and canted neck (IWAKI, Japan).

2.1.1. Cell Lines

Four different types of cell lines were used in this study. Of which, two were human cell lines. They were HeLa cells, a cervical adenocarcinoma cell line (ATCC, CCL-2) and A172 cells, a neuroblastoma cell line. HeLa cell line was originally derived from a 31 years old Negroid woman (Master, 2002). A172 cell line was originally derived from the glioblastoma brain tumour cells of a 53 year old male (Giard *et al.*, 1973). The passage number of HeLa cells and A172 cell lines used was between 80 and 100. In addition, C6/36 mosquito cell line was used for propagation of the WNV whereas Syrian golden baby hamster kidney (BHK)-21 cell line was

mainly used for plaque assay. The passage number of both cell lines used was between 50 and 80.

2.1.2. Media for Cell Culture

Dulbecco's Modified Eagle's media [(DMEM) (Sigma, USA – Appendix 1a)] was used as the growth medium to culture both HeLa and A172 cells. RPMI-1640 (Sigma, USA – Appendix 1b) was used to culture BHK cells and L15 (Sigma, USA – Appendix 1c) growth medium was used to culture C6/36 cells. DMEM, RPMI and L15 maintenance media (Appendix 1d) were used to culture virus-infected HeLa, A172, BHK and C6/36 cells respectively. The media were prepared according to manufacturer's specifications and these were further supplemented with 10 % fetal calf serum (FCS) for growth medium and 2 % FCS for maintenance medium. Sodium bicarbonate was added as a buffering agent, and the pH of the media was adjusted to 7.2.

2.1.3. Regeneration, Cultivation and Propagation of Cell Lines

Cells in cryo-vials were stored in liquid nitrogen. To revive the cells, each vial of the desired cell line was retrieved from liquid nitrogen storage and immediately thawed in a 37 °C water bath. When thawed, the cells were transferred into a 75 cm^2 culture flask and 15 ml of growth medium was added. The growth medium was needed to dilute the toxic effects of dimethysulphoxide (DMSO), which was present in the preserving medium. The cells in the flasks were then incubated at 37 °C with 5 % CO_2. The growth medium was decanted after 12 h and replaced with fresh medium, after which the cells were allowed to grow to confluence for about 3-4 days.

When the cells were confluent, the medium was discarded and the cell monolayer was rinsed once with 10 ml 1 X PBS (Appendix 2a). This was followed by the addition of two ml trypsin-versene solution (Appendix 2b) and incubated at 37 °C for about two min. Cells were then observed under microscope to ensure that they have detached. The flask was tapped gently to dislodge the cell monolayer. Two ml of growth medium was immediately added to inactivate the enzymatic effect of the trypsin-versene solution. The cell aggregates were resuspended by pipetting up and down gently for a few times. The suspension of cells was split into a seeding ratio of 1:4 for experiments and a seeding ratio of 1:8 for maintaining the cell lines, into 75 cm^2 culture flasks, and topped up to 10 ml with growth medium. The cells were cultivated at 37 °C, in a humidified 5 % CO_2 incubator (Lunaire, USA). The monolayer reached confluency in about three days and six days for seeding ratio of 1:4 and 1:8, respectively. The media were changed after every three days till the cells were confluent to sub-culture.

Cell cultivation in a 24-well tissue culture tray required cells from a 100 % confluent cell monolayer in a 75 cm^2 flask. The monolayer was split into a seeding ratio of 1:4 as describe above. Hence, one out of four ml of the cell suspension was further resuspended with 11 ml of medium before dispensing 0.5 ml into each well. The trays were then left at 37 °C in the 5 % CO_2 incubator (Lunaire, USA) until they were confluent unless describe otherwise .

2.2. Infection of Cells

2.2.1. Virus Strains

The virus used in this study was West Nile (Sarafend) virus [WN(S)V] – a gift from Emeritus Professor Westaway, Sir Albert Sakzewski Virus Research Laboratory, Queensland, Australia. It is used as a laboratory prototype for WNV. The virus was propagated in C6/36 cells throughout the study, and introduced into the human cell lines (HeLa cells and A172 cells) for infection studies. The virus was not 'adapted' to the human cell lines prior to infection, so as to ensure that a basal level of comparison can be obtained by using the same virus stock. This was also to prevent any form of attenuation to the virus when grown in the human cells (Dunster *et al.*, 1990).

2.2.2. Infection of Cell Monolayer and Production of Virus Pool

A confluent cell monolayer of about 3 days old in either a 75 cm^2 culture flask or 24-well tissue culture tray was used for infection. The growth medium was discarded and the monolayer was washed with three ml or one ml of Hanks medium (Sigma, USA – Appendix 3a) for a 75 cm^2 culture flask and a 24-well tissue culture tray, respectively. A volume of one ml or 0.1 ml of virus suspension with multiplicity of infection (MOI) of 10 was inoculated onto the cell monolayer of a 75 cm^2 culture flask and a 24-well tissue culture tray respectively. The flask was incubated at 37 °C for 1 h and rocked every 15 min to ensure even infection of the cell monolayer. After 1 h of virus adsorption, virus suspension was removed and washed as described above with Hanks medium before adding 10 ml or 1 ml of maintenance medium to a 75 cm^2 culture flask and a 24-well tissue culture tray, respectively. The infected cells were then incubated at 37 °C for 24 h. Mock-infected controls on HeLa cells and A172

cells were also prepared as describe above with 1 ml of Hanks medium instead of virus suspension.

At the end of the incubation period, the maintenance medium containing extracellular virus particles was then harvested. The supernatant was first spun on a bench top centrifuge (Sigma Model 3K15, USA) at 1,000 rpm for 10 min at 4 °C to remove cell debris. One ml of this supernatant was aliquoted into sterile cryo-vials, sealed and frozen immediately in cold ethanol (-80 °C). The vials were subsequently stored at -80 °C. To assay viral growth kinetics, confluent cultures in 25 cm^2 flasks were infected at the desired MOI. Cells from a replicate flask were counted prior to infection to accurately calculate the amount of virus needed. Virus was adsorbed for 1 h at room temperature with rocking at every 15 min, and the monolayers were rinsed four times to remove unbound virus before replacing 5 ml of DMEM containing 5 % FCS. Samples (0.5 ml) of culture fluid were removed at various times after infection and stored at −80 °C. Fresh medium (0.5 ml) was replaced at each time point. Virus titres were determined by plaque assay on BHK cells. The virus titres at each time point are the averages of the results of triplicate titrations from one experiment. In total, three separate experiments were carried out.

2.2.3. Plaque Assay

Virus stock was diluted in ten-fold serial dilutions with virus diluent from 10^{-1} to 10^{-8} dilutions. Aliquots containing 0.1 ml of the appropriate dilutions were inoculated onto a day-old confluent BHK cell monolayer (~ 10^5 cells) grown in a 24-well culture plate (Nunc, Denmark). The virus was allowed to adsorb to the cells at 37 °C for 1 h, with gentle rocking at 15 min intervals. Following that, excess inoculate

were removed and the wells were washed gently with virus diluent. One ml of overlay media (Appendix 3b) was added to each well. The plate was placed in a humidified 37 °C, 5 % CO_2 incubator (Lunaire, USA). After about two days of incubation, the overlay media was decanted and then stained with 1 % crystal violet solution (Appendix 3c) overnight at room temperature on a shaker. Thereafter, the plate was rinsed twice with water and dried in an oven. The number of plaques obtained was then counted.

The virus was plaqued on BHK cells, even though they had been passaged in HeLa and A172 cells, so that a basal level of comparison can be obtained. It had also been reported that HeLa cell plaque assays were unreliable (Dunster *et al.*, 1990).

2.3. Microscopy

2.3.1. Light Microscopy

When the monolayers reached 70 % confluency, the cells were infected with WN(S) virus. The flasks were incubated for 24 h until cytopathic effects (CPE) was observed. The flasks were then visualised under an optical microscope (IX81, Olympus, Japan) that was linked to a digital camera.

2.3.2. Indirect Immunofluorescence Microscopy

Cells were grown on coverslips for immunofluorescence microscopy. Glass coverslips of diameter 13 mm (ARH, UK) were washed with 90 % ethanol for 30 min and then boiled in double-distilled water for about 10 min. The coverslips were then left to air dry. Dry sterilization was done in a hot air oven at 160 °C (Jouan, USA) for

2 h. The individual coverslips were subsequently placed aseptically into a 24-well tissue culture tray (Nunc, Denmark). When the monolayers reached confluency of about 70 %, the cells were infected with WN(S)V as before. Mock-infected cells using virus diluent was used as controls. The plate was incubated at appropriate time points until it is ready for immunofluorescence microscopy studies.

The antisera used and their sources are described as below:

Table 2-1: Antibodies and their working dilution used in IFA.

Type of antibody	Name	Dilution
Primary antibodies	Rabbit polyclonal anti- WNV Envelope protein antibody (Millipore, USA)	1:500
	Mouse anti-$\alpha_v\beta_3$ integrins antibody (Chemicon)	1:500
Secondary antibodies	Alexa Fluor 488 Goat anti-mouse IgM (μ chain) (Invitrogen, USA)	1:500
	Alexa Fluor 594 Goat anti-mouse IgM (μ chain) (Invitrogen, USA)	1:500
	Alexa Fluor 594 Goat anti-rabbit IgM (μ chain) (Invitrogen, USA)	1:500

The infected and control cells were washed twice with cold 1 X PBS and then fixed with cold formaldehyde (Merck, Germany) for 10 min at room temperature and followed by Triton-X for 10 min at room temperature. This was followed by a wash in cold PBS for 15 min. The cells were then blocked with cold 0.1 % BSA (Appendix 4a) in PBS for 1 h to prevent non-specific attachment of antibodies.

Primary antibodies were diluted as detailed above in Table 1. Twenty µl of the diluted antibodies was spotted on parafilm. Coverslips seeded with cells were then inverted over the drop of antibody and incubated at 37 °C for 1 h in a humid chamber. After incubation, the excess antibodies were washed off thrice after incubating with PBS for 5 min each at room temperature. Species-specific secondary antibodies were appropriately diluted in PBS as detailed in Table 1. Coverslips were similarly treated with the secondary antibodies as described above. After incubation, the coverslips were washed three times with cold PBS for 5 min each. Following all these secondary labelling, twenty µl of DAPI (1: 20 dilution) was similarly treated to the cells to stain the nucleus at 37 °C for 15 min in a humid chamber. In addition, phallodin (Invitrogen, USA) is used at 1: 5000 dilution to stain actin filaments in the cells where appropriate.

A single drop of prolong ProLong® Gold Antifade Reagent (Invitrogen, USA) was placed on ethanol-cleaned glass slides and the coverslips were inverted over the ProLong reagent. Excess ProLong was blotted with a cleaning tissue, Kimwipe (Kimberly Clark, Canada). Fluorescence was visualised under optical immunofluorescence microscopy (IX81, Olympus, Japan) and Laser Scanning Spectral Confocal microscopy (A1R, Nikon, Japan) using oil immersion objectives. Where relevant, quantification of the fluorescent intensity was performed using the MetaMorph software (Universal Imaging Corporation, USA).

2.4. Molecular Biology techniques

2.4.1. Total RNA Isolation from Cell Culture

RNA is prone to disintegration from ubiquitous ribonucleases (RNase), therefore it is important to stabilize RNA and adopt proper RNA handling techniques. A cell monolayer was washed once with PBS to remove excess media. Total RNA isolation was carried out using QIAGEN RNeasy Mini Kit (QIAGEN GmbH, Germany) according to the manufacturer's recommended protocol. Briefly, a volume of 350 µl Lysis buffer was added immediately to the cells (5 x 10^6). This captures relevant RNA in cells by preventing unwanted changes in the gene-expression patterns due to RNA degradation or changes in the environment. After the lysis of cells to release RNA, homogenization of the sample was performed to reduce the viscosity of the cell lysates by shearing the high-molecular weight genomic DNA and other high-molecular weight cellular components to create a homogeneous lysate. Homogenization would disrupt the cells and thus increase the yield of RNA and this was carried out by transferring the lysates directly into a QIAshredder spin column (QIAGEN GmbH, Germany) and centrifuged at 13 000 X *g* for 2 min. Subsequently, 350 µl of 70 % ethanol was added and mixed well before transferring into a RNeasy spin column and centrifuged at 12 000 X *g* for 30 s. The flow through was then discarded and 700 µl of Buffer RW1 was added to the spin column, and centrifuged at 12 000 X *g* for 30 s. This was followed by washing with 500 µl of Buffer RPE twice, with centrifugation at 12 000 X *g* for 30 s after the first wash and 2 min after the second wash. RNA was eluted out in 30 µl of RNase-free water and stored at -20 °C for later use.

2.4.2. Small scale purification and screening of plasmid DNA

Small scale plasmid DNA preparation using alkaline lysis method was adopted. Single bacterial colony was picked and inoculated in 2 ml of LB medium (Appendix 5a) containing either 100 µg/ml of ampicillin or blasticidin (Invitrogen, USA). The culture was incubated at 37 °C with vigorous shaking for 16 h. The overnight culture was placed into a 2 ml tube and centrifuged at 12,000 X *g* for 5 min, followed by purification. Plasmid DNA was purified with PureLink Quick Plasmid Miniprep Kit (Invitrogen, USA). The medium was completely removed after centrifugation before the cells were resuspended in 250 µl Resuspension Buffer (R3) with RNase A. Then 250 µl of Lysis Buffer (L7) was added and mixed by inverting the tube. Next, 350 µl of Precipitation Buffer (N4) were added. The tube was centrifuged at 12,000 X *g* for 10 min to remove cell debris. The supernatant was applied to a silica-based spin column, followed by centrifugation at 12,000 X *g* for 1 min. The column was washed with 500 µl of Wash Buffer (W10) and subsequently with 700 µl of Wash Buffer (W9). The column was spun for another minute to remove residual buffer before 30 µl preheated (65 °C) TE Buffer was added to the center of the column. The column was incubated for 1 min at room temperature followed by centrifugation at 12,000 X *g* for 2 min. The DNA plasmid was stored at -20 °C for later use and aliquots for immediate use were stored at 4 °C.

2.4.3. RNA and DNA plasmid Quantification and Quality Determination

RNA and DNA concentration were determined by measuring the absorbance at 260 nm (A_{260}). An absorbance of 1 unit at 260 nm corresponds to either 40 µg of RNA or 50 µg of DNA per ml of sample. Nanodrop 1000 (Thermo Scientific, USA) was used to measure the quantity and quality with 2 µl of sample. The purity of RNA

was determined by taking the ratio of the readings at 260 nm and 280 nm (A_{260}/A_{280}). Pure RNA should have a A_{260}/A_{280} ratio of greater than 2 units and pure DNA should have a A_{260}/A_{280} ratio of greater than 1.80 units.

2.4.4. Determination of RNA and DNA plasmid Integrity

The integrity and size distribution of total RNA extracted was assessed by denaturing formaldehyde-agarose (FA) gel (Appendix 5e) electrophoresis. The respective ribosomal bands (1.9 kb and 5.0 kb for 18S and 28S rRNA, respectively) should appear as sharp bands on stained gels. Degraded RNA samples (smearing of the ribosomal bands) should not be used to proceed with downstream applications. Prior to running the gel, equilibrate the gel in 1 X FA gel running buffer (Appendix 5f) for at least 30 min. Two µl of RNA sample was mixed with 8 µl of RNA loading buffer (Appendix 5g) and mixed. Ten µl of each mixture was incubated for 5 min at 65 °C, and then chilled on ice. The equilibrated FA gel was electrophoreses at 100 V for 1.5 h. The gel was then incubated in 0.01% ethidium bromide containing TAE buffer for 30 min to stain the RNA for visualisation under the UV.

DNA plasmid was checked for contaminating genomic DNA and RNA by running agarose gel electrophoresis with 1 % TAE gel with TAE running buffer (Appendix 5h) at 150 V for 0.5 h. The gel was subsequently visualized under UV and images captured using ChemiGenius^2 (Syngene, UK).

2.4.5. Automatic DNA sequencing

DNA sequencing was carried out on an Applied Biosystems PRISM 3100A genetic analyzer with an ABI PRISM BigDye terminator cycle sequencing ready

reaction kit (Applied Biosystems, USA). Sequencing reaction of 10 µl contained 0.25 µg DNA template, 1.6 pmol primer and 4 µl BigDye terminator reaction mixture. The cycle sequencing was performed on iCycler PCR System (BioRad, USA) with following parameters: 38 cycles of 96 °C for 10 sec, 50 °C for 5 sec and 60 °C for 4 min. The reaction was purified by ethanol precipitation and the sample was resuspended in 6 µl of loading buffer followed by denaturing at 90 °C for 2 min. About 1.5 µl of denatured sample was loaded on 5 % acrylamide sequencing gel (18 g of urea, 5 ml of 50% long ranger acrylamide stock solution, 26 ml of distilled water and 5 ml of 10 X TBE) and was run on the ABI PRISM 377 sequencer for 9 h. The sequences were edited by the manufacturer's software. Sequencing results were checked using BLAST 2 sequences from the BLAST network server of the National Center for Biotechnology Information (NCBI).

2.4.6. Western blot

The WNV-infected cells were harvested from cell culture flask by using trypsin (Appendix 2b) and 5 ml of growth medium to deactivate the trypsin activity. Subsequently, cell suspension is spun at 350 rpm for 5 min at 4 °C. The supernatant was carefully removed without disturbing the cell pellet. The cells were kept at -80 °C if not processed immediately.

For 10^6 cells, 100 ul of cell lysis buffer (Miltenyi Biotec, Germany) was used in total protein extraction. After thorough mixing, the mixture was incubated for 1 h at room temperature. After incubation, it was transferred into 1.5 ml tube and heated for 5 min at 95 °C. Then the tube was spun at 10,000 X *g* for 10 min to remove the insoluble part. The supernatant as total protein extract was transferred to a new tube.

Protein samples were fractioned on SDS-polyacrylamide gel (12 % separating gel: 1.6 ml water, 2.0 ml 30 % acrylamide, 1.3 ml 1.5 M Tris.Cl (pH 8.8), 50 ul 10 % SDS, 50 ul 10% APS, 2 ul TEMED; 5 % stacking gel: 1.36 ml water, 333 ul 30 % acrylamide, 250 ul 1M Tris (pH 6.8), 20 ul 10 % SDS, 20 ul 10% APS, 2 ul TEMED). The samples were treated with equal volume of loading buffer [0.1 M Tris-HCl, pH 6.8, 20 % glycerol (V/V), 4 % SDS (W/V), 5 % ß-mercaptoethanol (V/V), 0.2 % bromophenol blue (W/V)] at 100 ^{o}C for 10 min. The running buffer (pH 8.3) contained the following reagents in one liter: 94 g glysine, 25 ml 10 % SDS and 15.1 g Tris.base. The electrophoretic unit was supplied with 50 V for 30 min, followed by 100 V for 2 h. For transferring proteins to PVDF membrane (Roche Diagnostics GmbH, Germany), the membrane was soaked in methanol and Transfer buffer (10% methanol, 0.01 M Tris.base, 0.096 M glysine) for 10 min, respectively. The Biorad Transblot machine was supplied with 10 V for 2 h. The membrane with proteins was then transferred into blocking buffer [5 % non-fat milk powder in TBST (10 mM Tris.Cl, pH 8.0, 150 mM NaCl, and 0.05 % Tween 20)] and the membrane was kept at 4 °C overnight with gentle shaking.

One ul of primary antibody (mouse anti-P_{Y397} FAK and mouse anti-actin, respectively) was added into 10 ml TBST buffer (1: 10,000 dilution) and the mixture together with membrane was shaken for 1 h at RT. Secondary antibody (goat anti-mouse) (1:10,000 diluted in TBST) was added to the membrane and incubated at RT for 1 h. The membrane was washed with TBST for 10 min for three times before and after adding antibodies.

2.5. Semi-Quantitative Reverse Transcription and Quantitative Real-Time PCR

2.5.1. Synthesis of Oligonucleotides

Appendix 6 lists the oligonucleotides (1st Base, Singapore) that were synthesized and used in this study. Sequences for the primers against target genes were primarily sourced from 'Primer 3'. It was used as a tool to generate optimal primers based on the target gene sequences [(http://fokker.wi.mit.edu/primer3/input.htm) (Rozen and Skaletsky, 2000)].

2.5.2. Semi-Quantitative Reverse Transcription PCR (RT-PCR)

Total cellular RNA was extracted as described previously. An additional DNase treatment step was included to remove all contaminating genomic DNA as qRT-PCR is a very sensitive quantification method. The qRT-PCR was performed in two steps; the first step was reverse transcription to generate first strand cDNA and then followed by real-time PCR. For first strand cDNA synthesis, 5 µg of total RNA was reverse transcribed using 200 units of SuperScript III Reverse transcriptase (Invitrogen, USA) in a total volume of 20 µl containing 500 µM dNTP mix, 5 mM $MgCl_2$, 20 mM DTT, 40U RNaseOUT, primed with 2.5 µM random hexamer. Reverse transcription was performed at 50 °C for 60 min, followed by 85 °C for 5 min, according to the manufacturer's protocol.

With 0.1 ug cDNA, PCR reaction was carried out in a 50 ul reaction mixture (5 ul of 10 X Taq buffer, 5 ul of 2mM dNTP mix, 1 uM of specific primers dimers, 1 ul of Promega Taq polymerase and top up to 50 ul with sterile distilled water) with the

following PCR steps: 1 cycle of 2 mins at 95 °C, 30 cycles of 30 s at 95 °C, 30 s at 55 °C and 20 s at 72 °C, 1 cycle of 8 mins at 72 °C and 1 cycle of 10 °C for infinite time till collection of tubes. PCR products were then run on the agarose gel as described in section 2.4.4. to check on the bands.

2.5.3. Real-Time PCR

For real-time PCR, 25 µl reaction mixture containing 2 µl of diluted cDNA (1: 100 dilution), 12.5 µl of SYBR GreenER™ qPCR SuperMix for ABI PRISM® instrument (Invitrogen, USA) and 0.2 µM of both forward and reverse primers (1St Base, Singapore) (Appendix 6) was used. A negative template control that contained all SYBR green reagents except DNA was performed in parallel. Reactions were cycled at 50 °C for 2 min and then 95 °C for 2 min, followed by 45 cycles of 95 °C for 15 s, 60 °C for 30 s and 72 °C for 30 s, followed by a melting curve analysis. These were performed on ABI PRISM® instrument (ABI, USA). Each gene was quantified 3 times, with a triplicate sample each time. This was to increase the statistical power and to average the readings.

A calibration curve containing 5 points ranging from 100 fg to 1 ng of cDNA was used as a standard. The 18S rRNA gene was used as an internal control for normalization, as it is a putative housekeeping gene. Other common housekeeping genes, such as beta-actin were found to be differentially expressed during virus infection. The threshold cycle (C_T) values were then translated into relative copy numbers of cDNA by using the comparative C_T ($\Delta\Delta C_T$) method of calculation (Livak and Schmittgen, 2001) as follows:

Relative change = $2^{-\Delta\Delta C}{}_T$, where $\Delta\Delta C_T = (C_{T,\,Target} - C_{T,\,18S})_{virus}$

2.6. Gene Silencing with microRNA (miRNA)

2.6.1. Generation of pcDNA ™ 6.2-GW/miR expression clone

The miRNA was generated with BLOCK-iT Pol II miR RNAi Expression Vector Kit (Invitrogen, USA) according to manufacturer's protocols. Briefly, single-stranded DNA oligos (Appendix 6) encoding pre-miRNA of interest are designed with an online tool, BLOCK-iT RNAi Designer [(https://rnaidesigner.invitrogen.com/rnaiexpress/) (Invitrogen, USA)]. The single-stranded oligos are annealed to generate a double-stranded (ds) oligo as follows: a 20 µl reaction mixture (5 µl of 200 µM top strand oligo & bottom strand oligo each, 2 µl of 10 X oligo annealing buffer and 8 µl of DNase/RNase-free water) was heated at 95 °C for 4 min and cooled at room temperature for 10 min. The ds oligo was then diluted to 500 nM with DNase/RNase-free water and further diluted to 10 nM with Oligo Annealing Buffer. The ds oligo was cloned into pcDNA ™ 6.2-GW/miR in the reaction mix [4 µl of 5 X ligation buffer, 2 µl of pcDNA ™ 6.2-GW/miR (5ng/ µl), 4 µl of 10nM ds oligo, 9 µl of DNase/RNase-free water and 1 µl of T4 DNA ligase (1U/ µl)] incubated for 5 min at room temperature. The ligated product was transformed into One Shot TOP10 chemically competent *E.coli* with 2 µl of the ligation reaction mix. The cells and ligation reaction mix were incubated on ice for 30 min before heat-shocking the cells at 42 °C for 30 s without shaking and immediately transferred to ice. Subsequently, 250 µl of room temperature S.O.C. medium was added and incubated at 37 °C for 1 h with shaking. After shaking, 100 µl of bacterial culture was spread on a pre-warmed LB agar plate containing 50 µg/ml of spectinomycin and incubated overnight at 37 °C. A few colonies were selected and cultured overnight in LB containing 50 µg/ml of spectinomycin. The pcDNA ™ 6.2-GW/miR with the ligated ds oligo was isolated as described above, quantitated and sequenced using the

miRNA forward sequencing primer (Appendix 6) to check the integrity of the ds oligo.

2.6.2. Transient silencing of *FRMD4A* & *INDO* in A172 cells

The pcDNA ™ 6.2-GW/miR expression plasmid DNA (0.8ug) was diluted in 50 ul of Opti-MEM® I Medium without serum. In another sterile 5 ml tube, 2 µl of Lipofectamine ™ 2000 (Invitrogen, USA) was diluted in 50 ul of Opti-MEM® I Medium without serum. After 5 min of incubation, the diluted DNA was combined with the diluted Lipofectamine™ 2000, and was further incubated for 20 min at room temperature, forming the DNA- Lipofectamine ™ 2000 complexes. The DNA-Lipofectamine™ 2000 complexes were added into the 24-well plate containing 500 ul of growth medium containing serum with a confluent layer of A172 cells. The plate was incubated overnight at 37 °C in a CO_2 incubator. The media containing the DNA-Lipofectamine ™ 2000 complexes was removed the next day and replaced with complete culture medium. The effect of transient silencing was analysed the following day (48 h post transfection) or the cells were collected and stored in -80 °C till further analysis was needed.

2.7. Cloning of full-length FRMD4A and truncated FRMD4A

2.7.1. First strand cDNA synthesis

The cloning of 3120 bp FRMD4A was carried out firstly by performing first strand cDNA synthesis with the following kits and its recommended protocol:

A. SuperScript™ III Reverse Transcriptase (Invitrogen, USA). The reaction mix initially contained 1 µl of 50 µM of oligo $(dT)_{20}$, 2 µg of total RNA, 1 µl of 10 mM of

dNTP Mix (10 mM each of dATP, dGTP, dCTP and dTTP at neural pH) and sterile, distilled water to make up 13 µl reaction volume. The mixture was heated to 65 °C for 5 min and incubated on ice for 5 min. Subsequently, 4 µl of 5 X First-Strand Buffer, 1 µl of 0.1 M DTT, 1 µl of RNaseOUT ™ Recombinant RNase Inhibitor (40 units/µl) and 2 µl of SuperScript™ III Reverse Transcriptase was added and mix well before incubating at 55 °C for 60 min and followed by heating at 70 °C for 15 min to inactivate the reaction. Finally, 1 µl of *E.coli* RNase H was added into the reaction mix and incubated at 37 °C for 20 min.

B. Transcriptor High Fidelity cDNA Synthesis kit (Roche, Germany). The reaction mix initially contained 1 µl of 50 pmol/ µl of oligo $(dT)_{18}$, 2 µg of total RNA, and sterile, distilled water to make up 11.5 µl reaction volume. The mixture was heated to 65 °C for 10 min and incubated on ice for 5 min. Subsequently, 4 µl of 5 X transcriptor High Fidelity Reverse Transcriptase Reaction Buffer, 1 µl of 0.1 M DTT, 0.5 µl of Protector RNase Inhibitor (40 units/µl), 2 µl of dNTPs (10 mM each) and 1 µl of High Fidelity Reverse Transcriptase was added and mix well before incubating at 55 °C for 60 min and followed by heating at 85 °C for 5 min to inactivate the reaction. Finally, 1 µl of *E.coli* RNase H was added into the reaction mix and incubated at 37 °C for 20 min. Similarly, reverse gene-specific primer was also used to perform the first strand cDNA synthesis with both kits instead of oligo $(dT)_{20}$.

2.7.2. PCR amplification of full-length and partial fragments of FRMD4A

The kits and recommended protocol used for PCR amplification are as followed:

A. High Fidelity PCR Enzyme Mix (Fermentas, USA), a 50 µl reaction mix includes 5 µl of 10X High Fidelity PCR Buffer with $MgCl_2$, 5 µl of 2mM dNTP mix, 1 µl of 10 µM primer pair, 5 µl of cDNA reaction mix and 0.5 µl of High Fidelity PCR Enzyme Mix (5 units/µl). The cycling conditions are 94 °C for 2 min for initial denaturation, followed by 35 cycles of denaturation at 94 °C for 30 s, annealing at the appropriate temperature depending on the primer melting temperature (Tm) and elongation at 72 °C for 3 min (full-length) or at 1 min/kb of PCR target and lastly, final elongation at 72 °C for 10 min.

B. KapaFidelity DNA polymerase kit (Bio Laboratories, Singapore), a 50 µl reaction mix includes 5 µl of 10X reaction buffer, 3 µl of 25mM $MgCl_2$, 1.5 µl of 10 mM dNTP mix, 1.5 µl of 10 µM primer pair, 5 µl of cDNA reaction mix and 2 µl of KapaFidelity DNA polymerase (1units/µl). The cycling conditions were 95 °C for 2 min for initial denaturation, followed by 35 cycles of denaturation at 98 °C for 15 s, annealing at the appropriate temperature depending on the primer melting temperature (Tm) and elongation at 72 °C for 2 min (full-length) or at 0.5 min/kb of PCR target and lastly, final elongation at 72 °C for 1 min.

C. Phusion High-Fidelity DNA Polymerase (Finnzymes, Finland), a 50 µl reaction mix includes 5 µl of 10 X Phusion HF Buffer with (1.5mM) $MgCl_2$, 1 µl of 10 mM dNTP mix, 1 µl of 10 µM primer pair, 5 µl of cDNA reaction mix and 1 µl of Phusion

High-Fidelity DNA Polymerase (2 units/µl). The cycling conditions are 98 °C for 30 s for initial denaturation, followed by 35 cycles of denaturation at 98 °C for 10 s, annealing at the appropriate temperature depending on the primer melting temperature (Tm) and elongation at 72 °C for 2 min (full-length) or at 30 s/kb of PCR target and lastly, final elongation at 72 °C for 10 min.

The amplification of the full length FRMD4A starts from 329 bp (FRMD4A 329) to 3509 bp (FRMD4A 3509) of the mRNA sequence found in NCBI (Accession no. NM_018027). The amplification of the partial FRMD4A fragments includes:

A. 329 bp (FRMD4A 329) to 1611 bp (FRMD4A 1611) which consists of the FERM domain.
B. 1592 bp (FRMD4A 1592) to 2419 bp (FRMD4A 2419)
C. 2403 bp (FRMD4A 2403) to 3509 bp (FRMD4A 3509).

The primer sequences in bracket are listed in Appendix 6. Amplification of these partial FRMD4A fragments was carried out using High Fidelity PCR Enzyme Mix (Fermentas, USA).

2.7.3. Cloning of FERM domain into GFP vector

The FERM domain of *FRMD4A* (329bp-1611bp) was amplified with newly designed primers (Appendix 6) using High Fidelity PCR Enzyme Mix (Fermentas, USA) and cloned into pcDNA3.1/CT-GFP-TOPO vector (Invitrogen, USA) using TOPO cloning technology according to manufacturer's protocols. This cloning required the inclusion of salt (200 mM NaCl, 10 mM $MgCl_2$). The salt prevented topoisomerase I from rebinding and potentially nicking the DNA after ligating the PCR products and dissociating from DNA. The result is more intact molecules present which leads to

higher transformation efficiencies. The TOPO reaction includes: 4 ul of fresh PCR product, 1 ul of salt solution and 1 ul of TOPO vector. The reaction mixture was incubated for 1 h at room temperature. The ligated product was then transformed into One Shot TOP 10 Chemically Competent *E.coli* and incubated on ampicillin plate overnight at 37 °C according to the manufacturer's protocol. A few colonies were selected and cultured overnight in LB containing 100 μg/ml of ampicillin. The plasmid was isolated as described in section 2.4.2., quantitated and sequenced using the GFP reverse primer (Appendix 6).

2.7.4. Bioinformatic Analyses

Conserved domain query was carried out with the NCBI Conserved Domain Database (CDD) (www.ncbi.nlm.nih.gov/Structure/cdd/cdd.shtml). The amino acid homology of FRMD4A as compared to erythroid protein 4.1 was obtained by getting the amino acid sequence of both proteins from NCBI database and compared using Cluster W (www.ebi.ac.uk/clustalw/). In addition, the multiple sequence alignment of the TALIN, RADIXIN, FAK and FRMD4A proteins was done using Cluster W.

CHAPTER 3.

RESULTS

3.1. Validation of microarray analysis of *FRMD4A* and *INDO*

West Nile virus (WNV)-infected A172 cells (glioblastoma) and WNV-infected HeLa cells (cervical adenocarcinoma) were observed to consistently produce virus titre of 10^5 PFU/ml and 10^8 PFU/ml at 24 h post-infection, respectively (Figure 3-1A). In addition, WNV-infected A172 cells had less efficient virus growth kinetic as compared to WNV-infected HeLa cells even though both have similar growth pattern (Figure 3-1B). As such, it was hypothesized that a more effective anti-viral mechanism was present in A172 cells. This anti-viral mechanism could be the reason behind the lower virus titre in WNV-infected A172 cells. A genomic study was then carried out using microarray technology previously (Koh and Ng, 2005). The main aim of that study was to determine the differentially expressed genes that could play a role in the different cell permissivity to infection between A172 cells and HeLa cells. From the differentially expressed genes, two genes, *FRMD4A* and *INDO*, with the highest significant fold change were identified and selected for further research. The fold difference of these two genes was validated using semi-quantitative reverse transcription polymerase chain reaction (RT-PCR) and quantitative real-time PCR.

A.

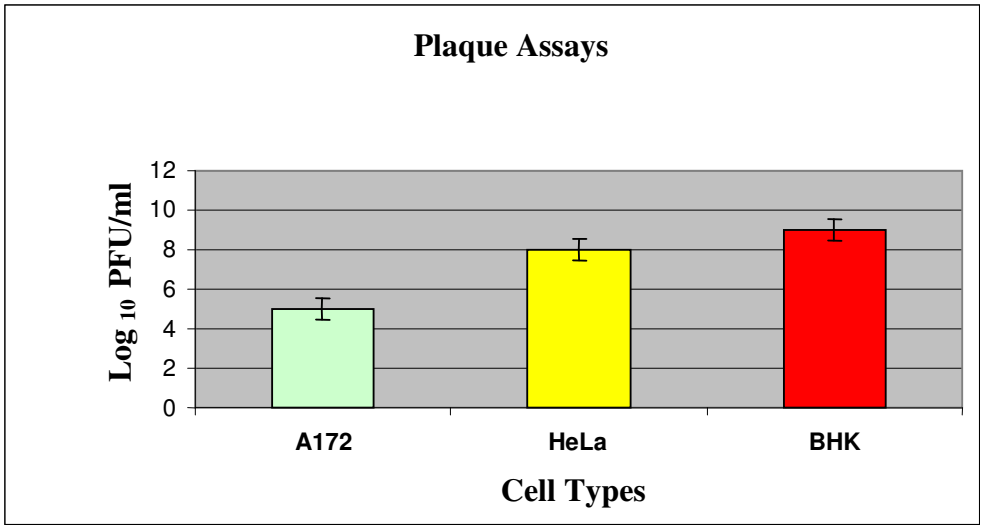

B.

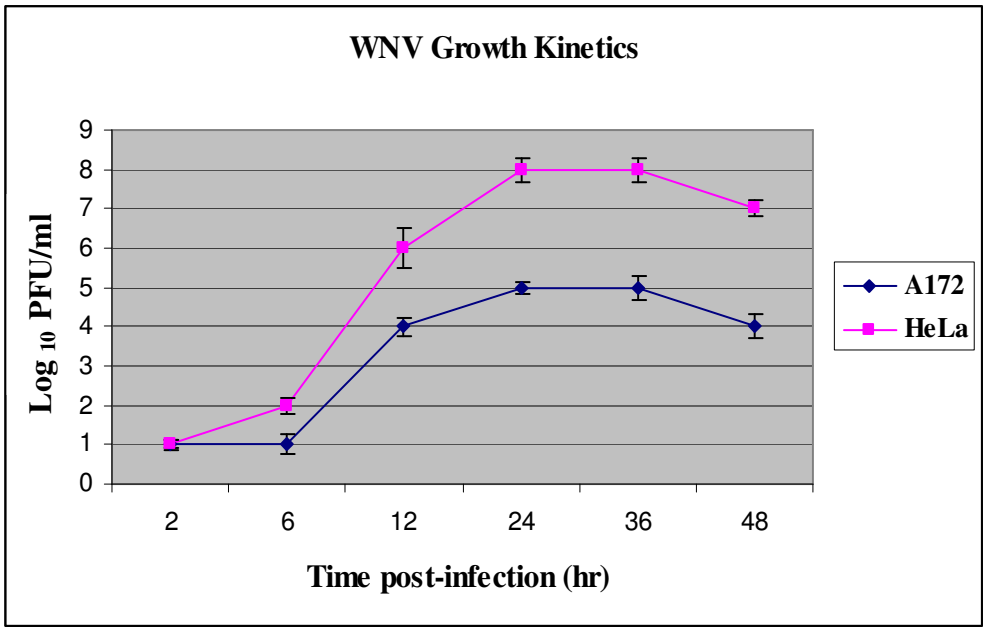

Figure 3-1. Differential WNV infection in selected cells. A. WNV-infected A172 cells produce a lower virus titre than WNV-infected HeLa cells at 24 h post-infection with MOI of 10. WNV-infected BHK cells are used as a positive control for plaque assay to ensure that the assay process is standardised. B. Graphs of WNV growth kinetic in infected A172 cells and infected HeLa cells show that WNV infects A172 cells less efficiently as compared to HeLa cells. The virus titres at each time point are the averages of the results of triplicate titrations from one experiment. In total, three separate experiments were carried out. Error bars indicate standard deviation of the three separate experiments and are shown where appropriate. These results strongly suggest A172 cells may have a more effective anti-viral mechanism than HeLa cells.

3.1.1. Total RNA integrity and purity

Total RNA was extracted from A172 cells and HeLa cells. Subsequently, the total RNA was assessed on integrity and purity (Figure 3-2). The good integrity of total RNA gave two distinct sharp bands which corresponded to 18S and 28S ribosomal RNA (rRNA). The apparent ratio of 28S rRNA to 18S rRNA was approximately 2:1 based on fluorescence intensity of the bands (Figure 3-2A). In addition, the purity of extracted total RNA was considered good with $Asorbance_{260}/Asorbance_{280}$ (A_{260}/A_{280}) and A_{260}/A_{230} ratios ranging between 2 to 2.1 (Figure 3-2B). This indicated low contamination with compounds such as protein, guanidine isothiocyanate, EDTA and phenol. As such, the good integrity and high purity of total RNA would provide more accurate and reliable results of the downstream applications.

A.

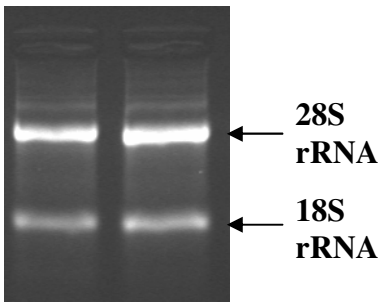

B.

Cells	260/280	260/230
A172	2.04	2.02
HeLa	2.09	2.06

Figure 3-2. Integrity and purity assessment of extracted total RNA with 2 % denaturing agarose gel (A) and Nanodrop (B) respectively. Two distinct 28S and 18S rRNA bands are used to assess the integrity of the total RNA. Ratio of 260/280 and 260/230 are used to assess the purity of the total RNA. This figure shows a representation of the common observation of rRNA bands and the ratio readings.

3.1.2. Primer specificity of *FRMD4A* and *INDO*

Primers (Appendix 6) were designed to amplify and detect specifically the presence of a short region of *FRMD4A* and *INDO*. The primers were specific as it produced a single band of the appropriate size after PCR (Figure 3-3). The specificity of these primers would also provide a more accurate and reliable results of the RT-PCR and real time PCR.

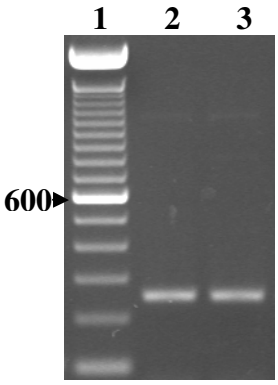

Lanes

1. **100bp Molecular Marker**
2. ***FRMD4A* (246bp)**
3. ***INDO* (234bp)**

Figure 3-3. Primer specificity of *FRMD4A* and *INDO* primers. These primers (Appendix 6) are subsequently used for checking mRNA expression of *FRMD4A* and *INDO*.

3.1.3. Endogenous control assessment

In order to make accurate comparison of the mRNA levels between different cell lines and between mock-infected and infected cell lines in RT-PCR and real time PCR, a suitable endogenous control that has a consistent mRNA level under all experimental conditions is required. *BETA-ACTIN (β-ACTIN)* and *18S rRNA* are the common endogenous control for RT-PCR and real time PCR as they belong to the housekeeping gene category. Standard curves of *β-ACTIN* and *18S rRNA* were obtained with different dilutions of total RNA extracted from mock-infected and infected A127 cells and HeLa cells using real-time PCR. Standard curve of *β-ACTIN*

from the mock-infected A172 cells showed significant difference from the rest of the standard curves obtained (Figure 3-4A). This could be due to the virus infection as it had been reported that actin filaments played a role in the maturation process of the WNV (Chu, *et al.*, 2003). However, there was no significant difference observed for the standard curves of *18S rRNA* (Figure 3-4B). Hence, *18S rRNA* was chosen as the endogenous control in this study.

A.

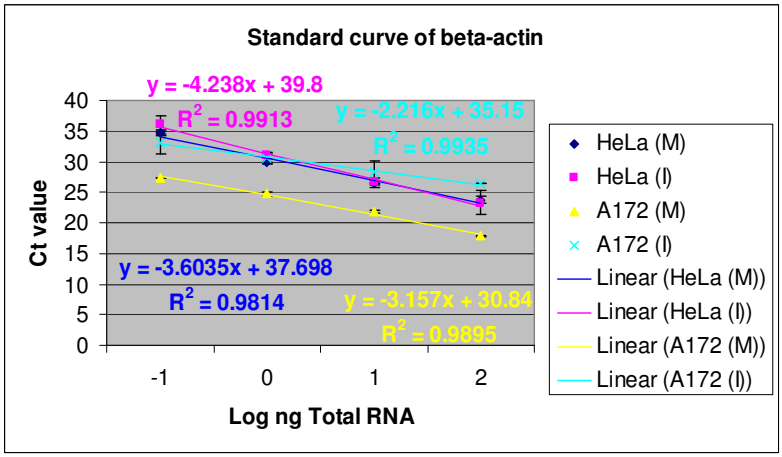

B.

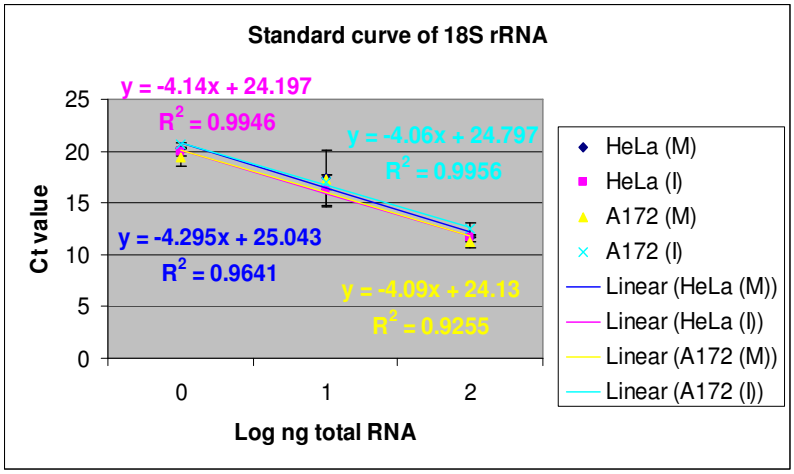

Figure 3-4. Endogenous control assessment for real-time PCR. A. *β-ACTIN* mRNA expression level is not consistent among the mock and infected cells. B. *18S rRNA* expression level is consistent and thus, it can serve as a better endogenous control than *β-ACTIN*.

3.1.4. Semi-quantitative RT-PCR

RT-PCR evidently showed that the mRNA expression levels of *FRMD4A* and *INDO* were differentiated prominently in expression in WNV-infected A172 cells when compared to WNV-infected HeLa cells (Figure 3-5A and B). This trend is correlated completely with the previous microarray analyses. Interestingly, it was observed that *FRMD4A* was only expressed in A172 cells but not in HeLa cells. However, the mRNA expression level of *FRMD4A* remained unregulated in A172 cells after virus infection (Figure 3-5A). This could be one of the intrinsic cellular factors that may be involved in the permissivity of A172 cells to WNV infection. Although its expression level was not influenced by the impact of virus infection, it might still play a role in WNV infection. On the contrary, the mRNA expression level of *INDO* was upregulated in infected A172 cells when compared to mock-infected A172 cells (Figure 3-5B). Hence, *INDO* may also be involved in the permissivity of A172 cells to WNV infection since its expression level was influenced by the impact of the WNV infection.

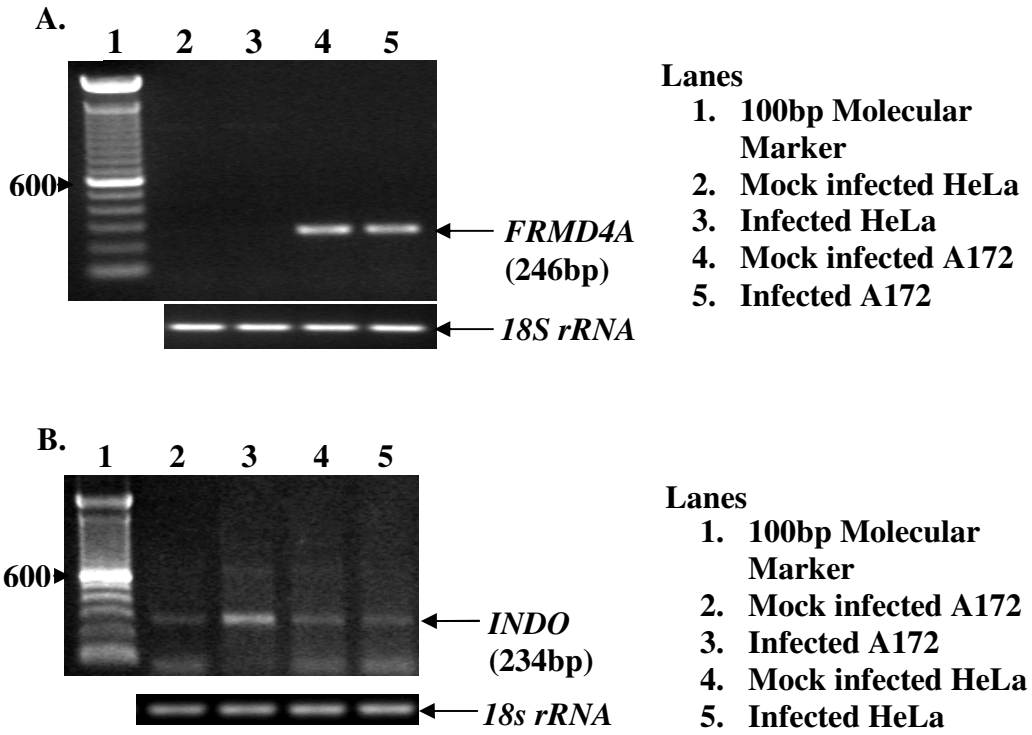

Figure 3-5. Semi-quantitative RT-PCR of *FRMD4A* (A) and *INDO* (B). Both mRNA expression of *FRMD4A* and *INDO* show higher level in infected A172 cells than in infected HeLa cells. However, the mRNA expression of *FRMD4A* is only observed in A172 cells but not in HeLa cells and mRNA expression of *INDO* is induced in infected A172 cells when compared to infected HeLa cells.

3.1.5. Real time PCR analyses

Dissociation curves of *FRMD4A* and *INDO* showed the primer specificity in real-time PCR. Dissociation curve of *FRMD4A* showed a single distinct peak at dissociation temperature of approximately 88 °C (Figure 3-6A). However, the dissociation curve of *INDO* showed two peaks. This was due to the existence of two isoforms of *INDO*, namely *INDO 1* and *INDO 2* in the amplified fragments of the same size as the two fragments were not observed in RT-PCR (Figure 3-5B). The two isoforms were made up of a number of different nucleotides resulting in the formation of different peaks with dissociation temperature difference of approximately 3 °C (Figure 3-6B). The No Template Control (NTC) was incorporated as a negative control to ensure that the amplified fragment is from the template and not other sources. The mRNA expression level of *FRMD4A* and *INDO* was observed to be significantly higher in infected A172 cells than in infected HeLa cells (Figure 3-7A & B; Figure 3-8). The fold difference of *FRMD4A* and *INDO* was approximately 11 and 10 units, respectively (Figure 3-9). These results again correlated well with the microarray analyses of *FRMD4A* and *INDO*.

A.

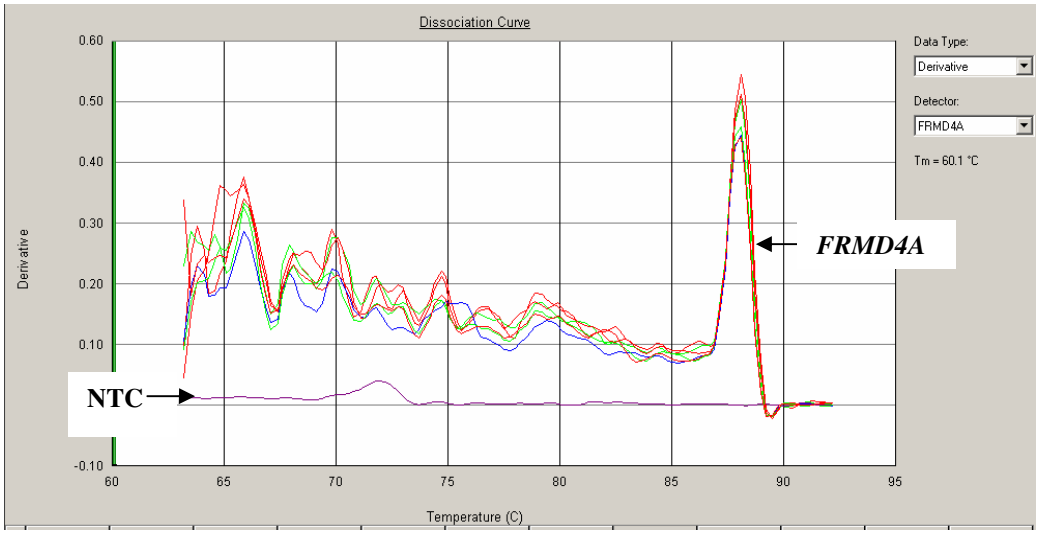

B.

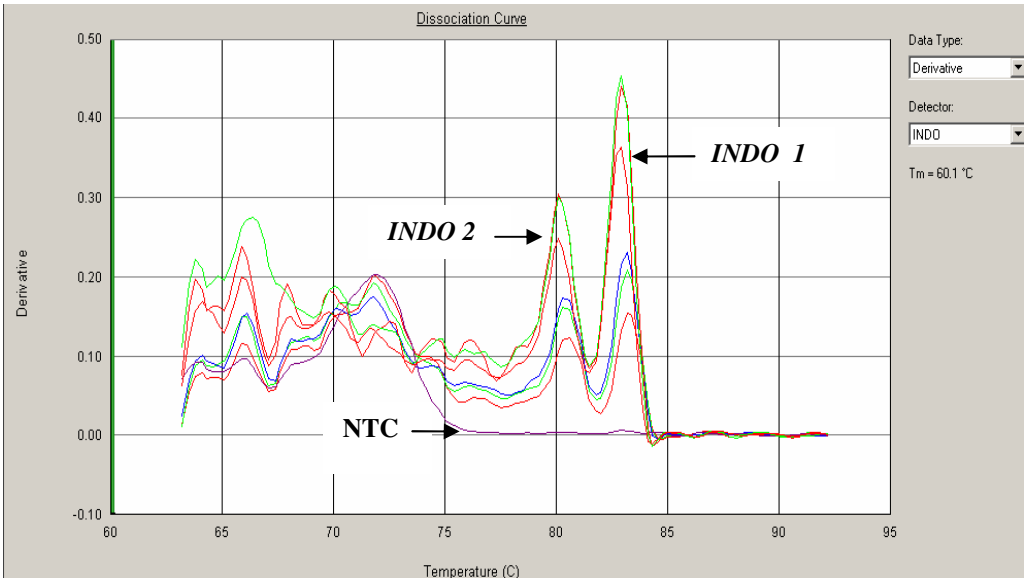

Figure 3-6. Dissociation curve of *FRMD4A* (A) and *INDO* (B). A. The single peak of *FRMD4A* represents the specificity of the primers. B. The double peaks of *INDO* represent the presence of two isoforms of *INDO* of the same fragment size but contain a few different nucleotides. This results in a dissociation temperature difference of approximately 3 °C. NTC- No template control. This figure is used as a representation of the replicates of real-time PCR results.

A.

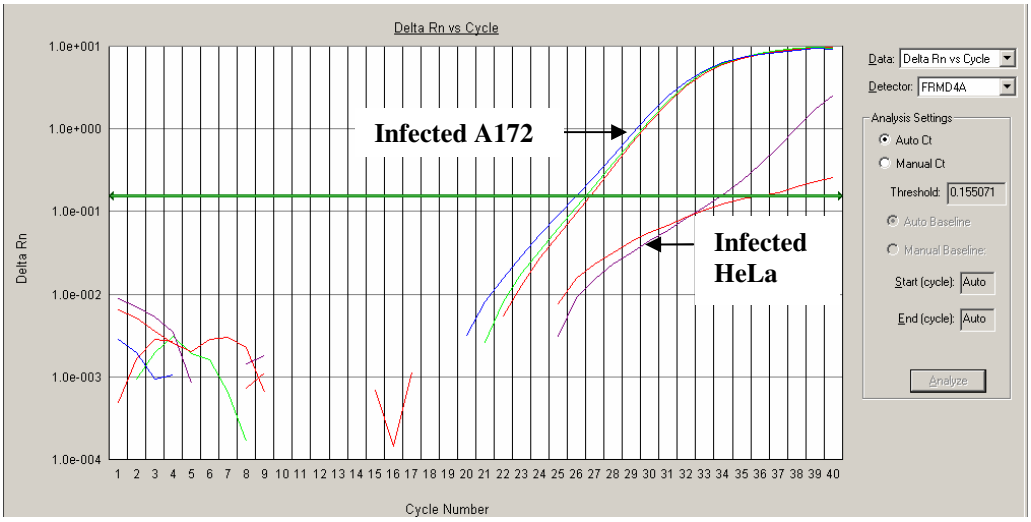

B.

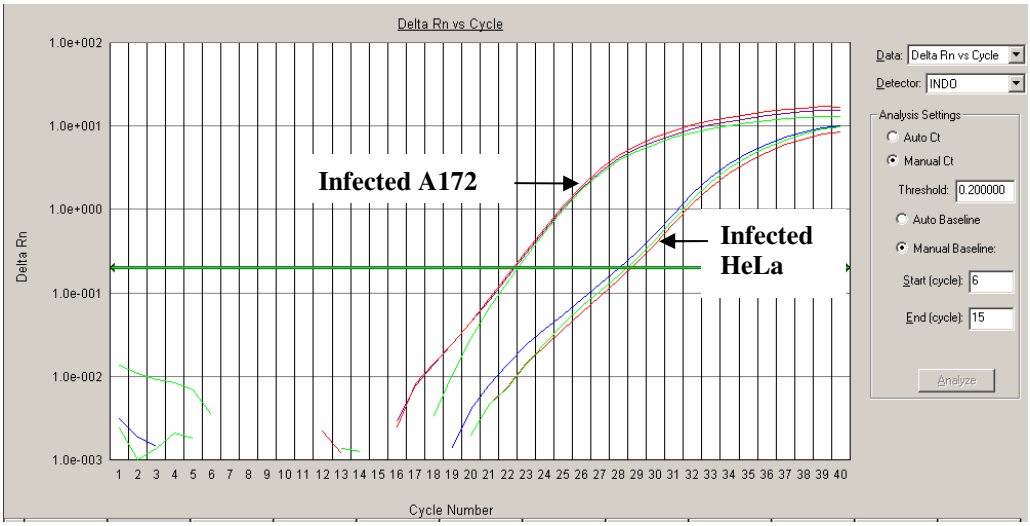

Figure 3-7. Real-time PCR analyses of *FRMD4A* (A) and *INDO* (B) in WNV-infected A172 and HeLa cells. A. WNV-infected A172 cells have lower cycle number (Ct) than infected HeLa cells and hence, higher mRNA expression level of *FRMD4A*. B. WNV-infected A172 cells have lower cycle number (Ct) than infected HeLa cells and hence, higher mRNA expression level of *INDO*. This figure is used as a representation of the replicates of real-time PCR results.

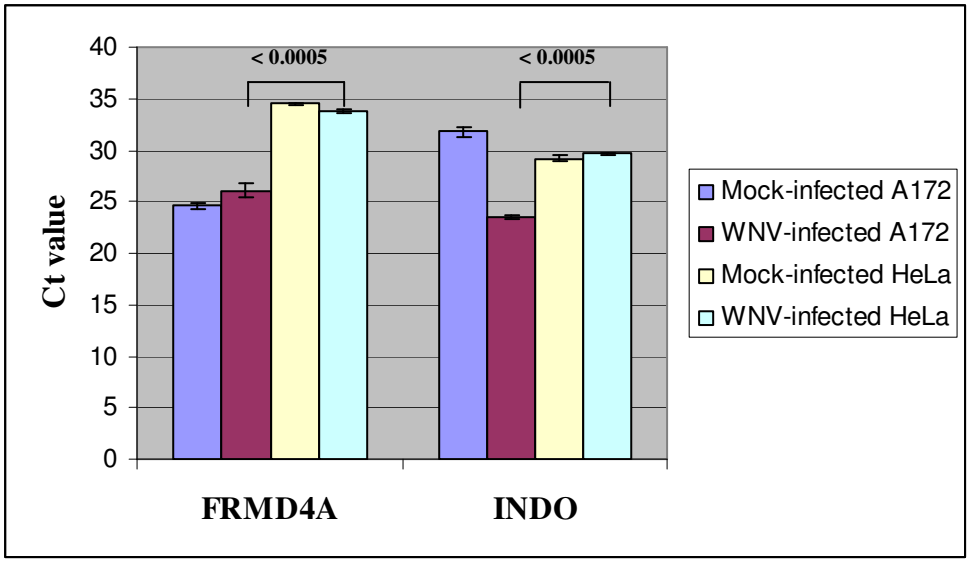

Figure 3-8. Real-time PCR analysis of *FRMD4A* and *INDO* mRNA expression level (Ct value) in A172 cells and HeLa cells. *FRMD4A* expression in WNV-infected A172 cells and WNV-infected HeLa cells show significant difference. However, mock-infected and WNV-infected of both A172 cells and HeLa cells do not show significant difference in *FRMD4A* expression. *INDO* expression in WNV-infected A172 cells and WNV-infected HeLa cells show significant difference. However, mock-infected and WNV-infected of both A172 cells and HeLa cells do not show significant difference in *INDO* expression.

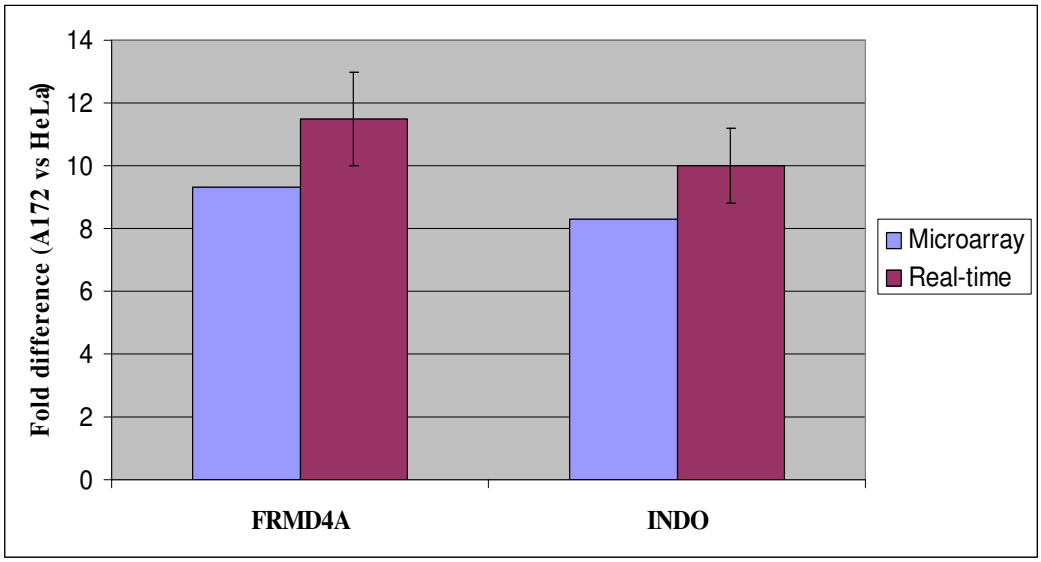

Figure 3-9. Relative fold change of *FRMD4A* and *INDO* between WNV-infected A172 cells and HeLa cells using real-time PCR. Real-time PCR results of both *FRMD4A* and *INDO* correlate well with microarray analyses. Fold change = $2^{-\Delta\Delta CT}$ (A172)/ $2^{-\Delta\Delta CT}$ (HeLa) where $\Delta\Delta CT$ = (CT, $_{Target}$ − CT, $_{18S\ rRNA}$) virus-infected.

3.2. Impact of silencing *FRMD4A* and *INDO* on WNV infection

FRMD4A and *INDO* had been shown and validated to have significantly higher differential expression in WNV-infected A172 cells than in WNV-infected HeLa cells. In order to find out whether these two genes had any influence on WNV infection, silencing of these two genes was carried out using microRNAs (miRNA) expression system. This expression system facilitates the generation of an expression construct that permits high-level expression of a pre-miRNA in mammalian cells for RNAi analyses of the target genes. The expression of pre-miRNA will subsequently be processed by Dicer into an approximately 22 nucleotides miRNA (mature miRNA) molecule. Mature miRNAs usually regulate gene expression by either mRNA cleavage or translational repression (Cullen, 2004). However, the engineered miRNAs produced by the BLOCK-iT™ Pol II miR RNAi Expression Vector Kits fully complement their target site and hence, cleave the target mRNA.

Since WNV infection can cause neurological diseases such as encephalitis and meningitis, it would be most appropriate to used A172 cells. A172 cells are human glioblastoma cells of central nervous system origin and, so it is more relevant and significant to study the two genes in A172 cells. Furthermore, A172 cells like the microglial cells are poorly permissive to the growth of WNV. Microglial cells are also thought to influence the neuropathogenesis of WNV infection (Cheeren *et al.,* 2005).

3.2.1. Construction of *FRMD4A*- and *INDO*- silencing plasmid

Antisense target sequence of 21 nucleotides (nt) (Appendix 6) of *FRMD4A* and *INDO* were selected using Invitrogen's BLOCK iT^{TM} RNAi Designer online tool. The respective site of these sequences was shown in Figure 3-10. The antisense target

sequence of *FRMD4A* was chosen outside the FERM domain. This was because based on literature review, there were many proteins found to have this FERM domain. In order not to affect the expression level of other FERM domain-containing proteins, it was logical to design the antisense target sequence outside the FERM domain.

Single-stranded (ss) DNA oligos of 64 nt were designed with the selected antisense target sequence of *FRMD4A* and *INDO*, respectively (Appendix 6). Double-stranded (ds) oligos of size that corresponded to 75 bp of the molecular marker were generated by annealing the commercially synthesized complementary ss DNA oligos (Figure 3-11A). The respective ds DNA oligos were then cloned into the pcDNA vector by ligation and transformation into *E. coli* to form pre-*FRMD4A* miRNA and pre-*INDO* miRNA expressing- vectors (Figure 3-11B). In addition, scramble (Scr) sequence was cloned into the vector to generate pre-Scr miRNA expressing-vector to determine the specificity of silencing (negative control) and to ensure no off-target effects.

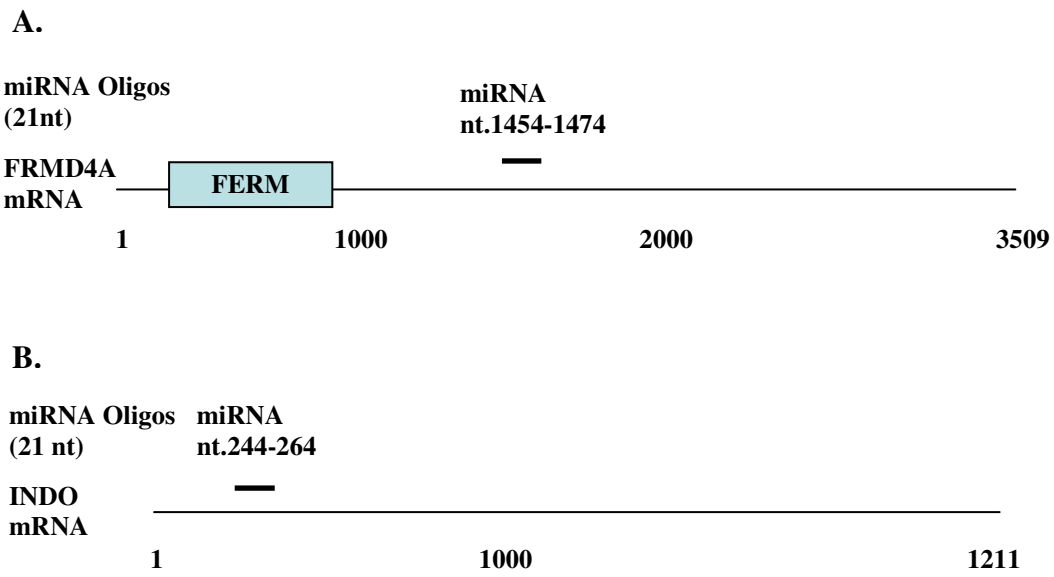

Figure 3-10. Schematic diagrams of *FRMD4A* (A) and *INDO* (B) mRNA, and their respective antisense target sequence sites. The sequence of antisense target sites used for silencing *FRMD4A* and *INDO* is selected using Invitrogen's BLOCK iT™ RNAi Designer online tool. A. The miRNA sequence for silencing *FRMD4A* is selected at nucleotide (nt) position 1454-1474, away from the FERM domain. This is to avoid unspecific silencing of other FERM domain-containing proteins. B. The miRNA sequence for silencing *INDO* is selected at nucleotide (nt) position 244-264. Based on the analysis of the online tool, both miRNA sequence of *FRMD4A* and *INDO* are one of the sequences that have the highest silencing probability.

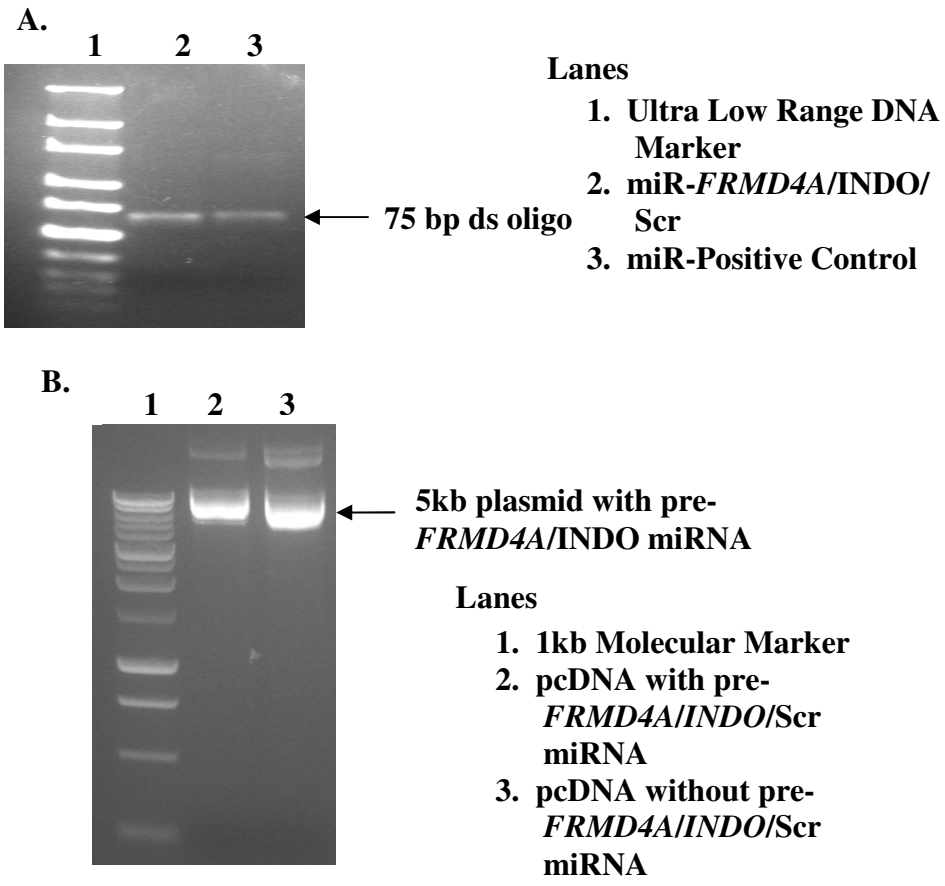

Figure 3-11. Generation of double-stranded (ds) oligo (A) and pre-miRNA-expressing vector for silencing (B). A. Single-stranded (ss) DNA oligos, designed using BLOCK-iT RNAi Designer, were successfully annealed to generate the ds oligo (75 bp). Commercially available ds miR-positive oligos are used for positive control. B. Ds miR- *FRMD4A*/*INDO*/Scramble (Scr) oligos were then ligated into pcDNA vector to generate the *FRMD4A*/*INDO*/Scr miRNA-expressing vector, respectively. Lane 2 shows the ds miR-*FRMD4A*/*INDO*/Scramble oligos successfully ligated into the pcDNA vector. This results in the higher molecular weight of the vector in Lane 2 as compared to the vector in Lane 3. This figure is a representation of the generation of pre-*FRMD4A, INDO* and Scr mi RNA expressing-vector.

3.2.2. Transient RNAi analysis of *FRMD4A* in A172 cells and its impact on virus infection

With the generated pre-miRNA vector for silencing *FRMD4A*, transfections of these vectors were performed. It was observed (Figure 3-12A) and quantitated by real-time PCR (Figure 3-12B) that the generated pre-miRNA vector was capable of reducing the mRNA expression level of *FRMD4A* by approximately 79 fold difference based on the Ct values obtained. As a result of this silencing, the virus titre increased by one log (Figure 3-13). This showed that *FRMD4A* is a potential anti-viral host factor. Expression level of *FRMD4A* was also not affected by miScr and hence, silencing of *FRMD4A* was specific and not due to off-target effects.

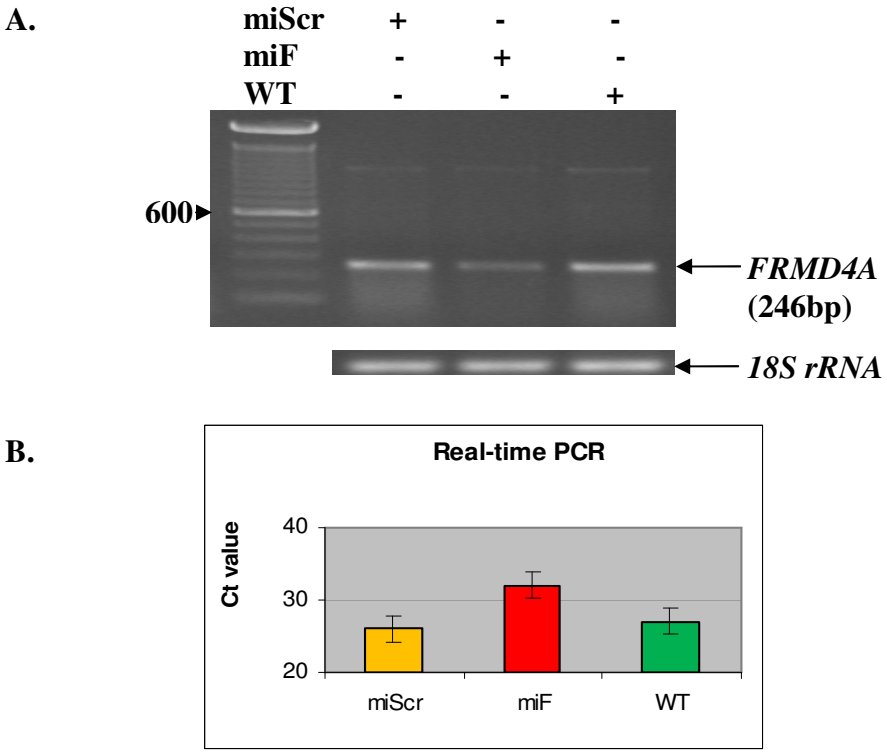

Figure 3-12. Transient silencing of *FRMD4A* in A172 cells. A. Pre-*FRMD4A* miRNA expressing-pcDNA vector (miF) is transfected into A172 cells to silence *FRMD4A*. Pre-Scramble miRNA expressing-pcDNA vector (miScr) is used as a negative control for silencing. B. Real-time PCR is used to quantitate the reduction of the mRNA level of *FRMD4A*. Transfection of miF successfully results in transient silencing of *FRMD4A*. miScr: transfection with pcDNA expressing pre-Scr miRNA; miF: transfection with pcDNA expressing pre- *FRMD4A* miRNA; WT: mock transfection.

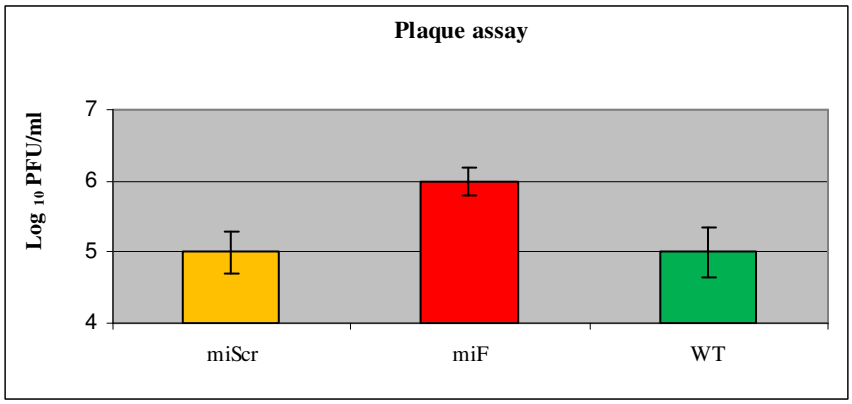

Figure 3-13. The impact of transient silencing *FRMD4A* on virus titre in A172 cells. With transient silencing of *FRMD4A*, the virus titre increases by one log as compared to mock-transfected A172 cells. miScr: transfection with pcDNA expressing pre-Scr miRNA; miF: transfection with pcDNA expressing pre-*FRMD4A* miRNA; WT: mock transfection.

3.2.3. Transient RNAi analyses of *INDO* in A172 cells and its impact on virus infection

In addition, pre-*INDO* miRNA expressing-pcDNA vector was transfected into A172 cells. It was observed (Figure 3-14A) and quantitated by real-time PCR (Figure 3-14B) that the generated pre-miRNA vector was capable of reducing the mRNA expression level of *INDO* by approximately 65 fold difference based on the Ct values obtained. However, as a result of this silencing, the virus titre remained consistently unchanged (Figure 3-15). Even though there is an induction of *INDO* in infected A172 cells as compared to mock-infected A172 cells, the role played by *INDO* may not be significant enough to affect virus replication. It was also observed that there is a change in *INDO* expression level as a result of the scrambled miRNA. This could be due to the silencing of other variants of *INDO* which could have very similar sequence as the scramble miRNA.

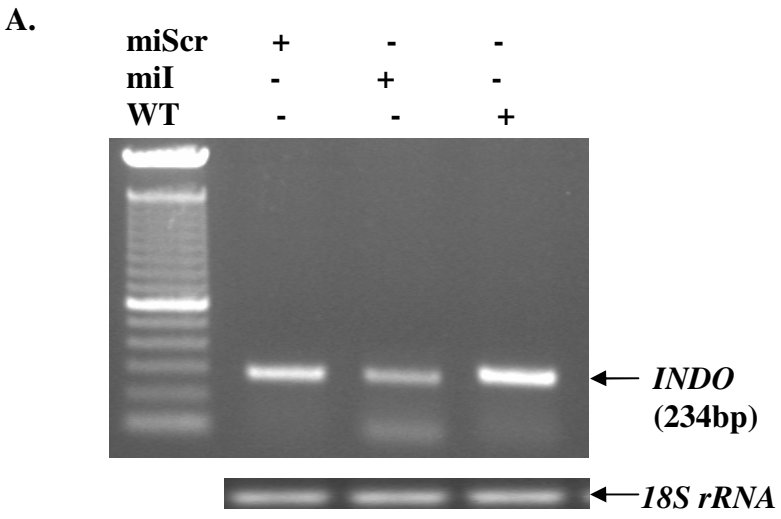

Figure 3-14. Transient silencing of *INDO* in A172 cells. Pre-*INDO* miRNA expressing-pcDNA is used for transfection. Pre-Scramble miRNA expressing-pcDNA vector (Scr) is used as a negative control for silencing. B. Real-time PCR is used to quantitate the reduction of the mRNA level of. *INDO*. Transfection of miI successfully results in silencing of *INDO*. miScr: transfection with pcDNA expressing pre-Scr miRNA; miI: transfection with pcDNA expressing pre-*INDO* miRNA; WT: mock transfection.

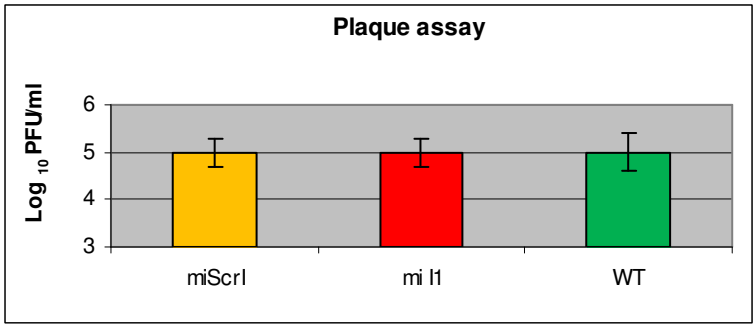

Figure 3-15. The impact of transient silencing *INDO* on virus titre in A172 cells. With transient silencing of *INDO*, the virus titre remains relatively similar. miScr: transfection with pcDNA expressing pre-Scr miRNA; miF: transfection with pcDNA expressing pre-*INDO* miRNA; WT: mock transfection.

3.3. Elucidation of the role of FRMD4A and its FERM domain in the less permissive A172 cells to WNV infection with bioinformatics and immunofluorescence microscopy

From the results of silencing *FRMD4A* and *INDO,* and their impact on virus infection based on the virus titre, it was more relevant to further study *FRMD4A* and its role in permissivity of A172 to WNV infection. Furthermore, it is a potential antiviral host protein that expresses only in A172, glioblastoma cells of central nervous system origin but not in HeLa cells.

3.3.1. Bioinformatics analyses of *FRMD4A*

Based on NCBI and conserved domain query, FRMD4A was found to belong to the 4.1 superfamily that contains a 4.1 ezrin radixin moesin (FERM) domain (Figure 3-16).

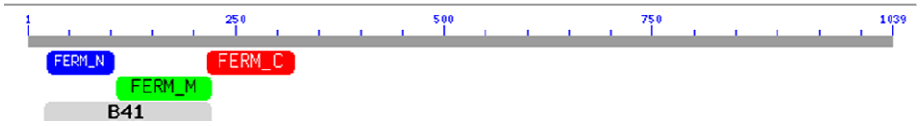

Figure 3-16. Conserved domains of FRMD4A. FERM domain consisting of three lobes (FERM-N, FERM-M, FERM-C) and B41 domain are conserved domains located at the N-terminal of FRMD4A protein.

The FERM domain of FRMD4A has 23% amino acid sequence homology to erythroid protein 4.1 (Figure 3-17). It is very similar to the FERM domain of talin, ezrin, radixin and moesin. In most cases, FERM domain has been shown to mediate intermolecular interactions between the transmembrane proteins such as integrins and the cytoskeleton.

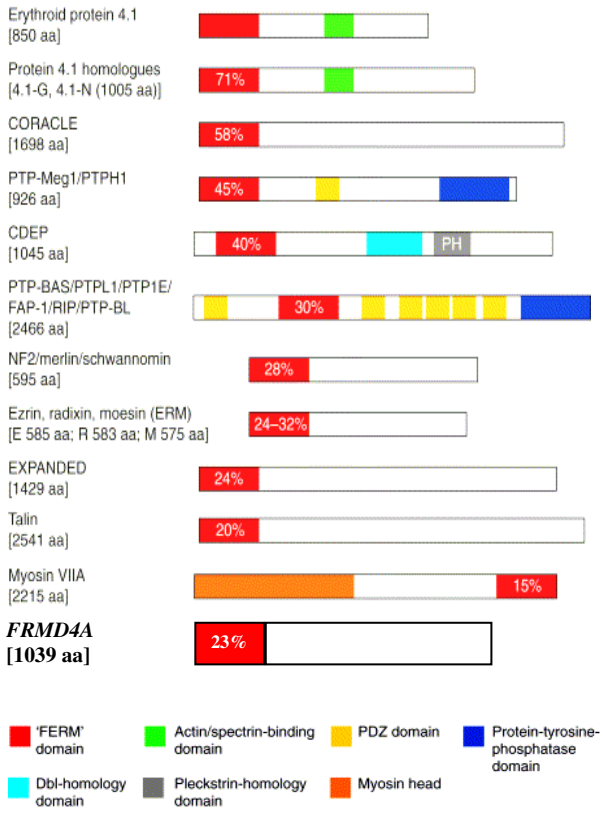

Figure 3-17. Amino acid sequence homology of FERM domain compared with that of erythroid protein 4.1. Similarly to most of the FERM domain-protein, FERM domain of FRMD4A is located at the N-terminal and has 23% amino acid sequence homology.

RADIXIN, TALIN and FAK are three FERM-domain containing proteins that had shown to interact with the integrin β-cytoplasmic tail (Athar *et al.,* 1998). Previously, it was found that the interaction of WNV with $\alpha_v\beta_3$ integrins mediates virus entry into the cells via the FAK activation and triggering of actin assembly

leading to clathrin-mediated endocytosis of virus particles (Chu & Ng, 2004). As such, a clustering of the FERM domain of RADIXIN, FRMD4A, TALIN and FAK was performed. It revealed two identical amino acids and a number of conserved substitutions of amino acids which correlated well to the binding region of integrin β-cytoplasmic tail (Figure 3-18A) (Tanentzapf and Brown, 2006). Furthermore, by comparing the scores derived from the clustering, it was observed that FRMD4A had the highest homology level as RADIXIN, which was also evident in Figure 3-15. The lowest homology level was observed with FAK, which may suggest FRMD4A could be a competitor of integrin-binding FAK (Figure 3-18B). It was observed that proteins such as RADIXIN (Tang *et al.,* 2007) and TALIN (Calderwood *et al.,* 2002) that were involved in the 'inside-out' signaling of integrin activation had a better homology score than FAK. This suggested that FRMD4A may be involved in the 'inside-out' signaling. Moreover, the score suggested that FRMD4A may have better or other binding sites like the RADIXIN and TALIN that can bind to integrin, competing with FAK in the process.

A.

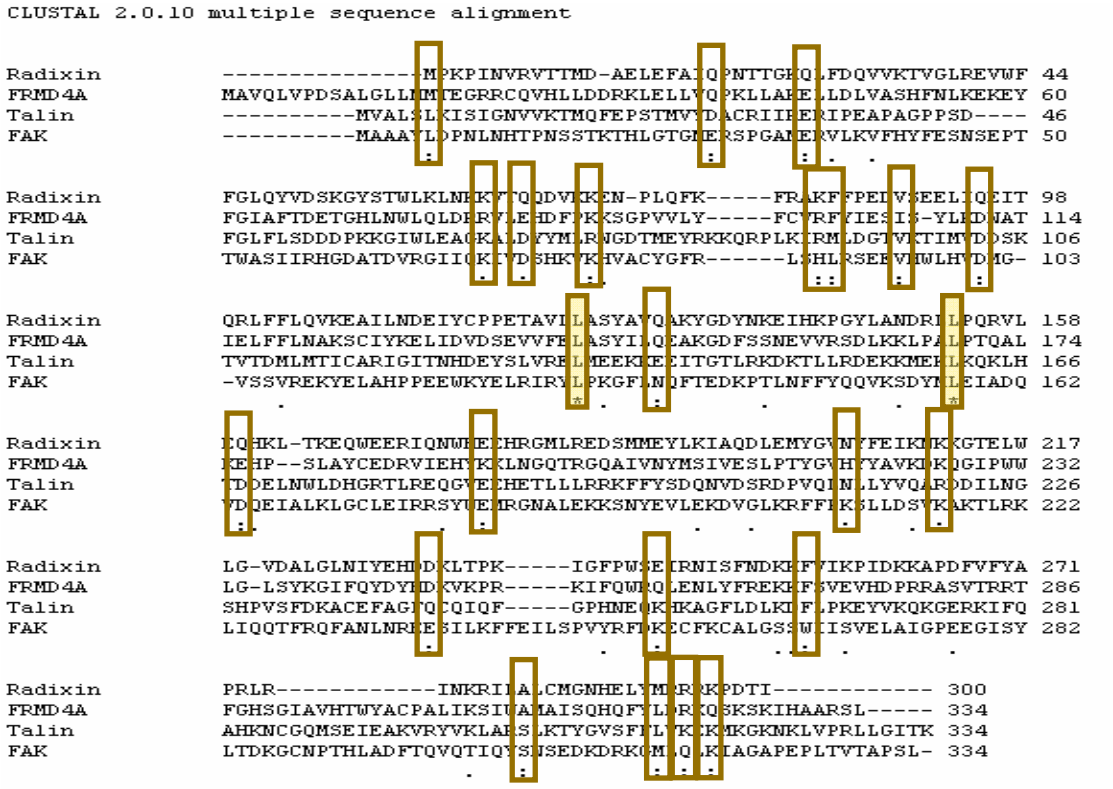

B.

SeqA	Name	Len(aa)	SeqB	Name	Len(aa)	Score
3	Radixin	300	4	FRMD4A	334	26
2	Talin	334	3	Radixin	300	15
2	Talin	334	4	FRMD4A	334	13
1	FAK	334	2	Talin	334	8
1	FAK	334	3	Radixin	300	8
1	FAK	334	4	FRMD4A	334	5

Figure 3-18. Clustering of the FERM domain of RADIXIN, FRMD4A, TALIN and FAK. A. The two identical lysine residues are associated with integrin β cytoplasmic binding site. '·' means semi-conserved substitution. ':' means conserved substitution. '*' means identical residues. B. FERM domain of FRMD4A has the highest homology to RADIXIN and the lowest homology to FAK.

3.3.2. Cloning of full length *FRMD4A* and its FERM domain

FRMD4A (NM_018027) has an mRNA of 6804 base pairs (bp) and coding sequence of 3509 bp, according to NCBI database. Many attempts to clone the full-length of this gene (3120 bp) were performed. However, none was successful. Forward and reverse primers were designed by first blasting the primer sequence with NCBI Blast to check for the specificity of the primer. Other parameters such as melting temperature, GC content, length of primer were also taken into consideration. Two different first strand cDNA synthesis kits were tried. They were Transcriptor High Fidelity cDNA Synthesis kit (Roche, Germany) and SuperScript^{TM} III Reverse Transcriptase (Invitrogen, USA). Furthermore, three different PCR kits with different polymerase were tested too. They were High Fidelity PCR Enzyme Mix (Fermentas, USA), KapaFidelity DNA polymerase kit (Bio Laboratories, Singapore) and Phusion High-Fidelity DNA Polymerase (Finnzymes, Finland). In addition, three-piece PCR strategy was performed but to no avail (Figure 3-19). In the end, the focus of the cloning was shifted to just the FERM domain as it was known to be functionally important as a linker between the transmembrane proteins and the cytoskeleton based on literature review. The segment 1A which consisted of FERM domain was amplified from 329bp-1611bp using newly designed primers (Appendix 6) (Figure 3-19C) and it was cloned into a vector with a GFP at the C-terminal of the segment 1A for downstream microscopy works.

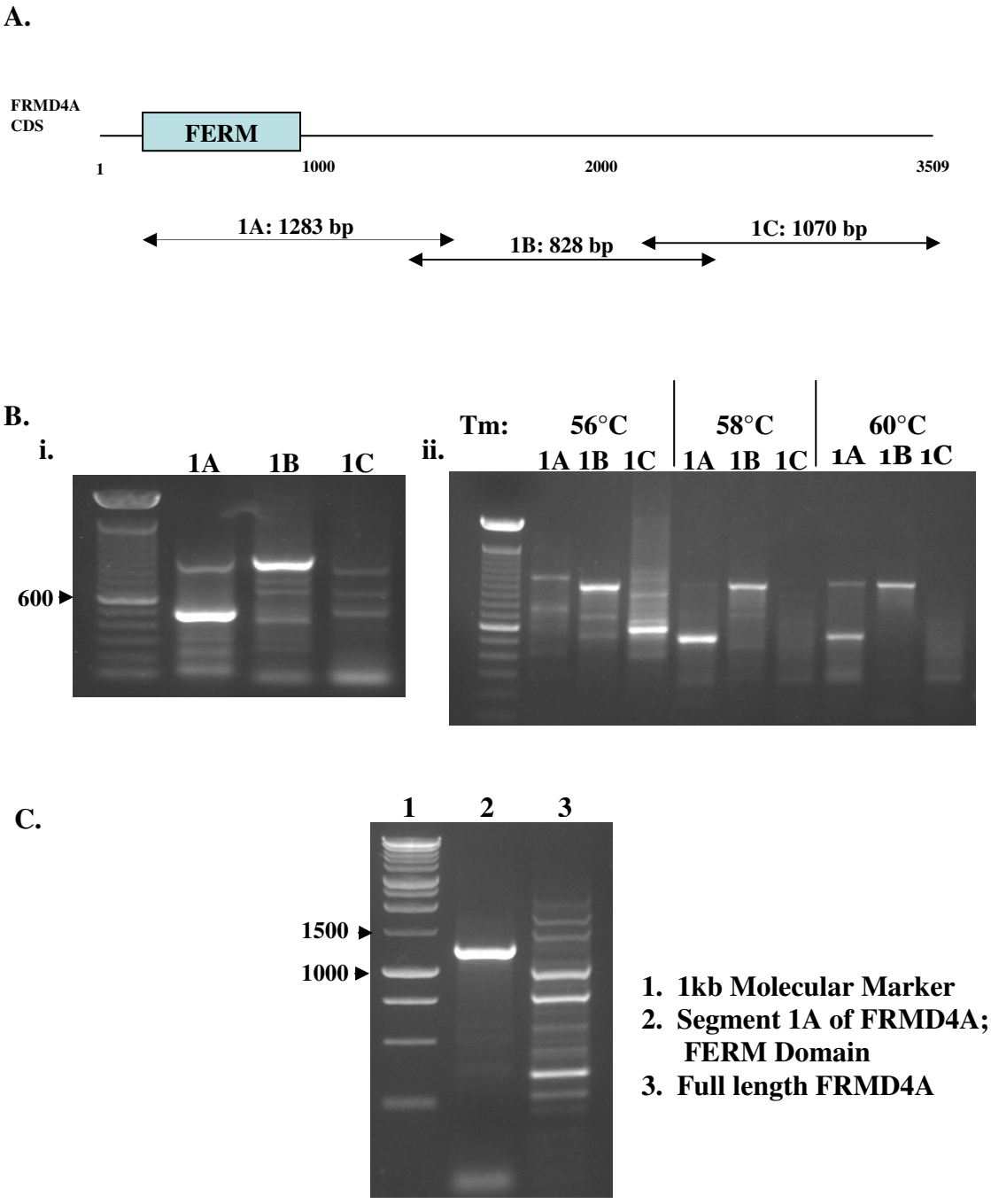

Figure 3-19. Cloning of full-length and FERM domain of *FRMD4A*. A. Schematic diagram of *FRMD4A* coding sequence of 3509 base pairs. The full length sequence was split up into three segments; 1A, 1283 bp long; 1B, 828 bp long; 1C, 1070 bp long. B. Three-piece PCR strategy to clone the full-length *FRMD4A* was also unsuccessful due to the production of unspecific and incorrect band size. (i). Increment of annealing temperature was also performed to reduce the unspecific bands and to achieve the correct size band, but to no avail (ii). C. Amplification of segment 1A of FRMD4A which consists of the FERM domain (Lane 2). Lane 3 is a representative figure of the many unsuccessful amplifications of the full length FRMD4A.

3.3.3. Colocalisation of WNV and integrins

Previous study had shown that WNV-integrin interaction mediated entry (Chu & Ng, 2004). Hence, based on bioinformatics analyses and literature review, it would be interesting to investigate the role of the FERM domain of FRMD4A in relation to WNV and integrin interaction-mediated entry. In Figure 3-20, A. represented the nuclei staining with DAPI; B. represented activated $\alpha_v\beta_3$ integrins detected with mouse anti-$\alpha_v\beta_3$ integrins antibody and stained with goat anti-mouse antibody conjugated with Alexa Fluor 488. The $\alpha_v\beta_3$ integrins are not strongly activated in all cells. However, when it is activated, it is found near the perinuclear region (white arrow in B); C. represented WNV detected with rabbit anti-WNV and stained with goat anti-rabbit antibody conjugated with Alexa Fluor 594. WNV is localized near the perinuclear region (white arrow in C) where the activated $\alpha_v\beta_3$ integrins are also localized; D. represented co-localizations of $\alpha_v\beta_3$ integrin (green) and the WNV (red) in infected A172 cells, represented in yellow. From Figure 3-20D, the colocalisation signal (yellow) from antibodies against WNV and $\alpha_v\beta_3$ integrin clearly shows that there is association between WNV and $\alpha_v\beta_3$ integrin. This was well-correlated to previous study (Chu & Ng, 2004) and it provided more confidence for this study to build on previous findings. However, it could be observed that some cells infected with WNV did not show strong colocalisation signal. This could be due to the fact that not all cells were intensely infected with WNV at that point of time. It could also be due to the entry of WNV via other mechanisms, instead of $\alpha_v\beta_3$ integrin.

3.3.4. No colocalisation between FERM domain of FRMD4A and actin filaments

In order to investigate whether the FERM domain interacts with the actin filaments, the following experiment was carried out. In Figure 3-21, A. represented

nuclei staining with DAPI; B. represented actin filaments detected with Phallodin; C. represented transfected FERM-GFP vector in A172 cells and FERM-GFP was localized near the perinuclear region; D. represented no co-localization of FERM-GFP (green) with the actin filaments (red) in A172 cells. Hence, the FERM domain was observed to have no association with the actin filaments (Figure 3-21). This is not surprising, as it has been reported in studies that actin binding sites are found at the C-terminal of the FERM domain-containing proteins and not at the FERM domain (Tanentzapf and Brown, 2006; Lee *et al.,* 2004a; Gary R and Bretscher A., 1995). In addition, the C-terminal of the FERM domain-containing proteins had a role involved in regulating the binding of the FERM domain to the integrin via this intramolecular autoinhibitory interaction (Lietha *et al.,* 2007).

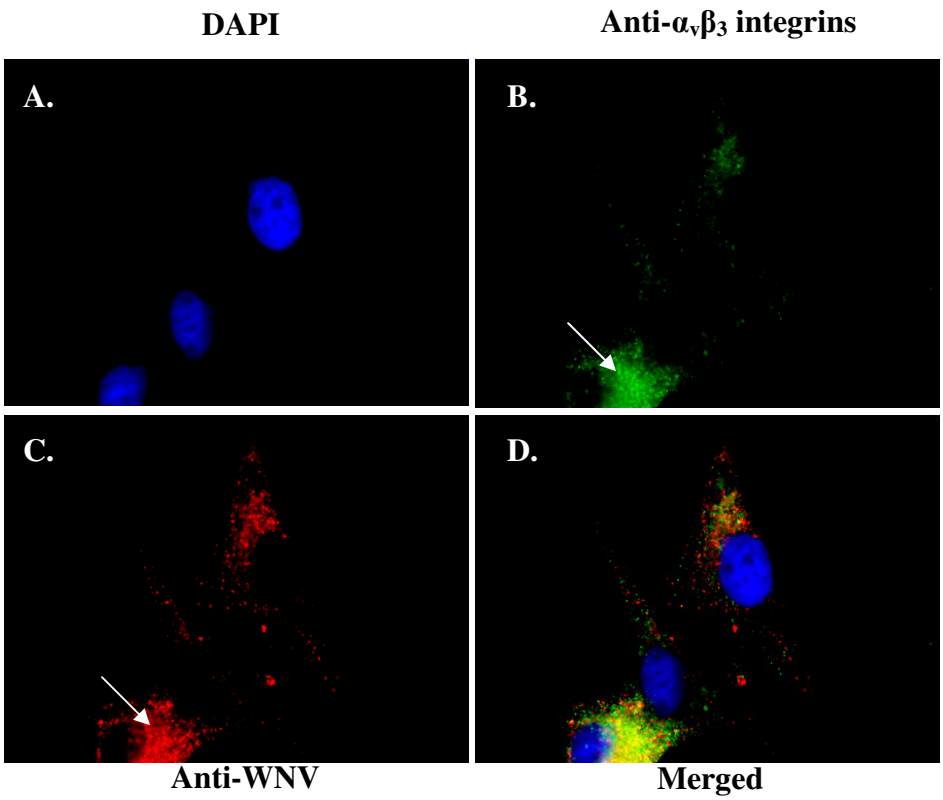

Figure 3-20. Immunofluorescence microscopy images of integrin (B) and WNV (C) association in WNV-infected A172 cells (D). A. Nuclei staining with DAPI. B. Activated $\alpha_v\beta_3$ integrins is detected with mouse anti-$\alpha_v\beta_3$ integrins antibody and stained with goat anti-mouse antibody conjugated with Alexa Fluor 488. The $\alpha_v\beta_3$ integrins are not strongly activated in all cells. When it is strongly activated, it is found near the perinuclear region (white arrow in B). C. WNV is detected with rabbit anti-WNV and stained with goat anti-rabbit antibody conjugated with Alexa Fluor 594. WNV is localized near the perinuclear region (white arrow in C) where the activated $\alpha_v\beta_3$ integrins are localized. D. Co-localizations of $\alpha_v\beta_3$ integrin (green) and the WNV (red) in infected A172 cells are represented in yellow.

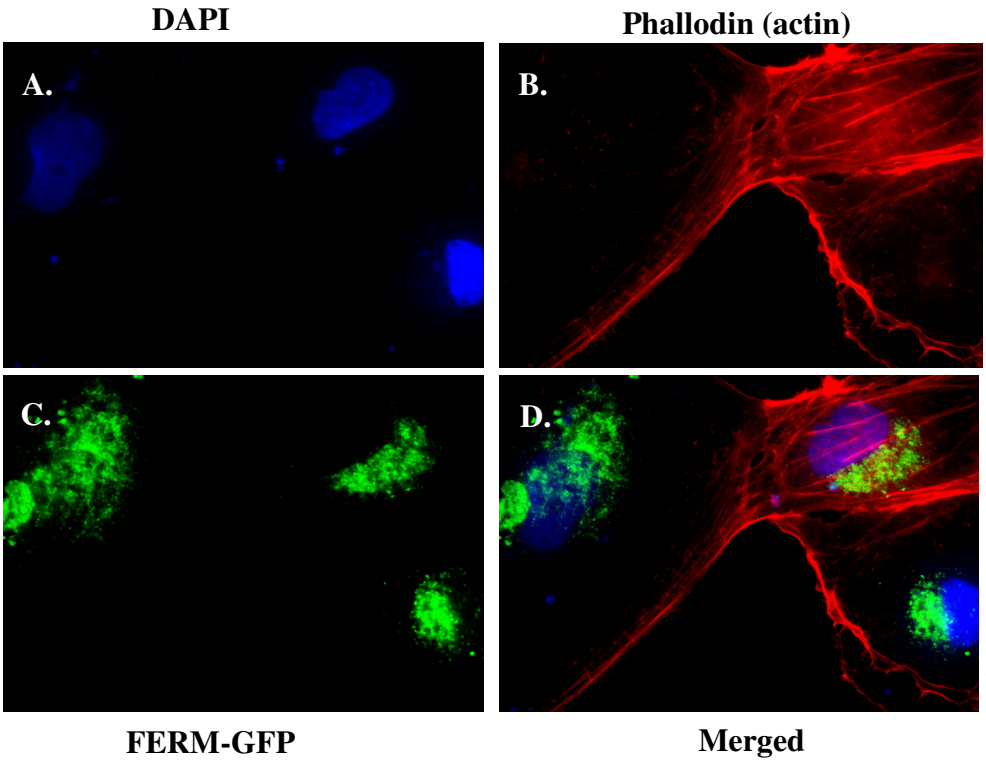

Figure 3-21. Immunofluorescence microscopy images of FERM-GFP and actin association. A. Nuclei staining with DAPI. B. Actin filaments are detected with phallodin. C. FERM-GFP vector was transfected into A172 cells and FERM-GFP was localized near the perinuclear region. D. No co-localization of FERM-GFP (green) and the actin filaments (red) in A172 cells is observed. FERM-GFP, similar to FERM domain of other FERM domain-containing protein does not interacts with actin (red).

3.3.5. Colocalisation of FERM domain of FRMD4A and Integrins

In order to investigate whether FERM domain of FRMD4A interacts with activated integrins, the following experiment was carried out. In Figure 3-22, A & Bi. represented nuclei staining with DAPI; A & Bii. represented activated $\alpha_v\beta_3$ integrins detected with mouse anti-$\alpha_v\beta_3$ integrins antibody and stained with goat anti-mouse antibody conjugated with Alexa Fluor 594. A & Biii. represented transfected FERM-GFP vector in A172 cells. In mock-infected A172, it was observed consistently that the FERM-GFP was localized at perinuclear region of the cell (Figure 3-22Aiii.) and had no association with the activated integrin (Figure 3-22Aiv.). Interestingly, when

the cells were infected with WNV 1 hr post infection, it was observed that the FERM-GFP had dispersed out, covering almost the entire perinuclear region (Figure 3-22Aiii.) and there was strong association with activated integrins (Figure 3-22Biv.).

3.3.6. Colocalisation of FERM domain of FRMD4A and WNV

In order to investigate whether WNV had any role in regulating the FERM domain of FRMD4A, the following experiment was carried out. In Figure 3-23, A. represented nuclei staining with DAPI; B. represented WNV detected with rabbit anti-WNV and stained with goat anti-rabbit antibody conjugated with Alexa Fluor 594. WNV was localized near the perinuclear region; C. represented transfected FERM-GFP vector in A172 cells and FERM-GFP was localized near the perinuclear region as well; D. represented some co-localizations signal of FERM-GFP (green) with WNV (red) in WNV-infected A172 cells, represented in yellow at 0.5 h post infection. It was observed that FERM-GFP had some form of association with WNV 0.5 h post infection (Figure 3-23D). This suggested that the dispersion of the FERM-GFP surrounding the entire perinuclear region might involve in the entry process of WNV. This preliminarily shows how FRMD4A targets WNV with its FERM domain and hinders WNV entry. However, more studies such as co-immunoprecipitation and time-course/live confocal microscopy are required to prove this.

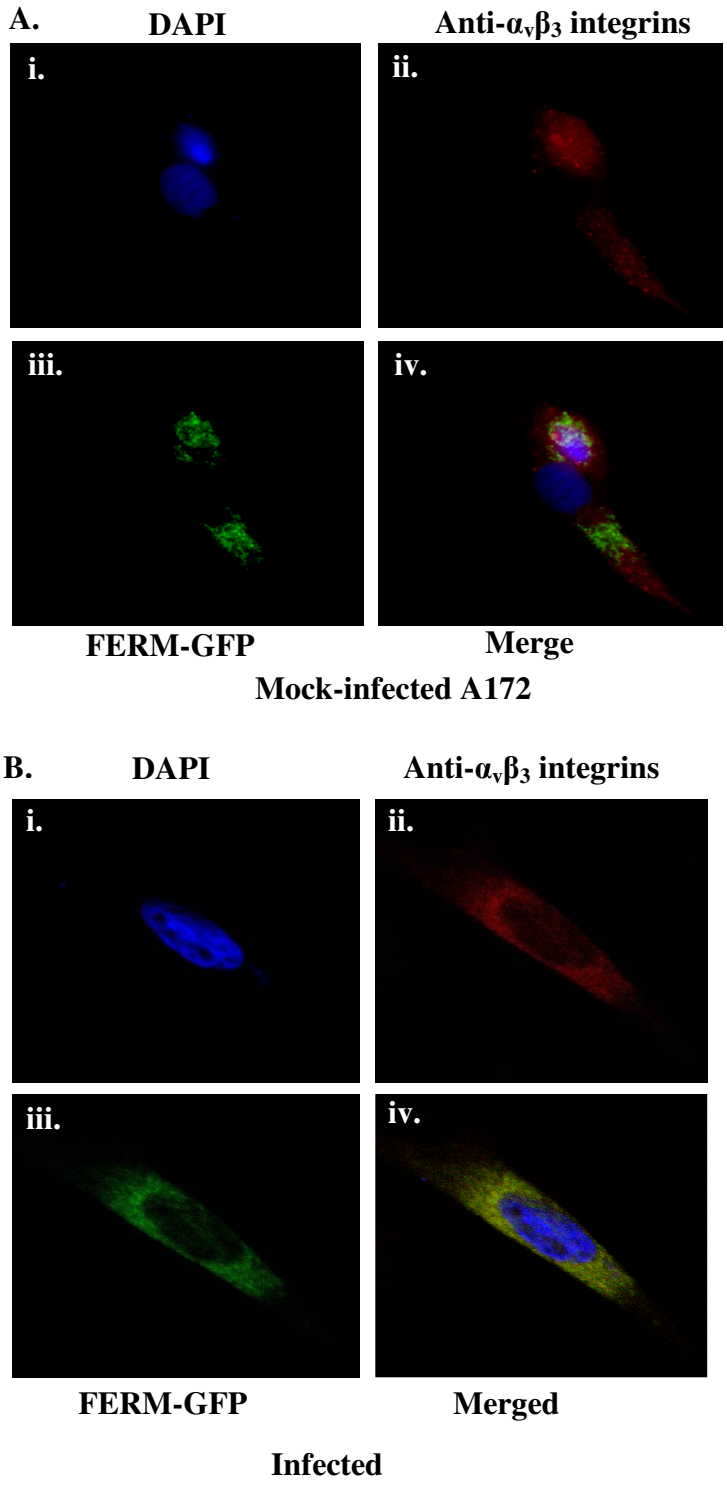

Figure 3-22. Immunofluorescence microscopy images of FERM-GFP and integrin association in mock-infected (A) and infected A172 cells (B). A. & B.i. Nuclei staining with DAPI. A. & B.ii. Activated $\alpha_v\beta_3$ integrins is detected with mouse anti-$\alpha_v\beta_3$ integrins antibody and stained with goat anti-mouse antibody conjugated with Alexa Fluor 594. A. & B.iii. FERM-GFP vector was transfected into A172 cells. In mock-infected cells, FERM-GFP is localized at perinuclear region (A.iii.) and does not colocalised (yellow) with the integrin (red) at 1h post infection (A.vi.). However, in infected cells, the FERM-GFP is dispersed (B.iii.) and it colocalises (yellow) with the integrin (red) at 1 h post infection (B.vi.).

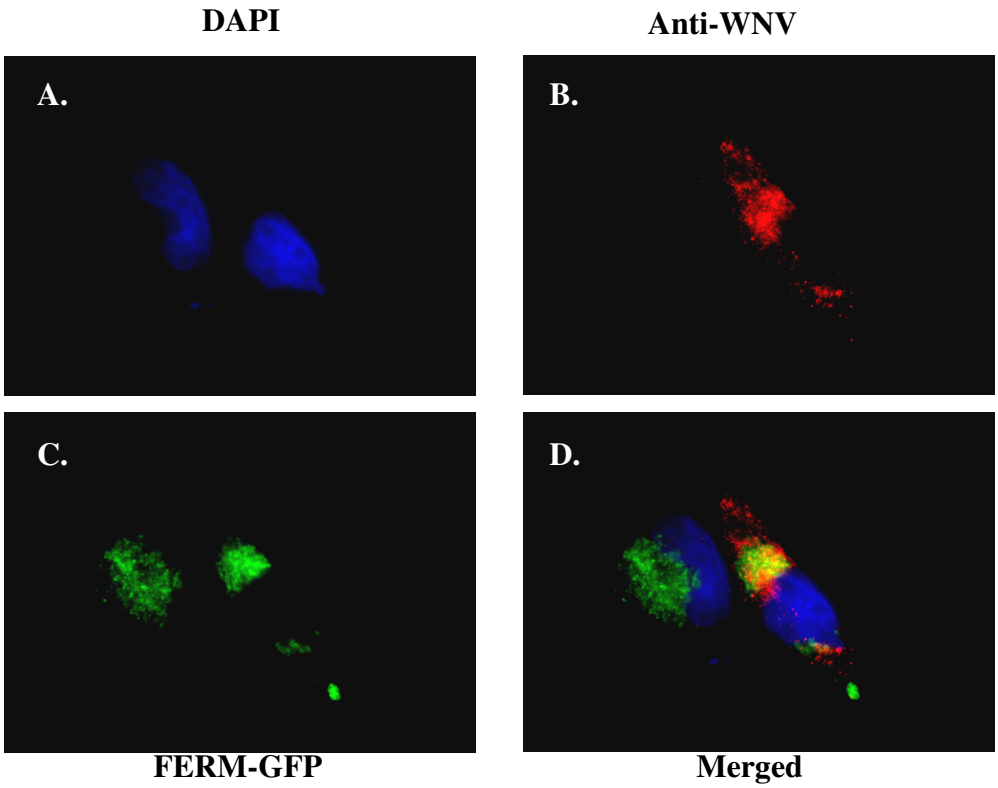

Figure 3-23. Immunofluorescence microscopy images of FERM-GFP and WNV association. A. Nuclei staining with DAPI. B. WNV is detected with rabbit anti-WNV and stained with goat anti-rabbit antibody conjugated with Alexa Fluor 594. WNV is localized near the perinuclear region. C. FERM-GFP vector was transfected into A172 cells and FERM-GFP was localized near the perinuclear region. D. Co-localizations of FERM-GFP (green) and the WNV (red) in infected A172 cells are represented in yellow at 0.5 h post infection.

3.3.7. FERM domain of FRMD4A regulate the level of phosphorylation of FAK tyrosine 397

Since FERM domain of FRMD4A colocalised with activated integrins that WNV mediated with to gain entry (Chu & Ng, 2004), it was hypothesized that FERM domain regulate the level of phosphorylation of FAK tyrosine 397, which could have resulted in the less permissive A172 cells to WNV. However, the level of phosphorylation in WNV-infected A172 cells transfected with plasmid expressing pre-*FRMD4A* miRNA (miF) and FERM-GFP showed insignificant fold difference

when compared to WNV-infected and mock-transfected A172 cells (WT) (Figure 3-24 & 3-25). There was only an approximately 0.2 fold increase in phosphorylation in miF as compared to WT (Figure 3-25). In addition, there was only an approximately 0.1 fold reduction in phosphorylation in FERM-GFP as compared to WT (Figure 3-25). Though the difference in the level of phosphorylation was not significant, the trend of phosphorylation in miF and FERM-GFP was as expected. The silencing of *FRMD4A* had resulted in an increase trend in the level of phosphorylation. On the other hand, the overexpression of FERM domain of FRMD4A had resulted in a decrease trend in the level of phosphorylation. The high level of activated FAK in WT was no surprising as FAK was overexpressed in many tumors including the brain (Natarajan *et al.,* 2003).

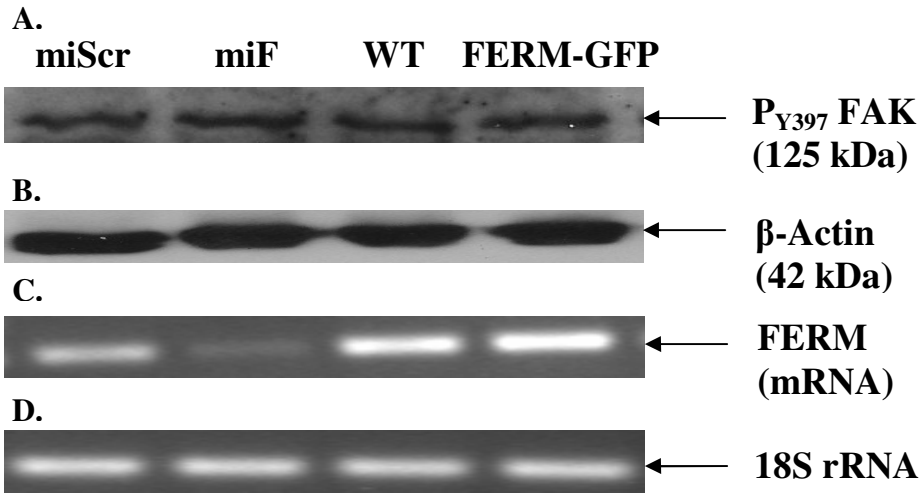

Figure 3-24. Phosphorylation of tyrosine 397 of Focal Adhesion Kinase (FAK) in WNV-infected A172 cells. A. The level of phosphorylation is compared among the following cells: i. WNV-infected A172 cells transfected with plasmid expressing pre-scramble miRNA (miScr); ii. WNV-infected A172 cells transfected with plasmid expressing pre-*FRMD4A* miRNA (miF); iii. WNV-infected and mock-transfected A172 cells (WT); iv. WNV-infected A172 cells transfected with plasmid expressing FERM-GFP (FERM-GFP).Both miF and FERM-GFP do not show significant difference in the degree of phosphorylation as compared to WT. B. Antibody against β-actin is used to ensure equal loading of the protein sample. C. FERM mRNA is semi-quantitated with reverse transcription PCR (RT-PCR) to ensure the effect of silencing and overexpression is present, respectively. D. RT-PCR is used to semi-quantitate the concentration of 18S rRNA to ensure equal loading of total cDNA sample loaded.

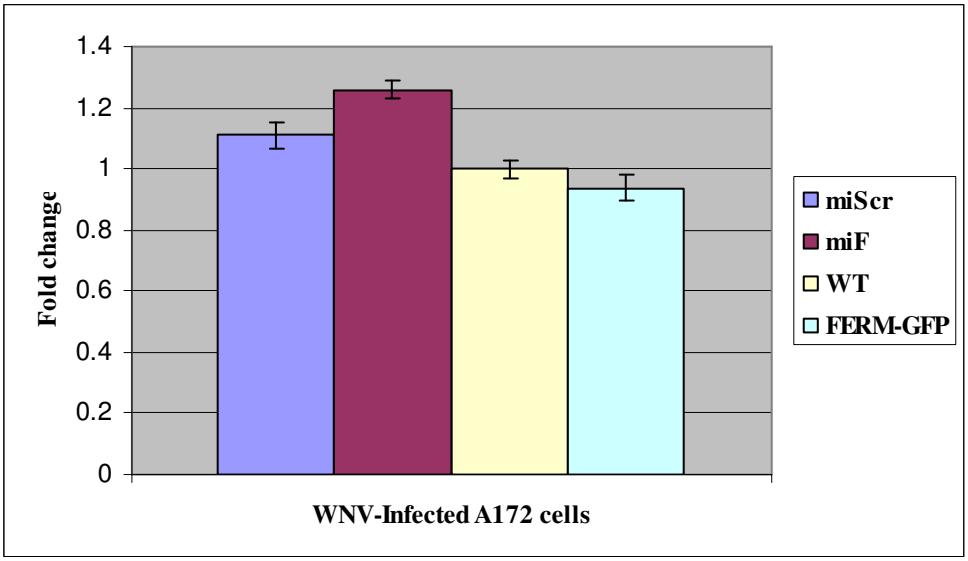

Figure 3-25. Semi-quantitation of FAK tyrosine 397 phosphorylation in the following cells: i. WNV-infected A172 cells transfected with plasmid expressing pre-scramble miRNA (miScr); ii. WNV-infected A172 cells transfected with plasmid expressing pre-*FRMD4A* miRNA (miF); iii. WNV-infected and mock-transfected A172 cells (WT); iv. WNV-infected A172 cells transfected with plasmid expressing FERM-GFP (FERM-GFP).

Chapter 4.

DISCUSSION & CONCLUSION

Differential West Nile virus (WNV) infection is known to occur in different cell types, depending on the permissiveness of the cell types to WNV. However, the mechanism of permissiveness is poorly understood. It has been reported that microglial cells are poorly permissive to WNV infection even though they may still influence the neuropathogenesis of WNV infection (Cheeren *et al.,* 2005). The higher resistance of microglial cells may explain the infrequent development of encephalitis in WNV infection. Hence, it is important to understand the mechanism behind this differential infection as it may help to explain the clinical manifestations of WNV infection. This differential infection most likely involves host-virus interactions that affect the virus entry, replication or assembly.

This study is based on the observation that A172 cells, a type of glioblastoma cells of central nervous system origin, was not as permissive or susceptible as HeLa cells to WNV infection (Figure 3-1). This provides a suitable platform to investigate the lesser permissivity of cells to WNV. The difference in permissivity could be due to the presence and the number of high affinity receptors for the virus particles as well as the presence of anti-viral factors in the cells. From the overall result of a previous genomic microarray study comparing the transcriptional level of host genes between WNV-infected A172 cells and WNV-infected HeLa cells (Koh & Ng, 2004), *FRMD4A* was found to have the highest differential expression among the genes selected (Figure 3-5A & 3-9). This molecular approach was chosen because it is able

to provide a global analysis of large number of genes relevant to the molecular pathogenesis of WNV simultaneously.

It was observed that *FRMD4A* only expressed in A172 cells but not in HeLa cells (Figure 3-5A). The expression of *FRMD4A* was also not regulated significantly in the presence of virus infection (Figure 3-5A). This suggests that *FRMD4A* is a factor that neither the host nor the virus is able to manipulate its mRNA expression level. After transient silencing of *FRMD4A*, it was observed that the virus titre increased by 10 fold (Figure 3-13). This shows that *FRMD4A* has an anti-viral role in A172 cells.

FRMD4A is a relatively new member of the protein 4.1 superfamily. It was first identified in a human brain cDNA sequencing project and was named KIAA1294 (Nagase *et al.*, 2000). It has a coding sequence of 3509 base pairs which encodes a protein that has a 4.1 ezrin radixin moesin (FERM) domain at the N-terminus (Figure 3-16). The FERM domain of FRMD4A is similar to the FERM domain of talin, ezrin, radixin and moesin. This is based on the amino acid sequence homology comparison (Figure 3-17) and the lack of association with the actin filaments (Figure 3-21). Hence, this suggests that FERM domain of *FRMD4A* may have similar roles as talin, ezrin, radixin and moesin. The FERM domain-containing proteins have been associated with mediating intermolecular interactions between the transmembrane proteins such as cadherins and the cytoskeleton (Tsukita *et al.,* 1992). Since *FRMD4A* is postulated to be a membrane-cytoskeleton linker and has an anti-viral role, it is hypothesized that it may be involved in regulating the entry of WNV via the activated integrin pathway as described by Chu and Ng (2004b).

The trials of cloning the full-length *FRMD4A* were unsuccessful after months of attempts with various parameter changes such as PCR kits, primers and annealing temperatures. One likely explanation would be the 3kb *FRMD4A* is too long to amplify. However, the strategy of generating 3 sub-fragments of *FRMD4A* to form the full-length with different parameters was also unsuccessful except for the generation of the first sub-fragment. The first sub fragment is mainly the FERM domain. One possible alternative would be to purchase from private company which have the isolated full-length cDNA clone. It may be costly but it would be more effective.

From the clustering result of the FERM domain of FRMD4A and those integrin-binding FERM domain-containing proteins (Figure 3-18A), and the colocalisation of FRMD4A FERM domain with the activated integrins (Figure 3-22B), it was observed that FERM domain of FRMD4A had a close association with $\alpha_v\beta_3$ integrins in WNV-infected A172 cells. Furthermore, FERM domain of FRMD4A did not have close association with activated $\alpha_v\beta_3$ integrins when it is not infected with WNV (Figure 3-22A). Hence, it was postulated that close association of the FERM domain with activated integrins required a feedback from the host after being infected with WNV. In addition, WNV may have a role in regulating this feedback by associating with FERM domain (Figure 3-23). From the clustering results, it was shown that FERM domain of FRMD4A may compete with FAK binding to the activated integrins and involve in 'inside-out' signaling like TALIN (Calderwood *et al.,* 2002) and RADIXIN (Tang *et al.,* 2007) (Figure 3-18).

Collectively, with all these preliminary results, an anti-viral mechanism that regulates the WNV entry into A172 cells is proposed. During normal cell state (Figure

4-1A), integrins are activated, leading to the recruitment and the autophosphorylation of FAK. This leads to the activation of FAK-Src signaling process which results in actin polymerisation required for cell survival and proliferation (Parsons, 2003). FRMD4A at this stage is postulated to be inactivated and localised near the perinuclear region. The inactivated FRMD4A may be due to the intramolecular autoinhibitory interaction where the C-terminal of the protein folds and binds to the FERM domain at the N-terminal, similar to other FERM domain-containing proteins such as FAK (Lietha *et al.,* 2007).

During the early WNV infection (Figure 4-1B), interaction of WNV with integrin mediates virus entry. The autophosphorylation of FAK in response to virus integrin engagement leads to the formation of phosphotyrosine docking sites for several classes of signaling molecules. This is necessary for the recruitment and activation of the downstream signaling molecules and signaling complexes that eventually lead to the triggering of actin assembly followed by the process of clathrin-mediated endocytosis of WNV particles (Chu and Ng, 2004). In response to the invasion of WNV, the host cells activate an anti-viral mechanism involving FRMD4A during this early infection (Figure 4-1B). As hypothesized, there may a feedback mechanism in the process of WNV entry that activates and disperses the FRMD4A to the surrounding perinuclear region (Figure 3-22B). FRMD4A may then bind competitively to the activated integrins and inhibits the FAK from binding to the integrin. As a result, this may indirectly hinders the process of clathrin-mediated endocytosis of WNV particles via the WNV-activated integrin mediated pathway (Figure 4-1B), and hence, resulting in the less permissive A172 cells to WNV infection.

This proposed anti-viral mechanism may still hold even though the difference in level of FAK tyrosine 397 phosphorylation is not too significant in transient *FRMD4A*-silenced A172 cells and FERM domain-overexpressed A172 cells (Figure 3-24 & 3-25). The small difference may be due to the higher intensity of endogenous FAK autophosphorylation (Natarajan *et al.,* 2003) as compared to the lower intensity of FRMD4A competitively binding to activated integrins in response to WNV infection. This may explain the consistent observation of WNV infection albeit at a lower level. Even though FRMD4A is postulated to resist WNV entry into A172 cells via the activated integrin pathway as the primary entry mechanism, the virus can also still gain entry via other mechanisms such as cholesterol-rich membrane microdomain (Medigeshi *et al.,* 2008).

Microglial cells, which are also poorly permissive to WNV growth, are best represented by A172 cells in this study. Activated microglial cells produce proinflammatory cytokines and chemokines upon infection by WNV as an immediate immune defence response against WNV. However, overproduction of cytokines

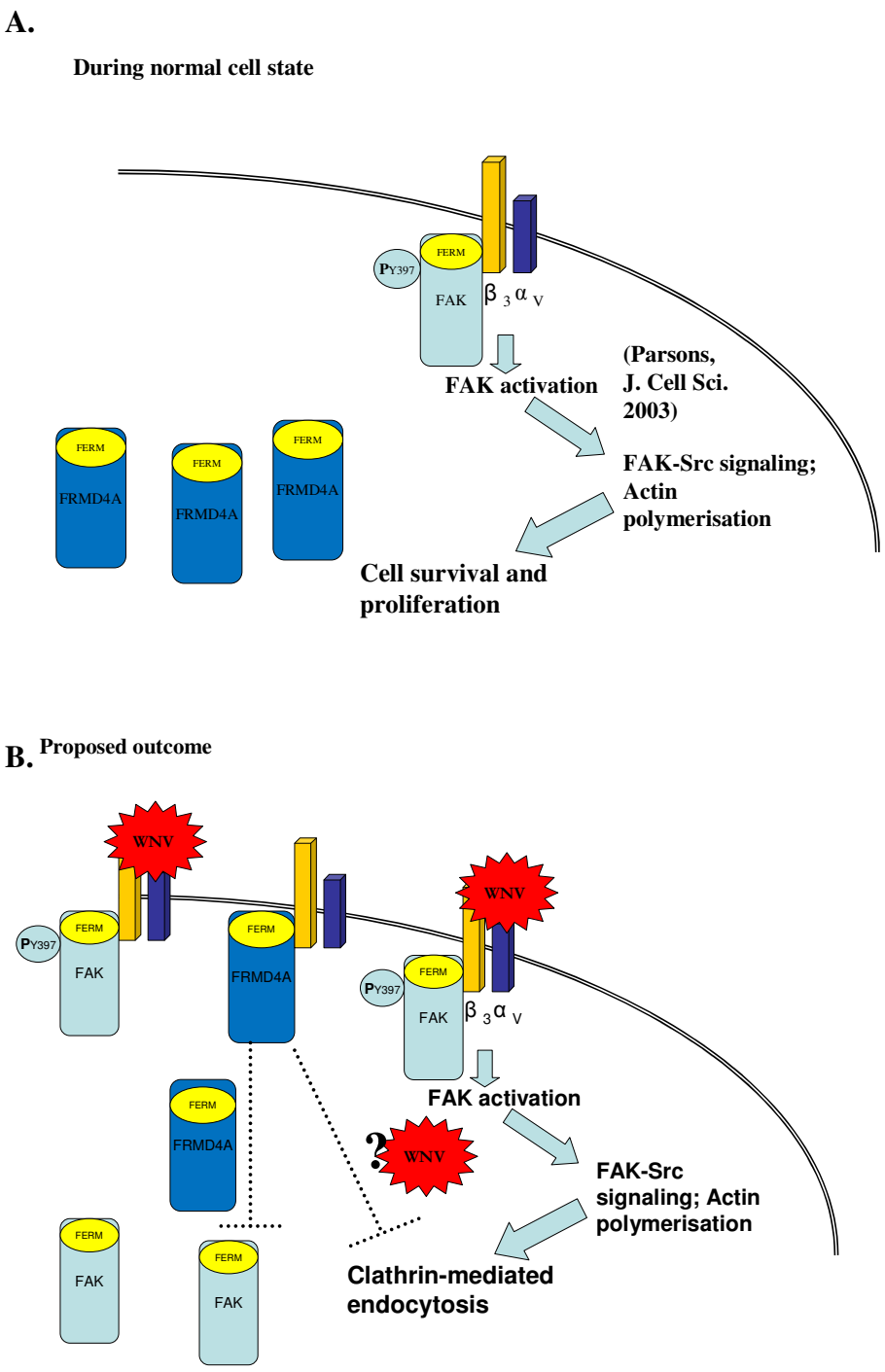

Figure 4-1. A cartoon of the proposed mechanism that regulates the WNV entry in WNV-infected A172. A. The roles and function of FAK at normal cell state. B. The roles and function of FAK and FRMD4A and the proposed outcome of the recruitment of FRMD4A to bind competitively to the integrins.

including TNF-α and IL-6 enhances neuronal injury (Meda *et al.,* 1995; Jeohn *et al.,* 1998). As such, activated microglial cells influence the neuropathogenesis of WNV

infection (Cheeren *et al.,* 2005). Hence, inhibition of WNV infection may be induced by FRMD4A regulating WNV entry into cells, together with the production of proinflammatory molecules. On the other hand, prolonged resistance in A172 cells may contribute to overproduction of proinflammatory cytokines leading to inflammation-induced cell death with resultant encephalitis. More studies such as time course/live confocal microscopy, co-immunoprecipitation, yeast-two hybrid and biochemical assays are required to confirm these preliminary findings. In addition, ELISA kit for detection of human phosphorylated (Tyr 397) FAK can be used to quantitatively evaluate the degree of phosphorylation in transient *FRMD4A*-silenced A172 cells and FERM domain-overexpressed A172 cells.

FRMD4A was postulated to play a role in regulating WNV entry. It is a potential anti-viral factor that is neither regulated by the host nor the virus. The FERM domain is strongly associated with activated integrins and is postulated to bind competitively to integrins and thus, inhibiting FAK binding to integrin during WNV infection. As a result, it prevents the integrin activated clathrin-mediated endocytosis of WNV into A172 cells. On this scenario, A172 cells become less permissive to WNV infection compare to cells such as HeLa cells which do not possess FRMD4A. Similarly to microglial cells, FRMD4A is likely to influence the neuropathogenesis of WNV infection.

References

Andrews DM, Matthews VB, Sammels LM. 1999. The severity of Murray Valley encephalitis in mice is linked to neutrophil infiltration and inducible nitric oxide synthetase activity in the central nervous system. *J Virol.* **73**:8781-8790.

Arturo LA, Fratkin J, Stokic DS, Harrington T, Webb RM, Slavinsky SA. 2003. West Nile poliomyelitis. *Lancet Infect Dis.* **3**:9-10.

Bartel DP. 2004. MicroRNAs: genomics, biogenesis, mechanism, and function. *Cell* **116**:281-297.

Bernard KA, Maffei JG, Jones SA, Kauffman EB, Ebel GD. 2001. West Nile virus infection in birds and mosquitoes, New York State, 2000. *Emerg Infect Dis.* **7**:679-685.

Beasley DW, Davis CT, Whiteman M, Granwehr B, Kinney RM, Barrett AD. 2004. Molecular determinants of virulence of West Nile virus in North America. *Arch Virol Suppl.* **18**:35-41.

Berthet FX, Zeller HG, Drouet MT, Rauzier J, Digoutte JP, Deubel V. 1997. Extensive nucleotide changes and deletions within the envelope glycoprotein gene of Euro-African West Nile viruses. *J Gen Virol.* **78**:2293-2297.

Bohnsack MT, Czaplinski K, Gorlich D. 2004. Exportin 5 is a RanGTP-dependent dsRNAbinding protein that mediates nuclear export of pre-miRNAs. *RNA* **10**:185-191.

Bompard G, Martin M, Roy C, Vignon F, Freiss G. 2003. Membrane targeting of protein tyrosine □hosphatases PTPL1 through its FERM domain via binding to phosphatidylinositol 4, 5-biphosphate. *J Cell Sci.* **116**:2519-2530.

Bretscher A, Edwards K, Fehon RG. 2002. ERM proteins and merlin:

integrators at the cell cortex. *Nat Rev Mol Cell Biol.* **3**:586-599.

Briese T, Glass WG, Lipkin WI. 2000. Detection of West Nile virus sequences in cerebrospinal fluid. *Lancet.* **355**:1614-1615.

Briese T, Rambaut A, Pathmajeyan M, Bishara J, Weinberger M, Pitlik S, Lipkin WI. 2002. Phylogenetic analysis of a human isolate from the 2000 Israel West Nile virus epidemic. *Emerg Infect Dis.* **8**:528-531.

Brinton MA. 1986. Replication of flaviviruses. In: Schlesinger S, Schlesinger M, editors. *Togaviridae and Flaviridae* The Viruses. Plenum, New York. Pp.329-376.

Brinton MA. 2002. The molecular biology of West Nile Virus: A new invader of the Western Hemisphere. *Annu Rev Microbiol.* **56**:371-402.

Burke DS, Monath TP. 2001. Flaviviruses. In *Fields Virology,* ed. Knipe DM, Howley PM. Philadelphia: Lippin-cott, Williams & Wilkins. 4th ed., pp.1043-1125.

Calderwood DA, Yan B, Pereda JM, Alvarez BG, Fujioka Y, Liddington RC, Ginsberg MH. 2002. The Phosphotyrosine Binding-like Domain of Talin Activates Integrins. *J Biol Chem.* **277**:21749-21758.

Calisher CH, Karabatsos N, Dalrymple JM, Shope RE, Porterfield JS. 1989. Antigenic relationships between flaviviruses as determined by cross-neutralization tests with polyclonal antisera. *J Gen Virol.* **70**:37-43.

Cantile C, Del Piero F, Di Guardo G, Arispici M. 2001. Pathologic and immunohistochemical findings in naturally occurring West Nile virus infection in horses. *Vet Pathol.* **38**:414–421.

Catteau A, Kalinina O, Wagner MC, Deubel V, Courageot MP, Despres P.

2003. Dengue virus M protein contains a proapoptotic sequence referred to as ApoptoM. *J Gen Virol.* **84**:2781–2793.

Ceccaldi PE, Lucas M, Despres P. 2004. New insights on the neuropathogenicity of West Nile virus. *FEMS Microbiol Lett.* **233**:1-6.

Celis JE, Kruhoffer M, Gromova I, Frederiksen C, Ostergaard M, Thykjaer T, Gromov P, Yu J, Palsdottir H, Magnusson N, Orntoft TF. 2000. Gene expression profiling: monitoring transcription and translation products using DNA microarrays and proteomics. *FEBS Lett.* **480**:2-16.

Cheeran MC, **Hu S**, **Sheng WS**, **Rashid A**, **Peterson PK**, **Lokensgard JR. 2005.** Differential responses of human brain cells to West Nile virus infection. *J Neurovirol.* **11**:512-524.

Chishti AH, **Kim AC**, **Marfatia SM**, **Lutchman M**, **Hanspal M**, **Jindal H**, **Liu SC**, **Low PS**, **Rouleau GA**, **Mohandas N**, **Chasis JA**, **Conboy JG**, **Gascard P**, **Takakuwa Y**, **Huang SC**, **Benz EJ Jr**, **Bretscher A**, **Fehon RG**, **Gusella JF**, **Ramesh V**, **Solomon F**, **Marchesi VT**, **Tsukita S**, **Tsukita S**, **Hoover KB, Louvard D, tonks NK, Anderson, JM, Fanning AS, Bryant PJ, Woods DF. 1998.** The FERM domain: a unique module involved in the linkage of cytoplasmic proteins to the membrane. *TIBS.* **23**:281-282.

Chowers MY, Lang R, Nasser F, David D, Giladi M. 2001. Clinical characteristics of the West Nile fever outbreak, Israel 2000. *Emerg Infect Dis.* **7**:611-614.

Chu JJH, Ng ML. 2002a. Infection of polarized epithelial cells with flavivirus West Nile: polarized entry and egress of virus occur through the apical surface. *J Gen Virol.* **83**:2427-2435.

Chu JJH, Ng ML. 2002b. Trafficking mechanism of West Nile (Sarafend) virus structural proteins. *J Med Virol.* **67**:127-136.

Chu JJH, Ng ML. 2003a. Characterization of a 105-kDa plasma membrane associated glycoprotein that is involved in West Nile virus binding and infection. *Virology.* **312**:458-469.

Chu JJH, Ng ML. 2003b. Actin filaments participate in West Nile (Sarafend) virus maturation process. *J Med Virol.* **71**:463–471.

Chu JJ, Ng ML. 2004b. Interaction of West Nile virus with $\alpha_V\beta_3$ integrin mediates virus entry into cells. *J Biol Chem.* **279**:54533-54541.

Cullen BR. 2004. Transcription and processing of human microRNA precursors. *Mol Cell.* **16**:861-865.

Daffis S, Samuel MA, Keller BC, Gale M Jr, Diamond MS. 2007. Cell-specific IRF-3 responses protect against West Nile virus infection by interferon-dependent and –independent mechanisms. *Plos Pathog.* **3**:e106.

Daffis S, Samuel MA, Suthar MS, Keller BC, Gale M Jr, Diamond MS. 2008. Interferon regulatory factor (IRF)-7 induces the antiviral interferon (IFN)-(alpha) response and protects against lethal West Nile virus infection. *J Virol.* **82**:8465-8475.

Davis WG, Blackwell JL, Shi PY, Brinton MA. 2007. Interaction between the cellular protein eEF1A and the 3'-terminal stem-loop of West Nile virus genomic RNA facilitates viral minus-strand RNA synthesis. *J Virol.* **81**:10172-10187.

Despres P, Fiamand M, Ceccaldi PE. 1996. Human isolates of dengue type 1 induce apoptosis in mouse neuroblastoma cells. *J Virol.* **70**:4090-4096.

Douglas MW, Kesson AM, King NJC. 1994. CTL recognition of West Nile virus-infected fibroblasts is cell cycle dependent and is associated with virus-induced increases in class I MHC antigen expression. *Immunology.* **82**:561-570.

Dunster LM, Gibson CA, Stephenson JR, Minor PD, Barrett AD. 1990. Attenuation of virulence of flavivirus following passage in HeLa cells. *J Gen Virol.* **71**:601-607.

Emmara MM, Brinton MA. 2007. Interaction of TIA-1/TIAR with West Nile and Dengue virus products in infected cells interferes with stress granule formation and processing body assembly. *Proc Natl Acad Sci USA.* **104**:9041-9046.

Fredericksen BL, **Keller BC**, **Fornek J**, **Katze MG**, **Gale M Jr. 2008.** Establishment and maintenance of the innate antiviral response to West Nile Virus involves both RIG-I and MDA5 signaling through IPS-1. *J Virol.* **82**:609-616.

Gary R, Bretscher A. 1995. Ezrin self-association involves binding of an N-terminal domain to a normally masked C-terminal domain that includes the F-actin binding site. *Mol Bio Cell.* **6**:1061-1075.

Gautreau A, Poullet P, Louvard D, Arpin, M. 1999. Ezrin, a plasma membrane-microfilament linker, signals cell survival through the phosphatidylinositol 3-kinase/Akt pathway. *Proc Natl Acad Sci USA.* 96: 7300–7305.

Giard DJ, Aaronson SA, Todaro GJ, Arnstein P, Kersey JH, Dosik H, Parks WP. 1973. *In vitro* cultivation of human tumors: establishment of cell lines derived from a series of solid tumors. *J Natl Cancer Inst.* **51**:1417-1423.

Giladi M, Metzkor-Cotter E, Martin DA, Siegman-Igra Y, Korczyn AD, Rosso R, Berger SA, Campbell GL, Lanciotti RS. 2001. West Nile encephalitis in Israel, 1999: the New York connection. *Emerg Infect Dis.* **7**:654–658.

Gubler DJ. 2007. The continuing spread of West Nile virus in the Western Hemisphere. *Clin Infect Dis.* **45**:1039–1046.

Gubler DJ, Kuno G, Markoff L. 2007. Flaviviruses. In: Knipe DM, Howley PM, eds. Fields virology, 5th ed. Philadelphia: Lippincott, Williams & Wilkins: pp 1153–1252.

Hamada K, Shimizu T, Matsui T, Tsukita S, Hakoshima T. 2000. Structural basis of the membrane-targeting and unmasking mechanisms of the radixin FERM domain. *EMBO J.* **19**: 4449-4462.

Hase T, Summers PL, Eckels KH, Baze WB. 1989. Maturation process of Japanese encephalitis virus in cultured mosquito cells *in vitro* and mouse brain cells *in vivo*. *Arch Virol.* **96**:135-151.

Hayes EB, Gubler DJ. 2006. West Nile virus: epidemiology and clinical features of an emerging epidemic in the United States. *Ann Rev Med.* **57**:181–194.

Hayes EB, O'Leary DR. 2004. West Nile virus infection: a pediatric perspective. *Pediatrics.* **113**:1375-1381.

Heinz FX, Allison SL. 2000. Structures and mechanisms in flavivirus fusion. *Adv Virus Res.* **55**:231-269.

Heinz FX, Roehrig JT. 1990. Flaviviruses in *Immuno-chemistry of Viruses II. The basis for Serodiagnosis and Vaccines.* MHV can Regenmortel and AR

Neurath, Eds. Elsevier, Amsterdam. Pp 289-305.

Heinz FX, Stiasny K, Puschner-Auer G, Holzmann H, Allison SL. 1994. Structural changes and functional control of the tick-borne encephalitis virus glycoprotein E by the heterodimeric association with protein prM. *Virology.* **198**:109-117.

Hilkens C, Is'harc H, Lillemeier BF, Strobl B, Bates PA, Behrmann I, Kerr IM. 2001. A region encompassing the FERM domain of Jak1 is necessary for binding to the cytokine receptor gp130. *FEBS.* **55**:87-91.

Hsu EC, Lin YC, Hung CS, Huang CJ, Lee MY, Yang SC, Ting LP. 2007. Suppression of hepatitis B viral gene expression by protein-tyrosine phosphatases PTPN3. *J Biomed Sci.* **14**:731-744.

Hunt TA, **Urbanowski MD**, **Kakani K**, **Law LM**, **Brinton MA**, **Hobman TC. 2007.** Interactions between the West Nile virus capsid protein and the host cell-encoded non-structure inhibitor, I2PP2A. *Cell Microbiol.* **9**:2756-2766.

Hunter, KW. 2004. Ezrin, a key component in tumor metastasis. *Trends Mol Med.* **10**:201–204.

Hurlbut HS, Rizk F, Taylor RM, Work TH. 1956. A study of the ecology of West Nile virus in Egypt. *Am J Trop Med.* **5**:579–620.

Ilkal MA, Mavale MS, Prasanna Y, Jacob PG, Geevarghese G. 1997. Experiment studies on the vector potential of certain *Culex* species to West Nile Virus. *Indian J Med Res.* **106**:225-228.

Jia XY, Briese T, Jordan I, Rambaut A, Chi HC, Mackenzie JS, Hall RA, Scherret J, Lipkin WI. 1999. Genetic analysis of West Nile New York 1999 encephalitis virus. *Lancet.* **354**:1971-1972.

Kanai R, Kar K, Anthony K, Gould LH, Ledizet M, Fikrig E, Marasco WA, Koski RA, Modis Y. 2006. Crystal structure of West Nile virus envelope glycoprotein reveals viral surface epitopes. *J Virol.* **80**:11000-11008.

Kesson, AM, King NJ. 2001. Transcriptional regulation of major histocompatibility complex class I by flavivirus West Nile is dependent on NF-kappa B activiation. *J Infect Dis.* **15**:947-954.

King NJC, Mullbacher A, Tian L, Rodger J, Lidbury B, Tha Hla R. 1993. West Nile virus infection induces susceptibility of *in vitro* outgrowth murine blastocysts to specific lysis by parentally directed alloimmune and virus-immune cytotoxic T cells. *J Reprod Immunol.* **23**:131-144.

Ko KK, Igarashi A, Fukai K. 1979. Electron microscopic observations on *Aedes albopictus* cells infected with dengue viruses. *Arch Virol.* **62**:41-52.

Kobayashi H, Sagara J, Kurita H, Morifuji M, Ohishi M, Kurashina K, Taniguchi S. 2004. Clinical significance of cellular distribution of moesin in patients with oral squamous cell carcinoma. *Clin Cancer Res.* **10**:572–580.

Koh WL, Ng ML. 2005. Molecular Mechanisms of West Nile virus pathogenesis in brain cell. Emerging Infectious Diseases. **11**:629-632.

Lanciotti RS, Ebel GD, Deubel V, Kerst AJ, Murri S, Meyer R, Bowen M, McKinney N, Morrill WE, Crabtree MB, Kramer LD, Roehrig JT. 2002. Complete genome sequences and phylogenetic analysis of West Nile virus strains isolated from the United States, Europe, and the Middle East. *Virology.* **298**:96-105.

Lee HS, **Bellin RM**, **Walker DL**, **Patel B**, **Powers P**, **Liu H**, **Garcia-Alvarez B**, **de Pereda JM**, **Liddington RC**, **Volkmann N**, **Hanein D**, **Critchley DR**,

Robson RM. 2004a. Characterization of an actin-binding site within the talin FERM domain. *J Mol Bio.* **343**:771-784.

Lee Y, Kim M, Han J, Yeom KH, Lee S, Baek SH, Kim VN. 2004b. MicroRNA genes are transcribed by RNA polymerase II. *EMBO J.* **23**:4051-4060.

Leyssen P, De Clercq E, Neyts J. 2008. Molecular strategies to inhibit the replication of RNA viruses. *Antiviral Res.* **78**:9–25.

Li L, **Lok SM**, **Yu IM**, **Zhang Y**, **Kuhn RJ**, **Chen J**, **Rossmann MG. 2008.** The flavivirus precursor membrane-envelope protein complex: structure and maturation. *Science.* **319**:1830-1834.

Li J, Loeb JA, Shy ME, Aashit KS, Tselis AC, Kupski WJ, Lewis RA. 2003. Asymmetric flaccid paralysis: a neuromuscular presentation of West Nile virus infection. *Ann Neurol.* **53**:703–710.

Lietha D, Cai X, Ceccarelli DF, Li Y, Schaller MD. 2007. Structural basis for the autoinhibition of focal adhesion kinase. *Cell.* **129**:1177–1187.

Lindenbach BD, Rice CM. 1999. Genetic interaction of flavivirus non-structural proteins NS1 and NS4A as a determinant of replicase function. *J Virol.* **73**:4611-4621.

Livak KJ, Schmittgen TD. 2001. Analysis of relative gene expression using real-time quantitative PCR and the $2^{-\Delta\Delta C}{}_{T}$ method. *Methods.* **25**:402-408.

Lucas M, Mashimo T, Frenkiel MP, Simon-Chazottes D, Montagutelli X, Ceccaldi PE, Guenet JL, Despres P. 2003. Infection of mouse neurons by West Nile virus is modulated by the interferon-inducible 2'-5' oligoadenylate synthetase 1b protein. *Immunol Cell Biol.* **81**:230-236.

Mackenzie JS, Barrett AD, Deubel V. 2002. The Japanese encephalitis serological group of flaviviruses: a brief introduction to the group. *Curr Top Microbiol Immunol.* **267**:1-10.

Manger ID, Relman DM. 2000. How the host 'sees' pathogens: global gene expression responses to infection. *Curr Opin Immunol.* **12**:215-218.

Marsh M, McMahon HT. 1999. The structural era of endocytosis. *Science*. **85**:215-220.

Martina BE, **Koraka P**, **van den Doel P**, **Rimmelzwaan GF**, **Haagmans BL**, **Osterhaus AD. 2008.** DC-SIGN enhances infection of cells with glycosylated West Nile virus in vitro and virus replication in human dendritic cells induces production of IFN-alpha and TNF-alpha. *J Virol.* **135**:64-71.

Mason PW. 1989. Maturation of Japanese encephalitis virus glycoproteins produced by infected mammalian and mosquito cells. *Virology.* **169**:354-364.

Masters JR. 2002. HeLa cells 50 years on: the good, the bad and the ugly. *Nat Rev Cancer.* **2**:315-319.

Matsumura T, Shiraki K, Sashikata T, Hotta S. 1977. Morphogenesis of dengue-1 virus in cultures of a human leukemic leukocyte line (J-111). *Microbiol Immunol.* **21**:329-334.

McManus MT, Sharp PA. 2002. Gene Silencing in Mammals by Small Interfering RNAs. *Nature Rev Genet.* **3**:737-747.

Medigeshi GR, Hirsch AJ, Streblow DN, Nikolich-Zugich J, Nelson JA. 2008. West Nile virus entry requires cholesterol-rich membrane microdomains and is independent of alphavbeta3 integrin. *J Virol.* **82**:5212-5219.

Miller BR, Nasci RS, Godsey MS, Savage HM, Lutwama JJ. 2000. First field

evidence for natural vertical transmission of West Nile virus in *Culex uni-vittatus* complex mosquitoes from Rift Valley province. *Am J Trop Med Hyg.* **62**:240-246.

Modis Y, Ogata S, Clements D, Harrison SC. 2004. Structure of the dengue virus envelope protein after membrane fusion. *Nature.* **427**:313-319.

Mukhopadhyay S, Kuhn RJ, Rossmann MG. 2005. A structural perspective of the *Flavivirus* lifecycle. *Nat Rev Microbiol.* **3**:13-22.

Murgue B, Murri S, Triki H, Deubel V, Zeller HG. 2001. West Nile in the Mediterranean basin: 1950–2000. In: White DJ, Morse DL, eds. *West Nile virus, detection, surveillance and control.* New York: New York Academy of Sciences: pp117–126.

Murgue B, Zeller H, Deubel V. 2002. The ecology and epidemiology of West Nile virus in Africa, Europe, and Asia. In: MacKenzie JS, Barrett ADT, Deubel V, eds. *Japanese encephalitis and West Nile viruses.* Berlin: Springer-Verlag: pp195–221.

Murphy FA. 1980. Togavirus morphology and morphogenesis, in *The Togavirus. Biology, Structure, Replication.* Schlesinger RW (ed.) Academic Press, New York. pp 241-316.

Nagase T, Kikuno R, Ishikawa KI, Hirosawa M, Ohara O. 2000. Prediction of the coding sequences of unidentified human genes. XVI. The complete sequences of 150 new cDNA clones from brain which code for large proteins in vitro. *DNA Res.* **7**:65-73.

Natarajan M, Hecker TP, Gladson CL. 2003. FAK signaling in anaplastic astrocytoma and glioblastoma tumors. *Cancer J.* **9**:126-133.

Ng ML. 1987. Ultrastructural studies of Kunjin virus-infected *Aedes albopictus* cells. *J Gen Virol.* **68**:577-582.

Ng ML, Howe J, Sreenivasan V, Mulders JJ. 1994. Flavivirus West Nile (Sarafend) egress at the plasma membrane. *Arch Virol.* **137**:303-313.

Ng ML, Tan SH, Chu JJH. 2001. Transport and budding at two distinct sites of visible nucleocapsids of West Nile (Sarafend) virus. *J Med Virol.* **65**:758-764.

Nowak T, Farber PM, Wengler G, Wengler G. 1989. Analysis of the terminal sequences of West Nile virus structural proteins and of the *in vitro* translation of these proteins allow the proposal of a complete scheme of the proteolytic cleavages involved in their synthesis. *Virology.* **169**:365-376.

Omalu BI, Shakir AA, Wang G, Lipkin WI, Wiley CA. 2003. Fatal fulminant pan-meningo-polioencephalitis due to West Nile virus. *Brain Pathol*. **13**:465–472.

Paddison PJ, Caudy AA, Bernstein E, Hannon GJ, Conklin DS. 2002. Short Hairpin RNAs (shRNAs) Induce Sequence-Specific Silencing in Mammalian Cells. *Genes Dev.* **16**: 948-958.

Papin JF, Vahrson W, Dittmer D. 2004. SYBR green-based real-time quantitative PCR assay for detection of West Nile virus circumvents false-negative results due to strain variability. *J Clin Microbiol.* **42**:1511-1518.

Parquet MC, Kumatori A, Hasebe F, Morita K, Igarashi A. 2001. West Nile virus-induced bax-dependent apoptosis. *FEBS Lett.* **500**:17-24.

Parsons J. 2003. Focal adhesion kinase: the first ten years. *J Cell Sci.* **116**:1409-1416.

Petersen LR, Roehrig JT. 2001. West Nile Virus: a reemerging global

pathogen. *Emerg Infect Dis.* **7**:611-614.

Rozen S, Skaletsky HJ. 2000. Primer3 on the WWW for general users and for biologist programmers. In: Krawetz S, Misener S (eds) Bioinformatics Methods and Protocols: Methods in Molecular Biology. Humana Press, Totowa, NJ: pp 365-386.

Saha S, Rangarajan PN. 2003. Common host genes are activated in mouse brain by Japanese encephalitis and rabies virus. *J Gen Virol.* **84**:1729–1735.

Sampson BA, Ambrosi C, Charlot A, Reiber K, Veress JF. 2000. The pathology of human West Nile virus infection. *Human Pathol.* **31**:527-531.

Samuel MA, Diamond MS. 2005. Alpha/beta interferon protects against lethal West Nile virus infection by restricting cellular tropism and enhancing neuronal survival. *J Virol.* **79**:13350-13361.

Sangster MY, Heliams DB, Mackenzie JS, Shellam GR. 1993. Genetic studies of flavivirus resistance in inbred strains derived from wild mice: evidence for a new resistance allele at the flavivirus resistance locus (*Flv*). *J Virol.* **67**:340-347.

Schneider-Schaulies J. 2000. Cellular receptors for viruses: links to tropism and pathogenesis. *J Gen Virol.* **81**:1413–1429.

Seligman SJ, Bucher DJ. 2003. The importance of being outer: consequences of the distinction between the outer and inner surfaces of flavivirus glycoprotein E. *Trends Microbiol.* **11**:108-110.

Serrels B, Serrels A, Brunton VG, Mark H, McLean GW, Gray CH, Jones GE, Frame MC. 2007. Focal adhesion kinase controls actin assembly via a FERM-mediated interaction with the Arp2/3 complex. *Nat Cell Biol.* **9**:1046-1056.

Shen J, Devery JM, King NJ. 1995. Early induction of interferon-independent virus-specific ICAM-1 (CD54) expression by flavivirus in quiescent but not proliferating fibroblasts – implications for virus-host interactions. *Virology.* **208**:437-449.

Shen J, T-To SS, Schrieber L, King NJC. 1997. Early E-Selectin, VCAM-1, ICAM-1, and late MHC antigen induction on human endothelial cells by flavivirus and comodulation of adhesion molecule expression by immune cytokines. *J Virol.* **71**:9323-9332.

Shi PY. 2002. Strategies for the identification of inhibitors of West Nile virus and other flaviviruses. *Curr Opin Invest Drugs.* **3**:1567-1573.

Shrestha B, Gottlieb D, Diamond MS. 2003. Infection and injury of neurons by West Nile encephalitis virus. *J Virol.* **77**:13203–13213.

Silva MC, Guerrero-Plata A, Gilfoy FD, Garofalo RP, Mason PW. 2007. Differential activation of human monocyte-derived and plasmacytoid dendritic cells by West Nile virus generated in different host cells. *J Virol.* **81**:13640-13648.

Smithburn KC, Hughes TP, Burke AW, Paul JH. 1940. A neurotropic virus isolated from the blood of a native of Uganda. *Am J Trop Hyg.* **20**:471-492.

Solomon TJ, Winter PM. 2004. Neurovirulence and host factors in flavivirus encephalitis-evidence from clinical epidemiology. *Arch Virol Suppl.* **18**:161-170.

Sriurairatna S, Bhamarapravati N. 1977. Replication of dengue-2 virus in *Aedes albopictus* mosquitoes. An electron microscopy study. *Am J Trop Med Hyg.* **26**:1199-1205.

Stadler K, Allison SL, Schalich J, Heinz FX. 1997. Proteolytic activation of

tick-borne encephalitis virus by furin. *J Virol.* **71**:8475-8481.

Steele KE, Linn MJ, Schoepp RJ, Komar N, Geisbert TW, Manduca RM, Calle PP, Rapahel BP, Clippinger TL, Larsen T, Smith J, Lanciotti RS, Panella NA McNamara TS. 2000. Pathology of fatal West Nile virus infections in native and exotic birds during the 1999. *Vet Pathol.* **37**:208-224.

Tanentzapf G, Brown NH. 2006. An interaction between integrin and the talin FERM domain mediates integrin activation but not linkage to the cytoskeleton. *Nat Cell Biol.* **6**:601-606.

Tang P, Cao C, Xu M, Zhang L. 2007. Cytoskeletal protein radixin activates integrin alpha(M)beta(2) by binding to its cytoplasmic tail. *FEBS Lett.* **586**:1103-1108.

Tsukita SH, Tsukita SA, Nagafuchi A and Yonemura S. 1992. Molecular linkage between cadherins and actin filaments in cell-to-cell adherens junctions. *Curr Opin Cell Biol.* **4**:834-839.

Turell MJ, O'Guinn M, Oliver J. 2000. Potential for New York mosquitoes to transmit West Nile virus. *Am J Trop Med.* **62**:413-414.

Wang P, Dai J, Bai F, Kong KF, Wong SJ, Montgomery RR, Madri JA, Fikrig E. 2008a. Matrix metalloproteinase 9 facilitates West Nile virus entry into the brain. *J Virol.* **82**:8978-8985.

Wang S, Welte T, McGargill M, Town T, Thompson J, Anderson JF, Flavell RA, Fikrig E, Hedrick SM, Wang T. 2008b. Drak2 contributes to West Nile virus entry into the brain and lethal encephalitis. *J Immunol.* **181**:2084-2091.

Westaway EG, Ng ML. 1980. Replication of flaviviruses: Separation of membrane translation sites of Kunjin virus proteins and of cell proteins.

Virology. **106**:107-122.

Westaway EG, Mackenzie JM, Khromykh AA. 2002. Replication and gene function in Kunjin virus. *Curr Top Microbiol Immunol.* **267**:323-351.

Xiao SY, Guzman H, Zhang H, Travassos da Rosa AP, Tesh RB. 2001. West Nile virus infection in the golden hamster (Messocricetus auratus): a model for West Nile encephalitis. *Emerg Infect Dis.* **7**:714–721.

Yang JS, Ramanathan MP, Muthumani K, Choo AY, Jin SH, Yu QC, Hwang DS, Choo DK, Lee MD, Dang K, Tang W, Kim JJ, Weiner DB. 2002. Induction of inflammation by West Nile virus capsid through the caspase-9 apoptotic pathway. *Emerg Infect Dis.* **8**:1379-1384.

Yekta S, Shih IH, Bartel DP. 2004. MicroRNA-directed cleavage of HOXB8 mRNA. *Science.* **304**:594-596.

Yi R, Qin Y, Macara IG, Cullen BR. 2003. Exportin-5 mediates the nuclear export of premicroRNAs and short hairpin RNAs. *Genes Dev.* **17**:3011-3016.

Zeng Y, Yi R, Cullen BR. 2005. Recognition and cleavage of primary microRNA precursors by the nuclear processing enzyme Drosha. *EMBO J.* **24**:138-148.

Appendix 1: Media for Tissue Culture of Cell Lines

a) Dulbecco's Modified Eagle's Medium (DMEM): Growth Medium for HeLa and A172 Cells

Item	Amount	Source
DMEM Powder	17.3 g	Sigma, USA
$NaHCO_3$	2.2 g	Merck, Germany
Foetal Calf Serum (FCS)	100 ml	Hyclone, Switzerland
Autoclaved Type 1 Reagent Grade Water (E-pure)	900 ml	Barnstead, USA

One bottle of DMEM powder was dissolved in 900 ml of NANOpure water. 2.2 g of $NaHCO_3$ was then added and the pH adjusted to 7.2. Sterilization of media was carried out by filtration through a 0.22 μm filter (Sterivex G-S, Millipore, USA). The media was then stored in aliquots at 37 °C for two days to check for any contamination before storing in 4 °C.

b) RPMI-1640 Growth Medium for BHK Cells

Item	Amount	Source
RPMI Powder	16.4 g	Sigma, USA
$NaHCO_3$	2.2 g	Merck, Germany
Foetal Calf Serum (FCS)	100 ml	Hyclone, Switzerland
Autoclaved Type 1 Reagent Grade Water	900 ml	Barnstead, USA

(E-pure)		

One bottle of RPMI powder was dissolved in 900 ml of E-pure water. 2.2 g of $NaHCO_3$ was then added and the pH adjusted to 7.2. Sterilization of media was carried out by filtration through a 0.22 μm filter (Sterivex G-S, Millipore, USA). The media was then stored in aliquots at 37 °C for two days to check for any contamination before storing in 4 °C.

c) L-15 Growth Medium for C6/36 Cells

Item	**Amount**	**Source**
L-15 Powder	13.8 g	Sigma, USA
$NaHCO_3$	2.2 g	Merck, Germany
Foetal Calf Serum (FCS)	100 ml	Hyclone, Switzerland
Autoclaved Type 1 Reagent Grade Water (E-pure)	900 ml	Barnstead, USA

One bottle of L-15 powder was dissolved in 900 ml of E-pure water. 2.2 g of $NaHCO_3$ was then added and the pH adjusted to 7.2. Sterilization of media was carried out by filtration through a 0.22 μm filter (Sterivex G-S, Millipore, USA). The media was then stored in aliquots at 37 °C for two days to check for any contamination before storing in 4 °C.

d) Maintenance Medium (DMEM) for HeLa and A172 Cells, Maintenance Medium (RPMI) for BHK and Maintenance Medium (L-15) for C6/ 36

Item	**Amount**	**Source**
DMEM/ RPMI/ L-15 Powder	17.3g/16.4g/13.8g	Sigma, USA
Foetal Calf Serum	20 ml	Hyclone, Switzerland
$NaHCO_3$	2.2 g	Merck, Germany
Autoclaved Type 1 Reagent Grade Water (E-pure)	980 ml	Barnstead, USA

One bottle of the DMEM/RPMI/L-15 powder was dissolved in 980 ml of water, and 2.2 g of $NaHCO_3$ was then added. The pH was adjusted to 7.2 and sterilization was carried out by filtration through a 0.22 μm filter (Sterivex G-S, Millipore, USA). The media was then stored in aliquots at 37 °C for two days to check for any contamination before storing in 4 °C.

Appendix 2: Reagents for Subculturing of Cells

a) 10 X Phosphate Buffered Saline [(PBS) (pH7.4)]

Item	**Amount**	**Source**
NaCl	80.0 g	Merck, Germany
KCl	2.0 g	Merck, Germany
KH_2PO_4	2.0 g	Merck, Germany
Na_2HPO_4	11.5 g	Merck, Germany
Type 1 Reagent Grade Water (E-pure)	900 ml	Barnstead, USA

To prepare 10 X PBS stock solution, the specified items were added to 900 ml of E-pure water and the pH adjusted to 7.4. The solution was topped up to 1 litre and then autoclaved at 121 °C for 15 min. The stock solution was then stored at room temperature. To prepare the working 1 X PBS, the stock solution was diluted 1:10 with E-pure water. The solution was then autoclaved at 121 °C for 15 min and subsequently stored at 4 °C.

b) 10 X Trypsin/Versene (ATV) Solution

Item	**Amount**	**Source**
NaCl	80.0 g	Merck, Germany
KCl	4.0 g	Merck, Germany
D-glucose	10.0 g	Analar, UK
$NaHCO_3$	5.8 g	Merck, Germany
Trypsin	5.0 g	Difco, New Zealand
Versene (EDTA)	2 g	Sigma, USA
Autoclaved Type 1 Reagent Grade Water (E-pure)	90 ml	Barnstead, USA

The items were added to 90 ml of E-pure water and the mixture was heated to 30 °C with occasional shaking (for 3-4 hr) to dissolve the trypsin. The solution was topped up to 100 ml before filtered through a 0.22 μm filter (Sterivex G-S, Millipore, USA). Ten ml of this solution was added to 90 ml of sterile E-pure water to give 1 X ATV solution.

Appendix 3: Reagents for Infection of Cells & Plaque Assays

a) Hanks Medium (Virus Diluent)

Item	**Amount**	**Source**
Hank's Balanced Salt Solution	11.0 g	Sigma, USA
10 % Bovine Serum Albumin	1 ml	CSL, Australia
$NaHCO_3$	2.2 g	Merck, Germany
Autoclaved Type 1 Reagent Grade Water (E-pure)	99 ml	Barnstead, USA

All items were dissolved in the water to give 100 ml. The solution was sterilized by filtration through a 0.22 μm filter unit (Sterivex G-S, Millipore, USA). The media was then stored in aliquots at 37 °C for two days to check for any contamination before storing in 4 °C.

b) Overlay Medium

Item	**Amount**	**Source**
M199 Powder	11.0 g	Sigma, USA
Foetal Calf Serum	40 ml	Hyclone, Switzerland
$NaHCO_3$	4.4 g	Merck, Germany
Autoclaved Type 1 Reagent Grade Water (E- pure)	460 ml	Barnstead, USA

The reagents were dissolved in the water to produce a 2 X concentrate nutrient medium. Two hundred ml of this 2 X concentrate medium was added to an equal volume of 2.5 % carboxymethyl-cellulose solution (See Appendix 3d).

c) 1% Crystal Violet Staining Solution

Item	Amount	Source
Crystal Violet Powder	1.85 g	BDH, UK
37 % Formaldehyde	250 ml	Merck, Germany
PBS	120 ml	see Appendix 2a

d) 2.5% Carboxymethyl-Cellulose Solution

Item	Amount	Source
Sodium salt of Carboxymethyl-Cellulose	2.5 g	CalBiochem, USA
Type 1 Reagent Grade Water (NANOpure)	100 ml	Barnstead, USA

2.5 g of sodium salt of carboxymethyl-cellulose (Aquacide II, CalBiochem, USA) was added to 100 ml of the water. The solution was mixed, autoclaved for 15 min at 121 °C and stored at 4 °C.

Appendix 4: Reagent for Indirect Immunofluorescence Microscopy

a) 10% Bovine Serum Albumin (BSA)

Item	Amount	Source
Bovine serum albumin powder, Fraction V	10 g	Gibco BRL, USA
PBS	100 ml	see Appendix 1g
Glycerol	9 ml	Merck, Germany

The solution was aliquoted and stored at –20 °C. To obtain 0.1% BSA, 1 ml of 10% BSA was diluted in 100 ml of PBS.

Appendix 5: Reagents for Molecular Biology Techniques

a) LB (Luria-Bertani) Medium & Plates

Item	Amount	Source
Tryptone	10 g	Oxoid, United kingdom
Yeast extract	5 g	Oxoid, United kingdom
NaCl	10 g	Merck, Germany
Type 1 Reagent Grade Water (E-pure)	950 ml	Barnstead, USA
Molecular grade agarose powder (only necessary when making LB plates)	15 g	Biorad Laboratories, Singapore

The pH of the solution was adjusted to 7.0 with NaOH, followed by autoclaving on liquid cycle for 20 min at 15 psi. Antibiotic was added after the solution had cooled to around 55 °C. This was followed by pouring the LB-agar into the 10 cm plates and stored at 4 °C after it had harden.

b) Diethylpyrocarbonate (DEPC) Treated ddH_2O

Item	Amount	Source
Diethylpyrocarbonate (DEPC)	1.0 ml	Sigma, USA
Type 1 Reagent Grade Water (E-pure)	999 ml	Barnstead, USA

To make 1 litre of DEPC treated (RNase-free) water, 1ml of DEPC was added to 999 ml of water. The treated water was incubated overnight at room temperature with stirring. The water was then autoclaved at 121 °C for 15 min.

c) Ethidium Bromide (EtBr)

Item	**Amount**	**Source**
Ethidium Bromide (EtBr)	0.2 g	Sigma, USA
DEPC Water	20 ml	see Appendix 5b

EtBr was dissolved in 20 ml of DEPC water by stirring with a magnetic stirrer at room temperature for several hours. The solution was then stored in the dark at 4°C.

d) 10x Formaldehyde-Agarose (FA) Gel Buffer

Item	**Amount**	**Source**
200 mM 3-[N-morpholino]propanesulfonic acid (MOPS) (free acid)	41.86 g	Sigma, USA
50 mM Sodium acetate	4.1 g	Merck, Germany
10 mM EDTA	2.9 g	Merck, Germany
DEPC Water	to 1000 ml	see Appendix 5b

The pH of the buffer was adjusted to 7.0 with NaOH.

e) FA Gel

Item	**Amount**	**Source**
Agarose	1.2 g	BioRad Laboratories, Singapore
10 X FA Gel Buffer	10 ml	see Appendix 1o
37 % (12.3M) Formaldehyde	1.8 ml	Sigma, USA

Ethidium Bromide (10µg/ml)	1 µl	see Appendix 5c
DEPC Water	90 ml	see Appendix 5b

The agarose and 10 X FA gel buffer was mixed and topped up to 100 ml with DEPC water. It was then swirled and microwaved until completely dissolved. Formaldehyde and ethidium bromide was then added and mixed at 60 °C.

f) 1x Formaldehyde-Agarose (FA) Gel Running Buffer

Item	**Amount**	**Source**
10x FA Gel Buffer	100 ml	see Appendix 5d
37% (12.3M) Formaldehyde	20 ml	Sigma, USA
DEPC Water	880 ml	see Appendix 5b

Store at room temperature after preparation.

g) 5x RNA Loading Buffer

Item	**Amount**	**Source**
Bromophenol Blue	16 µl	Sigma, USA
Formamide	3.084 ml	Sigma, USA
37% (12.3M) Formaldehyde	720 µl	Sigma, USA
100% Glycerol	2 ml	Merck, Germany
500mM EDTA, pH8.0	80 µl	Merck, Germany
10x FA Gel Buffer	4 ml	See Appendix 5d
DEPC Water	to 10 ml	see Appendix 5b

Store at -20°C after preparation.

h) 50X and 1X TAE running Buffer and 1% Gel

Item	**Amount**	**Source**
Tris Base	242.28 g	USB Corporation, USA
Glacial Acetic Acid	57.1 ml	Merck, Germany
0.5 M EDTA (pH 8.0)	100 ml	BDH, Middle East
Type 1 Reagent Grade Water (E-pure)	840 ml	Barnstead, USA
Agarose gel (necessary when making 1% gel)	1 g in 100 ml of 1 X TAE	BioRad Laboratories, Singapore

EDTA of 0.5 M was prepared by adding 93.06 g of EDTA in 500 ml of Type 1 Reagent Grade Water (E-pure) at pH 8.0. The 1 X TAE was prepared by diluting 20 ml of 50 X TAE with 980 ml of Type 1 Reagent Grade Water (E-pure)

Appendix 6: List of Oligonucleotides

Gene	Symbol	Sequence (5'-3')
FRMD4A	**FRMD4A F**	**gcc caa aat gtg gag tga gt**
	FRMD4A R	**cct cgt gga atg gac gta gt**
INDO	**INDO F**	**Gcg ctg ttg gaa ata gct tc**
	INDO R	**cag gac gtc aaa gca ctg aa**
Antisense target sequence of *FRMD4A*		**aga acc tga aga cag cag gct**
Antisense target sequence of *INDO*		**tat gag atc agg cag atg ttt**
Double-stranded oligos for *FRMD4A* miRNA	**Top single-stranded oligo**	**tgc tga gaa cct gaa gac agc agg ctg ttt tgg cca ctg act gac agc ctg ctc ttc agg ttc t**
	Bottom single-stranded oligo	**cct gag aac ctg aag agc agg ctg tca gtc agt ggc caa aac agc ctg ctg tct tca ggt tct c**
Double-stranded oligos for *INDO* miRNA	**Top single-stranded oligo**	**tgc tgt atg aga tca ggc aga tgt ttg ttt tgg cca ctg act gac aaa cat ctc tga tct cat a**
	Bottom single-stranded oligo	**cct gta tga gat cag aga tgt ttg tca gtc agt ggc caa aac aaa cat ctg cct gat ctc ata c**
miRNA forward sequencing primer	**miRNA (+)**	**tcccaagctggctagttaag**
GFP reverse primer	**GFP (-)**	**gggtaagctttccgtatgtagc**
CMV promoter	**CMV F**	**cgcaaatgggcggtaggcgtg**
FRMD4A	**FRMD4A 329 F**	**attcgtgcatgggaatcg**
	FRMD4A 3509 R	**gggaggaatccaggaaacag**
	FRMD4A 1611 R	**tgagctcagcttctcggag**
	FRMD4A 1592 F	**ctccgagaagctgagctca**
	FRMD4A 2419 R	**cctcgtggaatggacgtagt**
	FRMD4A 2403 F	**acgtccattccacgagg**
	New FRMD4A 329 F	**cac cat ggc agt gca gct ggt**
	New FRMD4A 1611 R	**gtg tga gct cag ctt ctc gga gac aca g**